

DEPARTMENT OF PHYSICS AND
ASTRONOMY

RUPRECHT-KARLS-UNIVERSITÄT HEIDELBERG

Master thesis in Physics

submitted by

JAN THORBEN SCHNEIDER

born 4 May 1992 in Gießen, Germany

—

August 2018

PROSPECTS OF LATTICE IMPROVEMENTS IN
QUANTUM SIMULATIONS

JAN THORBEN SCHNEIDER

This Master thesis has been carried out by Jan Thorben Schneider

at the

Institute for Theoretical Physics

under the supervision of

PROF. DR. JÜRGEN BERGES

and

DR. PHILIPP HAUKE

—

August 2018



To the memory of my mother.

ABSTRACT

Quantum simulators may be utilised to solve the hitherto intractable problem of simulating lattice gauge theories in regimes where simulations on classical computers are challenging. Current experimental state-of-the-art realisations, however, incorporate only view qubits thus seriously hindering a faithful simulation of lattice gauge theories. While being restricted in system size we employ lattice improvements to facilitate an accurate description of the continuum theory. We choose $1 + 1d$ quantum electrodynamics to quantify improving only with higher derivatives by benchmarking to the non-perturbative particle production rate in the Schwinger mechanism. Numerical simulations proceed with classical-statistical as well as exact diagonalisation methods. The latter offers an accessible route to the strong coupling regime of QED where we can confirm the particle production rate to grow. The former reveals including only higher derivatives in the improvement programme does not yield significant alleviation in need for larger system sizes.

ACKNOWLEDGMENTS

First and foremost I wish to thank my family for enabling me to having been able to pursue this degree! I am thankful for the support they gave me.

I wish to thank my supervisors Jürgen Berges and Philipp Hauke to taken me as their master's student. It has been an incredibly interesting, fascinating and exciting year in which I learned quite a lot.

Last but not least I am thankful for the very welcoming and friendly colleagues I enjoyed having throughout this year. I relished every coffee break and lunch break for the utterly helpful, enlightening and always a bit funny discussions.

Cheers

CONTENTS

1	INTRODUCTION	1
2	FOUNDATIONS	5
2.1	Introduction to the Schwinger Model in the continuum	5
2.2	Lattice derivatives and doublers	10
2.3	The staggered fermion transformation in Hamiltonian formulation . . .	12
2.4	Introduction to Improvements & the Renormalisation Group	17
2.4.1	Integrating momentum shell-wise [1]	17
2.4.2	Renormalisation Group Flows [1]	20
2.4.3	Symanzik improvement programme	22
2.4.4	Canonical Mass Dimension	24
2.4.5	Improvement coefficients	25
2.4.6	Quantifying Improvements	27
2.5	Schwinger mechanism in a constant, homogeneous electric field	31
2.5.1	Particle Number definition	31
2.5.2	Fermionic Current Operator	33
2.5.3	Average Current & its improvement	34
2.5.4	Periodicity and Cutoff	36
2.5.5	Illustration	37
3	METHODS	39
3.1	Exact Diagonalisation	39
3.1.1	Solving Gauss law with periodic boundary conditions	40
3.1.2	Numerical simulation	43
3.2	Classical Statistical Simulation	45
3.2.1	Introduction	45
3.2.2	Validity	45
3.2.3	Equations of Motion	45
3.2.4	Initial conditions	46
4	QUANTUM COMPUTING WITH TRAPPED IONS	47
4.1	Hamiltonian of trapped ions	47
4.2	Single-qubit gate	48
4.3	Two-qubit gate	48
4.4	4-qubit gate	49
4.5	4-qubit gate sequence of 1st improvement	50
5	RESULTS: UV CONVERGENCE WITH LATTICE IMPROVEMENTS	53
5.1	Approaching the continuum – Exact Diagonalisation	53
5.2	Approaching the continuum – Classical Statistical Simulation	55
6	RESULTS: EXACT DIAGONALISATION SIMULATION OF STRONGLY COUPLED QED	63
6.1	Strongly coupled QED at $Lm = 7$ and $E/E_c = 1.5$	63
7	CONCLUSION & OUTLOOK	75
7.1	Conclusion	75
7.2	Outlook	77

A	ILLUSTRATION OF THE SCHWINGER EFFECT IN THE BRILLOUIN ZONE	79
B	FERMIONIC OPERATORS IN SPIN DOF	81
B.1	Jordan-Wigner transform	81
B.2	Hamiltonian	82
B.3	Translation of statistical propagator	82
B.4	Current operator	83
C	SUPPLEMENTARY PLOTS: UV CONVERGENCE SERIES	85
C.1	Exact Diagonalisation	85
C.2	Classical Statistical Simulation	88
D	ON THE EFFECTS OF OPEN BOUNDARY CONDITIONS	97
E	SUPPLEMENTARY PLOTS: STRONGLY COUPLED QED AT $Lm = 7, E/E_c = 1.5$ AND 'EVEN' SYSTEM SIZE	101
	BIBLIOGRAPHY	103

LIST OF FIGURES

Figure 2.1	Plot of unimproved and improved dispersion relation	28
Figure 2.2	Figure of merit δ -deviation.	29
Figure 2.3	$N = 500, am = 0.05, E/E_c = 1, e/m = 0.1$	38
Figure 3.1	Plot Potential $v(d; a; N)$	41
Figure 4.1	Illustration of energy levels in Mølmer-Sørensen gate	49
Figure 4.2	Gate sequence 4-qubit improvement term	51
Figure 5.1	UV convergence (ED), $Lm = 6$	54
Figure 5.2	Comparison CD and ED	55
Figure 5.3	UV convergence (CS), $E/E_c = 1$, fit	57
Figure 5.4	UV convergence (CS), $E/E_c = 1.5$, fit	58
Figure 5.5	UV convergence (CS), $E/E_c = 2$, fit	59
Figure 5.6	UV convergence (CS), $E/E_c = 5$, fit	60
Figure 5.7	UV convergence (CS), $E/E_c = 7$, fit	61
Figure 6.1	VEV of chiral condensate	67
Figure 6.2	VEV of particle number	68
Figure 6.3	Strongly coupled QED, particle number, 'odd' system size . . .	69
Figure 6.4	Strongly coupled QED, particle number, $N = 26$, unimproved vs improved	70
Figure 6.5	Strongly coupled QED, UV-convergence of particle number, 'odd' system size	71
Figure 6.6	Strongly coupled QED, modified particle number, 'odd' system size	72
Figure 6.7	Strongly coupled QED, total energy $\langle H \rangle$ and electric field energy $\langle H_E \rangle$	73
Figure A.1	Series of plots with the Brillouin zone.	80
Figure C.1	UV convergence (ED), $Lm = 5$	86
Figure C.2	UV convergence (ED), $Lm = 4$	87
Figure C.2	UV convergence (CS), $E/E_c = 1$	90
Figure C.2	UV convergence (CS), $E/E_c = 1.5$	92
Figure C.3	UV convergence (CS), $E/E_c = 2$	93
Figure C.4	UV convergence (CS), $E/E_c = 5$	94
Figure C.5	UV convergence (CS), $E/E_c = 7$	95
Figure D.1	Comparison OPB vs PBC, current heat map	98
Figure D.2	Comparison OPB vs PBC, local current	99
Figure E.1	Strongly coupled QED, particle number, 'even' N	102

INTRODUCTION

Quantum field theory (QFT) combines three of the most fundamental set of ideas in physics: quantum theory, the concept of fields, and special relativity [1]. As such, it has proven to be a highly successful framework underlying much of modern day physics. It is central to a wide range of subjects—like elementary particle physics, condensed matter physics, and cosmology [1].

Fundamental to any quantum field theory are fields which are classified according to their statistics in either of two types: bosonic fields, and fermionic fields.

Gauge theories are certain types of quantum field theories where physics is invariant under local so-called gauge transformations. They describe fermions, the quanta of excitation of fermionic fields, as the fundamental particles of matter, and bosons, the quanta of excitation of bosonic fields, as the mediators of the fundamental forces. Gauge theories are the generally accepted and highly successful framework describing the strong, weak, and electromagnetic interactions of the fundamental fields of the standard model [2]. The theory of quantum chromodynamics (QCD) is such a gauge theory. It describes the strong interaction between quarks and gluons.

The set of mathematical tools to uncover and predict the behaviour of quantum fields has long been limited to perturbation theory [2] in which the coupling constant, a number quantifying the interaction of two quantum fields, is required to be sufficiently small. In this approach one may picture the interplay of quantum fields with Feynman diagrams and particles as their constituents [1, 3]. This was most successfully applied to the theory of quantum electrodynamics (QED) [3]. Yet, this approach fails when the interaction strength becomes strong.

This is particularly true for the theory of quantum chromodynamics [2]. Only when Kenneth Wilson in 1974 showed how to rigorously formulate gauge theories on a discretised lattice mimicking space and time, it was possible to numerically study phenomena in QCD beyond perturbation theory [2, 4], like the confinement of quarks and gluons. The coupling constant not needed to be sufficiently small and the quantum fields at hand may be strongly interacting and correlating.

Ever since, the quest of simulating quantum field theories in numerical simulations has become a branch of physics in its own right [2]. Ever more numerical methods to tackle problems which answers lie beyond perturbation theory have been devised. Among the most successful ones is the quantum Monte Carlo method. However, when strongly correlated and interacting fermionic quantum fields are involved, the quantum Monte Carlo method suffers from the so-called sign problem, which means the general numerical solution to this method scales in complexity larger than any polynomial [5]. As a consequence, the application of quantum Monte Carlo methods to systems involving fermionic fields is limited to the special case of thermal equilibrium, in which case the quantum theory problem can be mapped on a statistical (classical) mechanics problem [6].

However, a vast range of phenomena out of thermal equilibrium are excluded. They require real-time evolution, which is still an open problem without a general solution.

Yet, a part of the problems which require real-time dynamics can be accurately approximated by classical-statistical simulations [6]. Those simulations have shown remarkable results in describing phenomena beyond perturbation theory and simulating real-time dynamics of gauge theories [6–8]. The classical-statistical approximation, however, describes the full quantum theory accurately only in the limit of strong gauge fields and weak couplings [6].

Tensor Network States (TNS), aka. Matrix Product States (MPS) in $1 + 1d$, may be considered another promising numerical method for real-time dynamics of lattice gauge theories [9, 10]. This method, however, is mostly restricted to physics of low energy states of $1 + 1d$ with a gapped Hamiltonian [11]. Furthermore, due to restricting the maximal entanglement entropy, it can typically only cover relatively short time scales [11].

It is fair to say that to this day, there are no satisfying general and comprehensive methods to unravelling phenomena out of equilibrium quantum fields display.

The field of quantum simulation has emerged in parallel to numerical efforts in answering questions of real-time dynamics of quantum fields and more general quantum many-body systems [12, 13]. The concept dates back to 1982 when Richard Feynman proposed to take advantage of the ‘quantumness’ of nature at small scales to simulate quantum behaviour in a controlled and orderly fashion [12, 13]. Underlying this proposal is the insight of QFT that fundamental constants like the charge or mass of an electron are neither fundamental nor constant! Rather the symmetries of the respective QFT and the dimension it is embedded in define its properties. Those ‘constants’ ought to be measured and by doing so the experiment confirms where in the range of all possible values the QFT is realised. This, in turn, implies one can observe the same physics if one was to implement the same symmetries of e.g. a fundamental gauge theory regardless of the actual size of the system.

Unfortunately, his idea was left unappreciated as there was no known systems which could serve as a quantum simulator [14]. Later in 1989 Deutsch [15] formulated the notion of a general purpose quantum computer, which could compute any quantum algorithm. He showed that, only a certain small set of manipulations on quantum states would be necessary for building a general purpose quantum computer. Together with the quantum error correction protocols by Shor [16] and Steane [17] this set the feasibility of quantum simulation in regimes much closer to realise [18]. Those ideas base on the notion of a digital quantum computer with a set of manipulations called quantum logic gates. Simulating the physics of any system requires to translate the laws of motion into a successive application of quantum logic gates which simulate the original physics in discrete steps with quantum bits (qubits) storing the quantum information. This take on quantum simulators is hence called *digital*.

Today, there are several concepts to quantum simulation [19]. In view of gauge fields as emerging degrees of freedom in condensed matter systems [20], and the high fidelity with which one can tune isolated ultra cold quantum gases [20, 21], one may consider to engineer such an isolated quantum system such that it displays e.g. a local gauge symmetry. The laws governing the evolution of the system of interest are mapped in a one-to-one correspondence to the system at hand [19]. Then, the degrees of freedom in the ultra cold quantum system serve as an analogue of the fundamental degrees of freedom in the theory one wishes to simulate. Hence, this take on quantum simulators

is generally called *analogue*.

Within this thesis, however, we want to focus on the digital take on quantum simulators. Most prominent realisations with trapped ions include Refs. [22, 23] and with superconducting qubit circuits Refs. [24]. Engineering trapped ions to simulate a quantum many-body system of interest has many advantages like very long-lived coherence times, strong Coulomb interaction facilitating two-qubit gates, and experimental demonstration of very high fidelities [19]. However, the current state-of-the-art experimental realisations come with the drawback of only having few qubit degrees of freedom of the order of 10 [23]. The restricted system size is seriously hindering the simulation of effects that are characteristic of the infinite degrees of freedom any quantum field theory has.

However, physicists who are trying to use such quantum simulators to simulate lattice gauge theories are not the first to face this kind of restriction in system size. The earlier mentioned lattice QFT community devised a methodology to overcome some of those restrictions which goes by the name of *lattice improvements*, first proposed by Symanzik in 1979 [25].

This thesis aims at applying lattice improvements to small system sizes in order to investigate the benefits of the very same in view of digital quantum simulators. As a testbed we opt for QED in $1 + 1d$ (aka. the Schwinger model) and the Schwinger mechanism of particle pair production to benchmark our findings as analytical predictions for a certain regime are well-known [26]. For our main method of simulating QED in $1 + 1d$ we choose exact diagonalisation as it constitutes an unbiased and exact method of simulation. Moreover, it is characterised by the same set of fundamental degrees of freedom as a digital quantum computer, making it our method of choice.

This thesis is structured as follows. In [Chapter 2](#) we lay out the theoretical foundations involved in the Schwinger model, the Hamiltonian approach to lattice QED, and lattice improvements. [Chapter 3](#) is dedicated to introducing the two methods of numerical simulation we employ: exact diagonalisation and classical-statistical simulations. In [Chapter 4](#) we review some foundations of quantum computing with trapped ions before we compute the quantum logic gate sequence which comes about after applying lattice improvements to lattice QED. Subsequently, we show the results of numerical simulations in [Chapter 5](#) and measure the quantitative benefits of lattice improvements in view of quantum simulations.

Within this chapter we wish to approach all of the theoretical foundations and physical principles relevant to describe lattice QED with staggered fermions and an improved Hamiltonian in the prospect of the Schwinger mechanism.

To this end, we first review the Schwinger model and some of its features in the continuum in [Section 2.1](#), after which we discuss the fermion doubling problem on the lattice and introduce a solution with staggered fermions in [Section 2.2](#) and [Section 2.3](#), respectively. Subsequently, we cover a revision on the renormalisation group, improvements and their connection in [Section 2.4](#). Finally, we conclude this chapter with the description of the Schwinger mechanism in a constant, homogeneous electric field in [Section 2.5](#).

2.1 INTRODUCTION TO THE SCHWINGER MODEL IN THE CONTINUUM

The Schwinger model describes Quantum Electrodynamics (QED) in $(1 + 1)d$, and it entails a non-trivial interaction of Dirac fermions with a gauge field. It is an often studied toy model for inspecting a wide range of interesting phenomena. For instance, it exhibits confinement of fermions, appearance of a massive boson field, breaking of the chiral symmetry through the axial anomaly, screening of any external charge and background electric fields, and infinite (continuous) degeneracy of the vacuum state of the theory without mass [\[27\]](#).

The QED Lagrangian is given by,

$$\mathcal{L} = \bar{\psi} (i\partial^\mu \gamma_\mu - eA^\mu \gamma_\mu - m) \psi - \frac{1}{4} F^{\mu\nu} F_{\mu\nu}, \quad (2.1)$$

where ψ and $\bar{\psi}$ is the Dirac spinor and its canonical conjugate describing the electron and positron, A^μ is the gauge vector field describing the photon, and $F_{\mu\nu} = \partial_\mu A_\nu - \partial_\nu A_\mu$ is the (electromagnetic) field strength tensor.

In $1 + 1$ dimensions there are only two anti-commuting elements of the Clifford algebra defined by

$$\{\gamma_\mu, \gamma_\nu\} = 2\eta_{\mu\nu}, \quad (2.2)$$

where $\eta_{\mu\nu} = \text{diag}(1, -1)$ is the Minkowski metric. Thus, we have only three anti-commuting Dirac matrices. Hence, one can choose a representation with Pauli matrices:

$$\gamma_0 = \sigma_z = \begin{pmatrix} 1 & 0 \\ 0 & -1 \end{pmatrix}, \quad (2.3)$$

$$\gamma_1 = i\sigma_y = \begin{pmatrix} 0 & 1 \\ -1 & 0 \end{pmatrix}, \quad (2.4)$$

$$\gamma_5 = \gamma_0\gamma_1 = \sigma_x = \begin{pmatrix} 0 & 1 \\ 1 & 0 \end{pmatrix}, \quad (2.5)$$

$$\{\gamma_\mu, \gamma_\nu\} = 2\eta_{\mu\nu}. \quad (2.6)$$

which will be of use some time later.

Please note that in $1 + 1d$ the electromagnetic coupling constant e has units of an inverse length, i.e. units of mass.

2.1.0.1 Temporal gauge

For the analysis of the Schwinger model we want to resort to the ‘temporal’ or ‘Weyl gauge’, $A_0(x) = 0$. Hence, the Lagrangian takes the form

$$\mathcal{L} = \bar{\psi} \left(i\partial_\mu \gamma^\mu - eA^1 \gamma_1 - m \right) \psi + \frac{1}{2} \left(\partial_0 A^1 \right)^2, \quad (2.7)$$

However, the temporal gauge is in a sense an *incomplete* gauge as we are left with a residual gauge redundancy, where equivalent configurations are linked by time-independent gauge transformations. Additionally, Gauss’s law is not obeyed at the operator level. It becomes a constraint on the physical Hilbert space. This is because setting $A_0 = 0$ in the Lagrangian prohibits us from varying with respect to A_0 or $\partial_0 A_0$. Thus, we cannot obtain Gauss’s law from a variational principle since Gauss’s law is actually the equation of motion obtained by the Euler-Lagrange equation for A_0 .

To see this, consider,

$$0 = \frac{\partial \mathcal{L}}{\partial A_0} - \partial_\mu \frac{\partial \mathcal{L}}{\partial (\partial_\mu A_0)}, \quad (2.8)$$

$$\frac{\partial \mathcal{L}}{\partial A_0} = e\bar{\psi}\gamma^0\psi + \frac{1}{2}\partial_\mu\partial^\mu A^0 - \frac{1}{2}\partial_\mu\partial^0 A^\mu, \quad (2.9)$$

$$\partial_\mu \frac{\partial \mathcal{L}}{\partial (\partial_\mu A_0)} = -\frac{1}{2}\partial_\mu\partial^\mu A^0 + \frac{1}{2}\partial_\mu\partial^0 A^\mu, \quad (2.10)$$

$$\Rightarrow 0 = e\psi^\dagger\psi + \partial_\mu\partial^\mu A^0 - \partial^0\partial_\mu A^\mu \quad (2.11)$$

with $A^0 = 0$ we obtain Gauss law,

$$0 = e\psi^\dagger\psi - \underbrace{\partial_1 \partial^0 A^1}_{=E} = e\psi^\dagger\psi - \partial_x E. \quad (2.12)$$

We can deduce from [Equation 2.7](#) that the conjugate momentum to A^1 , ($= \frac{\partial \mathcal{L}}{\partial \dot{A}^1}$), is minus the electric field:

$$-\dot{A}^1 = F^{10} = E \quad (2.13)$$

and impose canonical commutation relations

$$[A(x), E(y)] = i\delta(x - y) \quad (2.14)$$

Hence, we find the Hamiltonian to be

$$H = \int dx \left\{ i\bar{\psi}\gamma^1 (\partial_1 + ieA_1) \psi + m\bar{\psi}\psi + \frac{1}{2}E^2 \right\}. \quad (2.15)$$

At first sight, Gauss's law does not seem to be implemented into the theory when working in temporal gauge. However, this fact is mitigated by the following observation [27]: We wish to restrict the Hilbert space to the 'physical' subspace where

$$\left(\partial_x E(x) - e\psi^\dagger \psi \right) |\phi\rangle =: G(x) |\phi\rangle = 0, \quad (2.16)$$

and Gauss's law is fulfilled. Yet, the gauge field as the canonical conjugate of the electric field is a generator for linear shifts of the electric field. Together with the canonical commutation relation [Equation 2.14](#) one finds:

$$e^{-i \int dy \alpha(y) A(y)} G(x) e^{+i \int dy \alpha(y) A(y)} \quad (2.17)$$

$$= \partial_x [E(x) + \alpha(x)] - e\psi^\dagger(x)\psi(x) \quad (2.18)$$

$$= G(x) + \partial_x \alpha(x) \quad (2.19)$$

Subsequently, one may start with a subspace where

$$G(x) |\phi_{\text{phys}}\rangle = 0, \quad (2.20)$$

and construct another subspace by

$$|\phi_{\text{phys}}\rangle \longrightarrow |\phi_\alpha\rangle = e^{-i \int dy \alpha(y) A(y)} |\phi_{\text{phys}}\rangle, \quad (2.21)$$

ending up in a subspace for which

$$G(x) |\phi_\alpha\rangle = \partial_x \alpha(x) |\phi_\alpha\rangle. \quad (2.22)$$

Therefore, if the initial state fulfils Gauss's law any time evolved state of this initial state will too. Moreover, we see that the Schwinger Hamiltonian generates a Hilbert space which has infinitely many subspaces for which Gauss's law is pairwise differently implemented.

Fortunately, all operators $G(x)$ commute with each other and with H such that we may simultaneously diagonalise them [27]. Thus, we are free to impose the state condition of [Equation 2.20](#) as the Hamiltonian will never take us out of the subspace we previously called "physical". Actually, we are free to impose the more general state condition of [Equation 2.22](#) for any arbitrary function $\alpha(x)$. Then, however, Gauss's law is modified by a classical static background distribution $\rho_{\text{class}} = \partial_x \alpha(x)$.

Therefore, canonical quantisation of the Schwinger model in temporal gauge produces not only one but rather an infinite number of theories, all having different classical background fields. This should not be a big surprise as one expects to be able to formulate QED with any classical background field.

On physical grounds, we are restricting ourselves to the case where $\rho_{\text{class}} = \partial_x \alpha(x) = 0$, such that $\alpha(x)$ is a constant in space. A unitary transformation like [Equation 2.17](#) of the operator $E(x)$ shifts it by a constant, i.e. we implement a constant background field ϵ , which is equivalent to the presence of boundary charges at finite volume.

2.1.0.2 Constraining Hilbert space to the physical subspace

Throughout this thesis we are only interested in (initial) states of zero total charge. Hence, in this section we want to express the Hamiltonian constraint on the ‘physical’ sector of the Hilbert space \mathcal{H}_{phy} such that $\forall |\Psi\rangle \in \mathcal{H}_{\text{phy}}$:

$$Q_{\text{tot}} |\Psi\rangle = \int_{-\infty}^{\infty} dx \rho(x) |\Psi\rangle = 0, \quad (2.23)$$

$$\rho(x) = \psi^\dagger(x)\psi(x). \quad (2.24)$$

As mentioned above, any dynamics will stay inside the respective sector of the Hilbert space as $G(x)$ commutes with H .

First, consider the following Maxwell equation,

$$\partial_x E(x) = \sum_j e_j \delta(x - x_j) = e\rho(x), \quad (2.25)$$

which is solved by the Green’s function

$$\partial_x \Theta(x') = \delta(x - x'), \quad (2.26)$$

$$\partial_x^{-1} = \Theta(x). \quad (2.27)$$

This implies the general solution of [Equation 2.25](#) is given by

$$E(x) = \sum_j e_j \Theta(x_j) + e\epsilon, \quad (2.28)$$

where ϵ is a constant of integration and constitutes a constant background field.

Using [\(2.25\)](#), we can solve for $E(x)$ in terms of $\rho(y)$,

$$E(x) = e \int_{-\infty}^x dx' \rho(x'), \quad (2.29)$$

and substitute this into the Hamiltonian [\(2.15\)](#) and obtain

$$H = \int dx \psi^\dagger \gamma_0 \left(i\gamma_1 \partial^1 + e\gamma_1 A^1 + m \right) \psi(x) - \frac{e^2}{4} \int dx dy \rho(x) |x - y| \rho(y). \quad (2.30)$$

Now, we may use the residual gauge freedom when working in axial temporal gauge. That is, one can still perform spatially dependent only gauge transformations. With

$$\psi'(x) = e^{-i \int_{-\infty}^x dy A(y)} \psi(x), \quad (2.31)$$

we can eliminate the remaining $A(x)$ from the Hamiltonian:

$$H = \int dx \psi'^{\dagger} \gamma_0 \left(i\gamma_1 \partial^1 + m \right) \psi'(x) - \frac{e^2}{4} \int dx dy \rho'(x) |x - y| \rho'(y). \quad (2.32)$$

2.1.0.3 Bosonisation of the Schwinger Model

In this subsection we merely want to motivate and cite the bosonisation process fairly briefly. It will become of particular interest because the bosonised version of the Schwinger model offers a clear view of the relevant degrees of freedom in the infinite coupling limit. As we will show below, the Schwinger Model can not only be treated

perturbatively at small couplings in the fermionic formulation. It is also possible to employ perturbation theory in the mass at infinite coupling in the boson representation of the theory. For an in-depth treatment we refer the reader to [28].

With (2.32) we have managed to express the Hamiltonian only in terms of fermionic degrees of freedom (DoF). In fact, the Hamiltonian of (2.32) can be expressed only in terms of bosonic DoF. For this, consider the ‘two-currents’,

$$j^\mu(x) = \bar{\psi}(x)\gamma^\mu\psi(x), \quad (2.33)$$

$$j_5^\mu(x) = \bar{\psi}(x)\gamma^\mu\gamma^5\psi(x), \quad (2.34)$$

which are conserved [29]. Due to the identity in two dimensions $\gamma^5 = \gamma^0\gamma^1$, $\gamma^\mu\gamma^5 = \epsilon^{\mu\nu}\gamma_\nu$ ($\epsilon_{\mu\nu}$ is the Levi-Civita symbol), the axial and vector currents can be expressed by some scalar field ϕ as [28]:

$$j^\mu(x) = -\frac{1}{\sqrt{\pi}}\epsilon_{\mu\nu}\partial^\nu\phi \quad (2.35)$$

$$j_5^\mu(x) = -\frac{1}{\sqrt{\pi}}\partial^\mu\phi \quad (2.36)$$

Introducing some test charges $\rho_{ext} = \pm q_{ext}$ at $\pm\infty$, respectively, simply shifts

$$\rho \rightarrow \rho + \rho_{ext} = \frac{1}{\sqrt{\pi}}\partial^1(\phi + \phi_{ext}). \quad (2.37)$$

Hence, we obtain a boundary term for the charge density and via Gauß’s law one has a background electric field.

Subsequently, we substitute (2.37) into (2.32) which yields

$$H = \int dx \bar{\psi} \left(i\gamma_1\partial^1 + m \right) \psi - \frac{e^2}{4\pi} \int dx dy \partial^1(\phi + \phi_{ext}) |x - y| \partial^1(\phi + \phi_{ext}). \quad (2.38)$$

If we know integrate by parts and remind ourselves that the coupling has mass dimension in $1 + 1d$, we can see the mass term of the scalar field emerge [29].

In fact, one can show the operator identities [28, 29]

$$\bar{\psi}i\gamma_\mu\partial^\mu\psi = \frac{1}{2}\partial_\mu\phi\partial^\mu\phi, \quad (2.39)$$

$$\bar{\psi}\psi = -c\frac{e}{\sqrt{\pi}}\cos(2\sqrt{\pi}\phi), \quad (2.40)$$

with $c = \exp(-\gamma)/2\pi$ and $\gamma = 0.5774$ the Euler–Mascheroni constant.

We find after integrating by parts

$$H = \int dx \frac{1}{2}(\partial^\mu\phi)^2 + \frac{1}{2}\frac{e^2}{\pi}\left(\phi + \frac{\sqrt{\pi}q_{ext}}{e}\right)^2 - cm\frac{e}{\sqrt{\pi}}\cos(2\sqrt{\pi}\phi). \quad (2.41)$$

We may define the background field $\theta = 2\pi q_{ext}/e$ and shift the field ϕ by it to obtain the bosonised version of the Schwinger model [28, 29]

$$H = \int dx \frac{1}{2}(\partial^\mu\phi)^2 + \frac{1}{2}\frac{e^2}{\pi}(\phi)^2 - cm\frac{e}{\sqrt{\pi}}\cos(2\sqrt{\pi}\phi - \theta). \quad (2.42)$$

Note this Hamiltonian describes a massive Sine-Gordon model with mass $\frac{e}{\sqrt{\pi}}$. The massless Sine-Gordon model is known to be integrable, while the massive Sine-Gordon model is not.

However, in the limit $e/m \rightarrow \infty$, or equivalently $m/q \rightarrow 0$, the interaction term of (2.42) $\cos(2\sqrt{\pi}\phi - \theta)$ is suppressed by the mass term $(\phi)^2$. Thus, the strong coupling limit yields a free massive scalar theory.

2.1.0.4 Spontaneous symmetry breaking

Here, we wish to cite the well-known fact that the vacuum state of the massless Schwinger model spontaneously breaks chiral symmetry [29, 30]. The quantum expectation value of the chiral order operator $\bar{\psi}\psi$ with respect to the vacuum state of the massless Schwinger model $|\Omega\rangle$ takes on a non-zero value according to [29, 30]

$$\langle\Omega|\bar{\psi}\psi|\Omega\rangle = -c\frac{e}{\sqrt{\pi}}\cos(\theta), \quad (2.43)$$

although the Hamiltonian (2.15) in the case of $m = 0$ is symmetric under the symmetry transformation

$$\psi \rightarrow e^{i\alpha\gamma^5}\psi, \quad (2.44)$$

$$\bar{\psi} \rightarrow -\bar{\psi}e^{i\alpha\gamma^5}. \quad (2.45)$$

We shall write the background field θ as

$$\theta = 2\pi\frac{E}{E_c}\left(\frac{m}{e}\right)^2, \quad (2.46)$$

$$E_c = \frac{m^2}{e}, \quad (2.47)$$

and thus can follow that the massive Schwinger model in the limit of $e/m \rightarrow \infty \Leftrightarrow m/e \rightarrow 0$ and $E/E_c = \text{const.}$ yields a vacuum expectation value of [28–30]

$$\langle\Omega|\bar{\psi}\psi|\Omega\rangle = -c\frac{e}{\sqrt{\pi}} = -\frac{e^\gamma}{2\pi^{3/2}}e. \quad (2.48)$$

2.2 LATTICE DERIVATIVES AND DOUBLERS

In this section we wish to explain the fermion doubling problem which comes about when naively discretising fermions on the lattice.

Our analysis in this section shall be based on the simplifying case of the free theory. The action of a free fermion field in $1 + 1d$ in Minkowski spacetime is given by

$$S = \int d^2x \bar{\psi}(x) (\gamma^\mu \partial_\mu - m) \psi(x). \quad (2.49)$$

To formulate this theory on the lattice where on every site we place (fermionic) degrees of freedom ψ_n , we need to find a lattice representation of the derivative.

To this end we shall inspect the Taylor expansion of a function f :

$$f(x \pm a) = f(x) \pm af'(x) + \frac{a^2}{2}f''(x) \pm \frac{a^3}{3!}f'''(x) + \mathcal{O}(a^4). \quad (2.50)$$

Therefore, we may define the symmetric (naive) derivative as

$$\frac{f(x+a) - f(x-a)}{2a} = f'(x) + \mathcal{O}(a^2). \quad (2.51)$$

Consequently, one might formulate the continuum action of free fermions on the lattice naively as

$$S = a \sum_n \frac{i}{2a} \bar{\psi}_\alpha(n) \left((\gamma_0)_{\alpha\beta} \psi_\beta(n + e_0) + (\gamma_1)_{\alpha\beta} \psi_\beta(n + e_1) \right) - m \bar{\psi}_\alpha(n) \psi_\alpha(n) \quad (2.52)$$

$$= a \sum_n \bar{\psi}_\alpha(n) M_{\alpha\beta}(n, m) \psi_\beta(m) \quad (2.53)$$

with

$$M_{\alpha\beta}(n, m) = \frac{i}{2a} \sum_\mu (\gamma_\mu)_{\alpha\beta} (\delta_{n+e_\mu, m} - \delta_{n-e_\mu, m}) - m \delta_{\alpha\beta} \delta_{n, m}. \quad (2.54)$$

We may define the discrete Fourier transform as

$$\tilde{\psi}_\alpha(p) = \frac{1}{\sqrt{N}} \sum_{n=0}^{N-1} e^{-i \frac{2\pi n q}{N}} \psi_\alpha(n), \quad (2.55)$$

$$\psi_\alpha(n) = \frac{1}{\sqrt{N}} \sum_{q=0}^{N-1} e^{i \frac{2\pi n q}{N}} \tilde{\psi}_\alpha(q), \quad (2.56)$$

and find the action in Fourier space to be

$$S = a \sum_{q, p} \tilde{\psi}_\alpha^\dagger(p) \delta_{qp} \tilde{M}_{\alpha\beta}(p) \tilde{\psi}_\beta(p), \quad (2.57)$$

$$\text{with } M_{\alpha\beta}(p) = \frac{1}{a} \sum_\mu (\gamma_\mu)_{\alpha\beta} \sin(p^\mu a) - m \delta_{\alpha\beta}. \quad (2.58)$$

Here, we see that the matrix of the Dirac operator is diagonal in Fourier space. Hence, we can easily invert it in Fourier space and transform it back to real space.

It is well known how to invert this matrix formally and we shall only state the result. For computational details see [2].

One finds

$$\tilde{M}_{\alpha\beta}^{-1}(p) = i \frac{m + \sum_\mu \gamma_\mu \pi(p^\mu)}{m^2 + \sum_\mu \pi^2(p^\mu)}, \quad (2.59)$$

$$\text{with } \pi(p^\mu) = \frac{1}{a} \sin(p^\mu a). \quad (2.60)$$

This yields for the (naive) propagator in real space on the lattice

$$M_{\alpha\beta}^{-1}(x, y; a) = \int_{-\pi/a}^{\pi/a} \frac{d^d p}{(2\pi)^d} i \frac{m + \sum_\mu \gamma_\mu \pi(p^\mu)}{m^2 + \sum_\mu \pi^2(p^\mu)} e^{ip(x-y)}. \quad (2.61)$$

It is here, where we see why the naive lattice derivative yields troubling results. The continuum limit $a \rightarrow 0$ of (2.51) will not give the correct well-known continuum limit,

$$D = i \sum_\mu \gamma^\mu \partial_\mu - m, \quad (2.62)$$

$$D^{-1}(x-y) = \int_{-\infty}^{\infty} \frac{d^d p}{(2\pi)^d} i \frac{\sum_\mu \gamma_\mu p^\mu + m}{p^2 - m^2} e^{-ip(x-y)} \quad (2.63)$$

This is because the sine in the denominator of (2.51) has for every dimension two zeros; namely everywhere where p^μ has an entry of 0 or π/a , respectively. This extra zero in $\pi(p^\mu)$ compared to the continuum case p^μ gives rise to an extra low energy excitation, as the poles of the propagator gives rise to particles. This problem is referred to as the fermion doubling problem.

Our theory suffers fermion doubling as long as we not remedy this. There are many ‘cures’ for fermion doubling available. They all must obey the Nielsen-Ninomiya no-go theorem [31] that every real, local, chiral as well as translation symmetry obeying free fermion action will suffer from fermion doubling. Hence, any cure of the fermion doubling will necessarily violate one of the above assumptions.

In the next section we want to explain how Kogut and Susskind’s staggered fermions [32] break translational invariance and remove (most of) the fermion doublers.

2.3 THE STAGGERED FERMION TRANSFORMATION IN HAMILTONIAN FORMULATION

As we have seen in the previous section, the fermion doubling problem arise from the fact, that the naive discretisation of the derivative will yield unphysical contributions from the Brillouin zone boundary. One might think that we could eliminate these unphysical contributions by effectively halving the Brillouin zone, i.e. doubling the lattice spacing. To that end, one distributes all relevant degrees of freedom into one hypercube, such that the effective lattice spacing *doubled*. Consequently, we may be able to eliminate the doublers. However, this comes at the cost of explicitly breaking translational invariance, and doubling the lattice spacing and therefore halving the effective size of available points in the BZ.

Kogut and Susskind’s approach [32] to remove the fermion doublers can be outlined like this. We diagonalise the naive action in both the matrix indices n, m , labelling position, and α, β , labelling spinor entry. Then we spread those degrees of freedom onto a hypercube in our lattice thereby doubling the effective lattice spacing between the same degrees of freedom. A crucial observation one has to make is that a hypercube in d spatial dimensions has 2^d sites. However, a spinor has in d (d odd) spatial dimensions $2^{\frac{d+1}{2}}$ components (if d is even, the spinor has as many components as in $d - 1$ spatial dimensions). Thus, for d spatial dimensions one is forced to populate all 2^d sites of a hypercube with $2^{d - \frac{d+1}{2}} = 2^{\frac{d-1}{2}}$ different ‘species’ of fermions in order to maintain the effective doubling of the lattice spacing between the same degrees of freedom. In fact, those extra DoF might be considered as doublers.

In one spatial dimension we are fortunate enough to eliminate the doubler fermion entirely—without the otherwise applicable caveat of introducing new fermion species, also known as *tastes*.

Below we want to outline how the staggered fermion transformation, which diagonalises the naive action, looks like in the Hamiltonian picture in Minkowski spacetime. Due to the Hamiltonian description we opted for, the fundamental degrees of freedom are ψ^\dagger and ψ as opposed to $\bar{\psi}$ and ψ in the path integral approach. This change in variables must be accommodated for by a modified staggered fermion transformation which is usually not cited in the literature.

The transformation often referred to in the literature is in *euclidean* d -dimensional spacetime given by

$$\psi_a(x) = U_{ab}(x)\psi_b(x), \quad (2.64)$$

$$U_{ab}(x) = \left(\prod_{i=0}^d \gamma_i^{x_i} \right)_{ab}. \quad (2.65)$$

Then, the action

$$S = \sum_{\mathbf{n}} \sum_{\hat{\mu}} \bar{\psi}_{\mathbf{n}} \gamma_{\hat{\mu}} (\psi_{\mathbf{n}+\hat{\mu}} - \psi_{\mathbf{n}-\hat{\mu}}) + m \sum_{\mathbf{n}} \bar{\psi}_{\mathbf{n}} \psi_{\mathbf{n}}, \quad (2.66)$$

is diagonal in the variables ψ and $\bar{\psi}$ in the sense that there is only one independent label for the matrix connecting these two variables. This implies the spatial and spinor indices are mixed to give this new label in which the resulting matrix is diagonal. This does not pose a problem for a treatment where the path integral is the fundamental object, since the path integral measure is invariant under the variable transform $\psi^\dagger \rightarrow \bar{\psi}$. However, when changing to Minkowski spacetime and treating the Hamiltonian as the fundamental object of our theory, the same transformation which diagonalised the action in the above mentioned sense and in the variables $\psi, \bar{\psi}$ will not diagonalise the Hamiltonian in the variables ψ and ψ^\dagger . Hence, we may incorporate γ_0 in the staggered fermion transformation. As we will see later, the transformation we chose diagonalises the Hamiltonian in the above mentioned sense only if a representation of the Clifford algebra is chosen such that γ_0 is diagonal.

In general, transformation matrices U_R and U_L ,

$$\psi(n) = U_R(n)\phi(n) \quad (2.67)$$

$$\psi^\dagger(n) = \phi^\dagger(n)U_L(n) \quad (2.68)$$

will bring the Hamiltonian into diagonal form in the variables ϕ and ϕ^\dagger if they satisfy

$$U_L(n)\gamma_0\gamma_1U_R(n-1) = K_f(n-1), \quad (2.69)$$

$$U_L(n)\gamma_0\gamma_1U_R(n+1) = K_f(n+1), \quad (2.70)$$

$$U_L(n)\gamma_0U_R(n) = M_f(n), \quad (2.71)$$

$$U_L(n)U_R(n) = \mathbb{1}, \quad (2.72)$$

with $K_f(n \pm 1), M_f(n)$ being diagonal matrices.

A possible choice for the transformation matrix in $1 + 1d$ would be

$$U_R(n) = U(n), \quad U_L(n) = U^\dagger(n), \quad (2.73)$$

$$U(n) = (\gamma_0\gamma_1)^n. \quad (2.74)$$

Then, we find

$$\psi^\dagger(n)\gamma_0\psi(n) = \phi^\dagger(n)(-\gamma_1\gamma_0)^n\gamma_0(\gamma_0\gamma_1)^n\phi(n) \quad (2.75)$$

$$= \phi^\dagger(n)(-1)^n\gamma_1^n\gamma_0^n\gamma_0\gamma_0^n\gamma_1^n\phi(n) \quad (2.76)$$

$$= \phi^\dagger(n)(-1)^n\gamma_1^n\gamma_0^n\gamma_0^n\gamma_1^n(-1)^n\gamma_0\phi(n) \quad (2.77)$$

$$= \phi^\dagger(n)(-1)^n(-1)^n(-1)^n\gamma_0\phi(n) \quad (2.78)$$

$$= (-1)^n\phi^\dagger(n)\gamma_0\phi(n). \quad (2.79)$$

and, respectively,

$$\psi^\dagger(n)\gamma_0\gamma_1\psi(n\pm 1) = \phi^\dagger(n)(\gamma_0\gamma_1)^n\gamma_0\gamma_1(\gamma_0\gamma_1)^{n\pm 1}\phi(n\pm 1) \quad (2.80)$$

$$= \phi^\dagger(n)(-\gamma_0\gamma_0\gamma_1\gamma_1)^{n+1/2(1\pm 1)}\phi(n\pm 1) \quad (2.81)$$

$$= \phi^\dagger(n)\mathbb{1}^{n+1/2(1\pm 1)}\phi(n\pm 1) \quad (2.82)$$

$$= \phi^\dagger(n)\phi(n\pm 1). \quad (2.83)$$

Hence, the Hamiltonian is diagonal, provided a choice of representation where γ_0 is diagonal.

For $1 + 1d$ spinor fields, this is possible by choosing from (2.3).

This implies one can only realise uneven lattice derivatives $\partial^{(2n+1)}$ with staggered fermions as outlined below:

$$\psi^\dagger(n)\gamma_0\gamma_1\psi(n\pm l) = \phi^\dagger(n)(\gamma_0\gamma_1)^n\gamma_0\gamma_1(\gamma_0\gamma_1)^{n\pm l}\phi(n\pm l) \quad (2.84)$$

$$= \phi^\dagger(n)(\gamma_0\gamma_1\gamma_0\gamma_1)^{n+1-\frac{l+1}{2}\pm\frac{l+1}{2}}(\gamma_0\gamma_1)^{\pm(l-1)}\phi(n\pm l) \quad (2.85)$$

$$= \phi^\dagger(n)(\gamma_0\gamma_1)^{\pm(l-1)}\phi(n\pm l) \quad (2.86)$$

NB:

$$(\gamma_0\gamma_1)^{2n} = (\gamma_0\gamma_1\gamma_0\gamma_1)^n = (-\gamma_0\gamma_0\gamma_1\gamma_1)^n = (-\gamma_1\gamma_1)^n \quad (2.87)$$

$$= \mathbb{1}^n = \mathbb{1}, \forall n \in \mathbb{N} \quad (2.88)$$

This is also in accordance with the fact that staggered fermions ‘preserve’ a remnant – the axial symmetry – of the chiral symmetry [2, 29], as a second derivative term containing $\psi(n\pm 2)$ would explicitly break this remnant symmetry.

We gather, we are able to diagonalise the Hamiltonian by ‘mixing’ spin and configuration space. Hence, we have a Hamiltonian

$$H = \sum_{m,n=0}^{N-1} \sum_{a,b=0}^1 \phi_a^\dagger(n)h_{a,b}(n,m)\phi_b(m), \quad (2.89)$$

with

$$h_{ab}(n,m) = \delta_{a,b} \left(-\frac{i}{2a}\delta_{m,n+1} + \frac{i}{2a}\delta_{m,n-1} + m(-1)^n \right), \quad (2.90)$$

being a diagonal 2×2 matrix, which breaks translation invariance, thus fulfils a necessary requirement of the Nielsen-Ninomiya no-go theorem.

By mixing spatial and spinor index we achieved writing the Hamiltonian in a diagonal form in the sense that we couple the hermitian conjugate vector ϕ^\dagger via a diagonal matrix h to the vector ϕ . Consequently, the two components decouple and we wish to omit the latter since we know of the doubling problem which we have not remedied until now. Omitting the second degree of freedom, we write

$$H = \sum_{m,n=0}^{N-1} \phi^\dagger(n)h(n,m)\phi(m), \quad (2.91)$$

and we are left with only a single (spinless) fermionic degree of freedom [2]. We must, however, show that this is still of physical relevance. To this end we show that in the

limit of $a \rightarrow 0$ we can actually ‘rebuild’ the spinor components and retrieve the correct continuum action.

For this, consider the relabelling

$$\psi_\alpha(n) = \phi(2n + \alpha), \quad (2.92)$$

$$\psi_\alpha^\dagger(n) = \phi^\dagger(2n + \alpha), \quad (2.93)$$

$$\alpha \in \{0, 1\}.$$

Notice the index n for the spinor ψ labels spacetime points of a lattice with lattice spacing $2a$.

Together with $(-1)^{2n+\alpha} = (-1)^\alpha$, (2.91) takes the following form in the relabelled spinors:

$$H = \sum_{n=0}^{N/2-1} \sum_{\alpha=0}^1 \frac{-i}{2a} \phi^\dagger(2n + \alpha) [\phi(2n + \alpha + 1) - \phi(2n + \alpha - 1)] \quad (2.94)$$

$$+ \sum_{n=0}^{N/2-1} \sum_{\alpha=0}^1 m(-1)^\alpha \phi^\dagger(2n + \alpha) \phi(2n + \alpha). \quad (2.95)$$

Considering

$$\phi(2n + \alpha + 1) = \delta_{\alpha,0} \psi_1(n) + \delta_{\alpha,1} \psi_0(n + 1), \quad (2.96)$$

$$\phi(2n + \alpha - 1) = \delta_{\alpha,0} \psi_1(n - 1) + \delta_{\alpha,1} \psi_0(n), \quad (2.97)$$

we can write (2.94) as

$$H_{\text{stagg}} = \frac{1}{2} \sum_{n=0}^{\frac{N}{2}-1} \sum_{\alpha,\beta=0}^1 \psi_\alpha^\dagger(n) [\delta_{\beta,\alpha+1} i\partial_L + \delta_{\beta,\alpha-1} i\partial_R + m\delta_{\alpha,\beta}(-1)^\alpha] \psi_\beta(n) \quad (2.98)$$

$$= \frac{1}{2} \sum_{n=0}^{\frac{N}{2}-1} \left(\psi_0^\dagger(n), \psi_1^\dagger(n) \right) \begin{pmatrix} m & i\partial_R \\ i\partial_L & -m \end{pmatrix} \begin{pmatrix} \psi_0(n) \\ \psi_1(n) \end{pmatrix} \quad (2.99)$$

with

$$\partial_R \psi_\beta(n) = \frac{1}{a} (\psi_\beta(n + 1) - \psi_\beta(n)), \quad (2.100)$$

$$\partial_L \psi_\beta(n) = \frac{1}{a} (\psi_\beta(n) - \psi_\beta(n - 1)). \quad (2.101)$$

Notice that we are to require N to be even. Later, this will be emphasised with denoting the total number of lattice points as $2N$.

This Hamiltonian yields in the limit $a \rightarrow 0$ the correct continuum result [2, 33],

$$H = \int dx \psi^\dagger(x) \gamma_0 (i\gamma_1 \partial^1 + m) \psi(x), \quad (2.102)$$

with the representation of the Clifford algebra chosen in (2.3)ff. Furthermore, we removed the doublers from our theory by effectively doubling the lattice spacing through relabelling according to (2.96)f. This renders the BZ half the size and as such the lattice momentum π_q will only have one zero in the first Brillouin zone. For an explicit calculation of the fermion propagator see e.g. Refs. [2, 33].

At this point it should be stressed, that we achieved to remove the doublers at the cost of doubling the lattice spacing and halving the effective number of spinor DoF. The relabelling (2.96) implies that a staggered fermion lattice of $2N$ sites describes in fact only N physical fermions. However, the symmetric lattice derivative from (2.90) yields an accuracy of $\mathcal{O}(a^2)$.

Lastly, we want to remark that (2.73), the transformation which diagonalises the Hamiltonian, can readily be generalised to higher dimensions as

$$U(n^\mu) = \prod_{\mu=0}^d (\gamma_0 \gamma_\mu)^{n^\mu} . \quad (2.103)$$

However, as we already emphasised above, in more than 1 spatial dimension we are not fortunate enough to remove all the doublers and we are left with $2^{\frac{d-1}{2}}$ (d odd), $2^{\frac{d-2}{2}}$ (d even) doublers in d spatial dimensions [2, 33].

Summarising, we found a transformation which breaks translation invariance and brings the Hamiltonian in to a diagonal form in the sense of (2.90). Subsequently, we have shown after omitting the second degree of freedom in (2.90) we disposed of the doublers and we can retrieve the correct continuum result by relabelling according to (2.96). Consequently, we found a suitable fermion discretisation which does not suffer the doubling problem. Within the framework of this thesis we will choose the staggered fermion discretisation.

2.4 INTRODUCTION TO IMPROVEMENTS & THE RENORMALISATION GROUP

The concepts and the motivation behind lattice improvements in general can be appreciated in view of the renormalisation group. Hence, we first review in this section Wilson's approach to renormalisation [34], introduce the renormalisation group, and define the notion of relevant, marginal and irrelevant operators, since we use those to improve our lattice theory. This introduction is closely oriented towards chapter 12 of Peskin & Schroeder's book [1].

Subsequently, we want to introduce Symanzik's improvement programme in Section 2.4.3 and discuss what kinds of irrelevant operators are at our disposal to improve $1 + 1d$ QED in Section 2.4.4, before we opt only for higher kinetic terms for our improvement procedure.

In Section 2.4.5 we apply the knowledge acquired over the previous sections to improve the Hamiltonian for staggered fermions in $1 + 1d$.

We conclude this chapter with Section 2.4.6 where we attempt to quantify improvements.

2.4.1 Integrating momentum shell-wise [1]

In his 1974 paper [34], Kenneth Wilson put forward a highly successful approach to renormalisation. It is based on the functional integral method in which the degrees of freedom of a quantum field theory are variables of integration. The main idea is to work with cutoff regularisation and integrate out 'highly fluctuating field modes'.

For our introductory purposes, we shall work with a scalar ϕ^4 theory. Wilson's approach can be applied to other QFTs too as long as one respects all symmetries within the cutoff regularisation scheme. The generating functional in some d dimensional Minkowski spacetime is given by

$$Z[J] = \int \mathcal{D}\phi e^{i\int(\mathcal{L}+J\phi)} = \prod_k \left(\int d\phi(k) \right) e^{i\int(\mathcal{L}+J\phi)}, \quad (2.104)$$

where ϕ is the scalar field, \mathcal{L} is its Lagrangian density, J is the source term, and \mathcal{D} marks the functional integral measure defined as above. In order to sensibly talk about 'highly fluctuating field modes' i.e. field modes with 'high momenta', we need to perform a Wick rotation and formulate the field theory rather in euclidean spacetime:

$$t \rightarrow it \quad (2.105)$$

$$i \int \mathcal{L} \rightarrow - \int \mathcal{L}_E \quad (2.106)$$

In the following, we will drop the subscript E on all euclidean variables for conciseness of notation.

For simplicity, let us set the source field to $J = 0$. Then the generating functional reads as

$$Z[J] = \int [\mathcal{D}\phi]_{\Lambda} \exp \left\{ - \int d^d x \left(\frac{1}{2} (\partial_{\mu}\phi)^2 + \frac{1}{2} m_0^2 \phi^2 + \frac{\lambda_0}{4!} \phi^4 \right) \right\}, \quad (2.107)$$

$$[\mathcal{D}\phi]_{\Lambda} = \prod_{|k| < \Lambda} d\phi(k), \quad (2.108)$$

where we made the Lagrangian \mathcal{L} explicit, in which m_0 and λ_0 are the bare (unrenormalised) mass and coupling constant, respectively. In the Wilsonian approach of momentum shell-wise integration of the functional integral, momentum modes of the field are divided in two: The variable $\tilde{\phi}(k)$ shall be only non-vanishing iff $b\Lambda \leq |k| < \Lambda$ while the variable $\phi(k)$ (with a slight abuse of notation) shall be only non-vanishing iff $|k| < b\Lambda$. Our aim is to integrate out the highly fluctuating degrees of freedom. Hence, we split the Lagrangian as

$$Z = \int [\mathcal{D}\phi]_{b\Lambda} \mathcal{D}\tilde{\phi} \exp \left\{ - \int d^d x \left[\frac{1}{2} (\partial_\mu \phi + \partial_\mu \tilde{\phi})^2 + \frac{m^2}{2} (\phi + \tilde{\phi})^2 + \frac{\lambda}{4!} (\phi + \tilde{\phi})^4 \right] \right\} \quad (2.109)$$

$$= \int [\mathcal{D}\phi]_{b\Lambda} e^{-\int \mathcal{L}(\phi)} \int \mathcal{D}\tilde{\phi} \exp \left\{ - \int d^d x \left[\frac{1}{2} (\partial_\mu \tilde{\phi})^2 + \frac{m^2}{2} \tilde{\phi}^2 + \lambda \left(\frac{1}{6} \phi^3 \tilde{\phi} + \frac{1}{4} \phi^2 \tilde{\phi}^2 + \frac{1}{6} \phi \tilde{\phi}^3 + \frac{1}{4!} \tilde{\phi}^4 \right) \right] \right\} \quad (2.110)$$

The product $\phi\tilde{\phi}$ vanishes identically in this expression.

We learn that integrating over the high momentum modes $\tilde{\phi}$ is equivalent to the addition of ‘correctional’ terms proportional to powers of λ to the ‘standard’ Lagrangian $\mathcal{L}(\phi)$:

$$Z = \int [\mathcal{D}\phi]_{b\Lambda} \exp \left\{ - \int d^d x \mathcal{L}_{\text{eff}} \right\} \quad (2.111)$$

$$= \int [\mathcal{D}\phi]_{b\Lambda} \exp \left\{ - \int d^d x \left(\underbrace{\frac{1}{2} (\partial_\mu \phi)^2 + \frac{1}{2} m^2 \phi^2 + \frac{\lambda}{4!} \phi^4}_{\mathcal{L}_{\text{std.}}(\phi)} + \underbrace{\mathcal{O}(\lambda) + \mathcal{O}(\lambda^2) + \dots}_{\text{‘corrections’}} \right) \right\} \quad (2.112)$$

To this end, we will analyse this theory perturbatively in a Feynman diagram approach. Since we are interested in the case of $m^2 \ll \Lambda^2$, we will not only treat the terms proportional to λ as a perturbation but also the mass term.

Thus, the free theory of the high momentum modes $\tilde{\phi}$ is trivially solved by computing the propagator $\overline{\tilde{\phi}(k)\tilde{\phi}(p)}$:

$$\int \mathcal{L}_0(\tilde{\phi}) = \frac{1}{2} \int_{b\Lambda \leq |k| < \Lambda} \frac{d^d k}{(2\pi)^d} \tilde{\phi}^*(k) k^2 \tilde{\phi}(k), \quad (2.113)$$

$$\Rightarrow \frac{\int \mathcal{D}\tilde{\phi} \tilde{\phi}^*(k)\tilde{\phi}(p) e^{-S_0[\tilde{\phi}]}}{\int \mathcal{D}\tilde{\phi} e^{-S_0[\tilde{\phi}]}} =: \overline{\tilde{\phi}(k)\tilde{\phi}(p)} = \frac{1}{k^2} (2\pi)^d \delta^{(d)}(k-p) \Theta(k), \quad (2.114)$$

$$\text{where } \Theta(k) = \begin{cases} 1 & \text{if } b\Lambda \leq |k| < \Lambda \\ 0 & \text{otherwise} \end{cases} \quad (2.115)$$

Subsequently, we will follow the standard procedure by substituting every field $\tilde{\phi}$ in the interaction terms by its corresponding functional derivative $\frac{\delta}{\delta \tilde{j}}$ and expand the exponential. This follows closely usual perturbation theory. However, we only allow for low momentum modes ϕ to be external states and $\tilde{\phi}$ fields must be contracted internally, i.e. the propagator $\overline{\tilde{\phi}(k)\tilde{\phi}(p)}$ only occurs as an internal propagator.

First, we shall inspect the $\mathcal{O}(\lambda)$ contribution of the ‘correctional’ terms in (2.110). One of the terms might be

$$-\int d^d x \frac{\lambda}{4} \phi^2 \overline{\tilde{\phi}} \tilde{\phi} = -\frac{1}{2} \int d^d k \mu \phi^*(k) \phi(k), \quad (2.116)$$

where μ consists of the contraction $\overline{\tilde{\phi}(k)} \tilde{\phi}(p)$ and some numerical factors to suite above equation. This term looks just like a correction to the mass at $\mathcal{O}(\lambda)$. We will inspect further contribution from this perturbation series diagrammatically. The propagator of the highly fluctuating field $\tilde{\phi}$ shall be denoted in a dotted line while the propagator of the lower momentum modes by a straight line. Then, Equation 2.116 can be expressed by

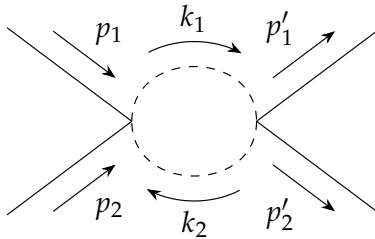


$$(2.117)$$

At $\mathcal{O}(\lambda^2)$ we will find, among others, these diagrams



$$(2.118)$$



$$=: -\frac{1}{4!} \int d^d k_1 \xi \phi^4. \quad (2.119)$$

Let us now inspect the contribution of Equation 2.119:

$$\xi \sim \frac{1}{k_1^2} \frac{1}{k_2^2} \quad (2.120)$$

$$= \frac{1}{k_1^2} \frac{1}{(p_1 + p_2 - k_1)^2} \quad (2.121)$$

We can now expand the second fraction in Equation 2.121 because we said earlier the momentum modes of $\tilde{\phi}(k_i)$ are larger than the momentum modes of $\phi(p_i)$.

$$\xi \sim \frac{1}{k_1^4} \left(1 + 2 \frac{p_1 + p_2}{k_1} + 3 \left(\frac{p_1 + p_2}{k_1} \right)^2 + 4 \left(\frac{p_1 + p_2}{k_1} \right)^3 + \dots \right) \quad (2.122)$$

Together with Equation 2.119 the first term of this series expansion in Equation 2.122 will yield a term only containing four powers of the field ϕ . It takes the form of a correction to the interaction. The higher terms of the series in Equation 2.122 will yield an operator containing derivatives acting on the fields ϕ .

In general one can deduce from this sketch that integrating out $\tilde{\phi}$ will generate *all possible* interactions of the fields ϕ and their derivatives which respect the original

symmetries of the theory. This integration generated also disconnected diagrams as seen in [Equation 2.118](#). With a standard combinatoric argument in QFT we can rewrite the sum of all diagrams as the exponential of all connected diagrams. Hence, we can conclude schematically

$$\mathcal{L}_{\text{eff}} = \frac{1}{2}(\partial_\mu\phi)^2 + \frac{1}{2}m^2\phi^2 + \frac{\lambda}{4!}\phi^4 + \{\text{sum of all connected diagrams}\}. \quad (2.123)$$

The contributions of all connected diagrams includes corrections to m^2 , like [Equation 2.116](#), and λ , like the first term of [Equation 2.122](#), as well as higher-dimensional operators. One might now go ahead and use the new Lagrangian \mathcal{L}_{eff} to compute observables like correlation functions. Any loop integral would be finite and only include modes up to $b\Lambda$ instead of the original cutoff Λ . The correction terms in \mathcal{L}_{eff} precisely compensate for this change.

2.4.2 Renormalisation Group Flows [1]

In the last section we left things at the effective Lagrangian \mathcal{L}_{eff} in which the momentum modes reach only $b\Lambda$ – unlike the Lagrangian we started with (there we allowed for momenta up to Λ). Now, we shall compare these two Lagrangians more thoughtfully. To this end, we will rescale momenta and lengths such that it appears we allowed for momenta up to the cutoff again:

$$k' = k/b \quad x' = xb. \quad (2.124)$$

As we have seen, the new addends in the effective action can be seen as correctional terms to the existing ones as well as entirely new terms. We will appreciate both thoughts in noting

$$\int d^d x \mathcal{L}_{\text{eff}} = \int d^d x \left[\frac{1}{2}(1 + \Delta Z)(\partial_\mu\phi)^2 + \frac{1}{2}(m^2 + \Delta m^2)\phi^2 + \frac{1}{4!}(\lambda + \Delta\lambda)\phi^4 + \Delta C(\partial_\mu)^4 + \Delta D\phi^6 + \dots \right] \quad (2.125)$$

$$= \int d^d x' b^{-d} \left[\frac{1}{2}(1 + \Delta Z)b^2(\partial_\mu\phi)^2 + \frac{1}{2}(m^2 + \Delta m^2)\phi^2 + \frac{1}{4!}(\lambda + \Delta\lambda)\phi^4 + \Delta C b^4(\partial_\mu)^4 + \Delta D\phi^6 + \dots \right]. \quad (2.126)$$

From this Lagrangian we could get the same free propagator as in [Equation 2.114](#) if we rescaled the field

$$\phi' = \left(b^{2-d}(1 - \Delta Z) \right)^{1/2} \phi. \quad (2.127)$$

NB: This is only sensible as long as we can treat all but the kinetic term as small perturbations. Hence, we need the couplings to be small, near the free theory. Then the corrections Δm^2 , $\Delta\lambda$, et cetera, originate from high orders of perturbation theory and thereby are small compared to leading order.

However, once we rescaled the field appropriately, the free theory looks the same as before. Yet, the interaction couplings have transformed:

$$\int d^d x \mathcal{L}_{\text{eff}} = \int d^d x \left[\frac{1}{2} (\partial_{\mu'} \phi')^2 + \frac{1}{2} m'^2 \phi'^2 + \frac{1}{4!} \lambda' \phi'^4 + C' (\partial_{\mu})^4 + D' \phi'^6 + \dots \right] \quad (2.128)$$

with

$$\begin{aligned} m'^2 &= (m^2 + \Delta m^2)(1 + \Delta Z)^{-1} b^{-2}, \\ \lambda' &= (\lambda + \Delta \lambda)(1 + \Delta Z)^{-2} b^{d-4}, \\ C' &= (C + \Delta C)(1 + \Delta Z)^{-2} b^d, \\ D' &= (D + \Delta D)(1 + \Delta Z)^{-3} b^{2d-6}. \end{aligned} \quad (2.129)$$

By successive application of this momentum shell-wise integration while in every step the fraction b is chosen infinitesimally close to 1, we can make the transformation of the coefficients in the effective Lagrangian (cf. Equation 2.129) continuous. This flow is referred to as the *renormalisation group flow* albeit this operation is *not invertible* implying this is truly not a group.

Suppose you wish to compute a correlation function of fields with momenta p_i much smaller than the cutoff. You might either use the original Lagrangian \mathcal{L} or the effective Lagrangian \mathcal{L}_{eff} one obtains when following the renormalisation group flow to momenta of the order of p_i . Both must yield the same results. However, in the former one encounters the effects of high momentum modes *only* when computing loop diagrams. In the later those effects have been absorbed in the new coupling constants. Renormalisation should then be viewed as a flow in the space of all possible coefficients which define a specific Lagrangian.

The simplest starting point to consider in the space of all possible Lagrangians is $0 = m = \lambda = C = D = \dots$, the free field Lagrangian $\mathcal{L}_0 = \frac{1}{2} (\partial_{\mu} \phi)^2$. By construction, the transformation laws we defined above leave \mathcal{L}_0 unchanged. Whenever this occurs, we speak of a *fixed point* of the renormalisation group transformation. As the free action is quadratic in the fields we call it the Gaussian fixed point. Here, the functional integral can be computed analytically.

In some neighbourhood of \mathcal{L}_0 we may approximate the effects of renormalisation by only keeping terms linear in λ in the transformation laws from (2.129). This simplifies them to

$$\begin{aligned} m'^2 &= m^2 b^{-2}, \\ \lambda' &= \lambda b^{d-4}, \\ C' &= C b^d, \\ D' &= D b^{2d-6}. \end{aligned} \quad (2.130)$$

Moreover, a general operator in d spacetime dimension containing N powers of a fermionic / bosonic field and P derivatives has canonical mass dimension

$$[O] = \begin{cases} N(\frac{d-2}{2}) + P & \text{scalar field} \\ N(\frac{d-1}{2}) + P & \text{fermionic field} \end{cases}, \quad (2.131)$$

and its corresponding coefficient transform like

$$C' = \begin{cases} b^{N(\frac{d-2}{2})+P-d}C & \text{scalar field} \\ b^{N(\frac{d-1}{2})+P-d}C & \text{fermionic field} \end{cases}. \quad (2.132)$$

Notice the exponent is precisely the mass dimension of the operator minus spacetime dimensions.

Successive application of the transformation law [Equation 2.132](#) down to a momentum scale accessible in an experiment will cause some coefficients to become vanishingly small. Conventionally, one speaks of those additional operators in \mathcal{L}_{eff} as perturbation to \mathcal{L}_0 and we group them according to the behaviour of their coupling constants:

Operators for which the coupling decreases by successive application of the transformation laws [\(2.132\)](#) are called *irrelevant*. Coupling constants which transform under [\(2.132\)](#) to a larger value correspond to *relevant* operators. Lastly, operators are called *marginal* when the value of their coupling constant does not change under [\(2.132\)](#). To find out whether these grow or decay, one must inspect higher order (quantum) corrections, as we left out terms of $\mathcal{O}(\lambda^2)$ and higher in the transformation laws.

Equivalently, an operator with canonical mass dimension d_i in d spacetime dimensions is relevant if $d_i < d$, irrelevant if $d_i > d$, and marginal if $d_i = d$.

2.4.3 Symanzik improvement programme

In this section we want to draw the connection from the renormalisation group to lattice improvements first discussed by Symanzik in 1979 [\[25\]](#). To this end, we remind ourselves to define a *quantum* field theory, it does not suffice to write down its classical Lagrangian $\mathcal{L}(x)$. One needs to define the functional integral aka. path integral:

$$\int D[\psi]D[\psi^\dagger] e^{i \int d^d x \mathcal{L}(x)}.$$

A valid method of obtaining a mathematically well-defined functional integral is to define the theory on a lattice with physical volume V and lattice spacing a . This procedure naturally introduces a cutoff at the ultraviolet ($\sim \frac{1}{a}$) and the infrared ($\sim \frac{1}{V}$) ends of the momentum spectrum, thus regularising the theory. One then has to take the thermodynamic limit $V \rightarrow \infty$ and the continuum limit $a \rightarrow 0$, respectively. While it is generally believed that finite-size effects concerning the limit $V \rightarrow \infty$ are controllable and observables which do not probe the topological nature of the theory display no trouble making features [\[35\]](#), the limit of taking the lattice spacing very much smaller than any other (physical) scale $a \rightarrow 0$ is in practice often only (too) slowly reached [\[36\]](#). Taking this limit might not always be straightforward.

The goal lattice improvements are aiming for, is to approach this continuum limit faster. To this end, we want to make the UV-cutoff effects explicit, which gives structural insight. At scales much larger than the spacing a , we expect the lattice theory to be effectively continuum-like. At such scales far away from the cutoff, the RG-flow should have renormalised the couplings of all irrelevant operators to zero.

The resulting effective action is conceptually the same as the one from (2.112). One might now expand this effective action in a power series of a [36],

$$S_{\text{eff}} = S_0 + aS_1 + a^2S_2 + \dots, \quad (2.133)$$

$$S_i = \int d^d x g_i(a, V, g_j, \dots) \mathcal{L}_i(x). \quad (2.134)$$

NB: S_0 is the continuum action.

Following our analysis from the previous section, for dimensional reasons all terms of the effective action which go with one power or higher in a must only contain irrelevant operators which respect the symmetries of the theory. Their correction to observables must hence vanish with $a \rightarrow 0$.

However, limited by computational complexity and finite hardware resources, one might find oneself in a situation where the limit of $a \rightarrow 0$ is not yet reached. For instance, in some QFT's the a -dependence in the running of the coupling goes like $a \log(a)$ which only slowly decays to the value of 0 in the limit $a \rightarrow 0$.

Alternatively, on any lattice with finite lattice spacing, we are excluding modes of excitation higher than $\sim \frac{1}{a}$. These highly oscillating modes, however, play an important role in a quantum field theory! As we have seen in Section 2.4.1, they contribute via renormalisation to real physical quantities like particle mass or coupling strength. Thus, we must include the effect of those highly fluctuating field modes on the lower modes [37].

The central idea of lattice improvements is to include lattice representations of the operators constituting $\mathcal{L}_i(x)$ from (2.133) with an appropriate coupling $c_i = -g_i$ such that the corresponding a -dependence gets canceled and the irrelevant operators imitate the renormalisation effect of high momentum modes on low momentum modes.

Now, the obvious question to answer is: What might be the appropriate value of the coupling c_i ? At first, this might seem like a tautologic question; If one exactly computed these couplings, one would have solved the problem of computing the observables in the first place.

Here we pick up the idea of rendering the a -effects explicit and employ lattice and continuum perturbation theory [25, 33, 36]. Knowing the continuum result from (continuum) perturbation theory, we can explicitly compute the a -dependence in lattice perturbation theory and counter the effects order by order in a with including \mathcal{L}_i and appropriate c_i . For this, we restrict ourselves to on-shell quantities and employ the equations of motion to eliminate further degrees of freedom in choosing the c_i . This is often referred to as classical or tree-level improvement. For instance, in consistently including all irrelevant operators respecting the symmetries and with canonical mass dimension $d_1 = d + 1$, which make up \mathcal{L}_1 from (2.133), one can completely remove the $\mathcal{O}(a)$ -dependence of some observable within perturbation theory, as there is no operator left which can affect an observable to $\mathcal{O}(a)$ within perturbation theory.

An important caveat is that this relies on perturbation theory and therefore it is unclear whether this improvement scheme works for strong couplings where perturbation theory does not hold.

Lastly, we want to remark that the involved and intricate quest of emulating the effect of *all* high momentum modes on lower ones is taken on in the approach of so called *perfect actions*. It involves the exact solution of renormalisation group transformations like we looked at in Section 2.4.2, which is known for few special cases. For further reference see e.g. [38, 39].

2.4.4 Canonical Mass Dimension

In the previous section we discussed that in order to improve a QFT we need to explicitly add all operators with mass dimension up to some order.

The canonical mass dimension of an operator O with N powers of a Dirac spinor field ψ and P derivatives in d spatial dimensions is

$$[O] = N\frac{d}{2} + P, \quad (2.135)$$

whereas the mass dimension of the corresponding coupling is given by

$$[O]_g = d + 1 - [O]. \quad (2.136)$$

We established above that irrelevant operators have positive mass dimension (while the coupling constant has negative), relevant operators have negative mass dimension, and marginal operators have zero mass dimension.

Since we are investigating the physics of QED in $1 + 1d$, we list the mass dimension of several couplings corresponding to different operators in $1 + 1d$ QED, where d is the spatial dimension:

$$[\bar{\psi}\psi]_g = -2\frac{d}{2} + d + 1 = +1, \quad (2.137)$$

$$\left[(\bar{\psi}\gamma_\mu\psi)^2\right]_g = -4\frac{d}{2} + d + 1 = d - 2 = 0, \quad (2.138)$$

$$\left[(\bar{\psi}\psi)^3\right]_g = -6\frac{d}{2} + d + 1 = 2d - 3 = -1, \quad (2.139)$$

$$\left[\bar{\psi}\mathcal{D}^2\psi\right]_g = -2\frac{d}{2} - 2 + d + 1 = -1, \quad (2.140)$$

$$\left[(\bar{\psi}\gamma_\mu\psi)^4\right]_g = -8\frac{d}{2} + d + 1 = 3d - 4 = -2, \quad (2.141)$$

$$\left[\bar{\psi}\mathcal{D}^3\psi\right]_g = -2\frac{d}{2} - 3 + d + 1 = -2, \quad (2.142)$$

$$\left[(\bar{\psi}\mathcal{D}\psi)^2\right]_g = -4\frac{d}{2} - 2 + d + 1 = -2 \quad (2.143)$$

$$\left[(\bar{\psi}D_\mu\psi)^2\right]_g = -4\frac{d}{2} - 2 + d + 1 = -2. \quad (2.144)$$

In order to improve the Hamiltonian of $1 + 1d$ QED and remove *all* lattice artefacts to $\mathcal{O}(a)$ we would naively assume to include the derivative term from Equation (2.140) as well as the cubic interaction term from Equation (2.139). However, we will not include a lattice representation of those operators in our theory, as we are considering staggered fermions which obey in $1 + 1d$ the axial symmetry. Those two operators would explicitly break this symmetry. This is reflected in our earlier finding in Section 2.3, that staggered fermions can only implement uneven lattice hopping terms. Moreover, it is consistent with our finding that staggered fermions are accurate up to $\mathcal{O}(a^2)$ and operators of canonical mass dimension 1 need not to be considered. Consequently, we are only to include the third derivative from (2.142), the Thirring-like interaction term from (2.141) as well as the squared first derivatives in (2.144) and (2.144), respectively.

Introducing new interaction terms into our theory requires us to perform lattice perturbation theory, in order to obtain an on-shell result on the lattice, as well as perturbation theory in the continuum to have a referencing result, with which we must check against, in order to determine the improvement coefficients c_i . This process is somewhat more involved and we will not pursue this in the framework of this thesis.

Henceforth, we will only introduce higher-order derivatives as irrelevant operators to improve our lattice theory.

In this framework we are limiting ourselves on a ‘subspace’ of what improvements might be able to offer. Now, it is only the free theory which we can be sure of is freed from *all* $\mathcal{O}(a^2)$ lattice artefacts. Coming from the free theory, we are promoting the derivatives to covariant derivatives. The RG flow for the interacting theory will generate more than derivatives terms, as we have already seen from [Section 2.4.2](#). In the limit of small couplings, i.e. in the neighbourhood of the Gaussian Fixed Point, we assume the results for the free theory to still be applicable to the interacting theory.

By introducing only irrelevant kinetic operators in $1 + 1d$ – in the context of high momentum modes affecting lower ones via renormalisation – we are neither fully capturing the effect of *all* of them on to the lower modes, nor do we include consistently irrelevant operators to a given order in a .

On the other hand, introducing only higher derivative terms can give an intuition of what improvements are providing; namely correcting the dispersion relation on the lattice to be accurate up to higher orders in a . This will be discussed in the next section.

As we will see later, in the interacting case after promoting the $U(1)$ symmetry to a gauge symmetry and promoting the derivative to a covariant derivative, we find that improving the kinetic terms of the Hamiltonian yields an improvement in the kinetic observables like the current.

2.4.5 Improvement coefficients

In this section we want to familiarise ourselves with improvements. To this end we will show, using the example of the (free) energy dispersion relation, that improvements reduce the lattice artefacts of some observable. The energy dispersion relation offers a very intuitive picture of what improvements can provide.

The above mentioned demonstration will be performed in the Hamiltonian framework of lattice gauge theories. As explained in [Section 2.4.3](#), Symanzik’s improvement programme is formulated in the functional integral approach to lattice QFT, where the degrees of freedom are *classical* variables of integration. Luo *et al.* argue one can expand this programme to the Hamiltonian approach in which the classical degrees of freedom are quantised according to canonical quantisation [40]. They demonstrate the *classically improved quantum Hamiltonian* has formally reduced $\mathcal{O}(a)$ dependence and can in fact be obtained in two different ways. First, one might obtain the classical improved Hamiltonian via Legendre transform from the classically improved action, and then canonically quantise it. Or equivalently, one might start with the (unimproved) classical action, construct the quantum Hamiltonian via the transfer matrix and then add appropriate operators to reduce the $\mathcal{O}(a)$ -dependence [40].

We shall consider the Hamiltonian in temporal axial gauge

$$\begin{aligned}
H_{\text{lat}} = & m \sum_{n=0}^{2N-1} (-1)^n \psi_n^\dagger \psi_n + \frac{a}{2} \sum_{n=0}^{2N-1} E_n^2 \\
& - c_1 \frac{i}{2a} \sum_{n=0}^{2N-2} [\psi_n^\dagger U_n \psi_{n+1} - \text{h.c.}] \\
& - c_3 \frac{i}{2a} \sum_{n=0}^{2N-4} [\psi_n^\dagger U_n U_{n+1} U_{n+2} \psi_{n+3} - \text{h.c.}], \tag{2.145}
\end{aligned}$$

where a is the (spatial) lattice spacing, ψ_n denotes the discretised version of the spinor field, U_n is the link variable which relates to the gauge field like $U_n = \exp\{ieaA_n\}$, c_1 and c_3 are the improvement coefficients corresponding to the first and third derivative of the fermion field ψ , respectively.

The choice of $c_1 = 9/8$, $c_3 = -1/24$, as Naik proposed [41], is the on-shell improvement up to $\mathcal{O}(a^4)$. To see this, let us take (2.145) in the limit of $e = 0$, i.e. the free theory. Then, we can diagonalise H_{lat} explicitly, read off the dispersion relation, and observe an $\mathcal{O}(a^4)$ improvement, as we will show now. Defining the Fourier transform as

$$\psi_n = \frac{1}{\sqrt{2N}} \sum_q e^{i\pi q n / N} \tilde{\psi}_q, \tag{2.146}$$

$$\tilde{\psi}_q = \frac{1}{\sqrt{2N}} \sum_n e^{-i\pi q n / N} \psi_n, \tag{2.147}$$

and taking $e = 0$, we find [42]

$$H_{\text{free}} = \sum_{q=0}^{N-1} \begin{pmatrix} \tilde{\psi}_q^\dagger & \tilde{\psi}_{q+N}^\dagger \end{pmatrix} \begin{pmatrix} \pi(q) & m \\ m & -\pi(q) \end{pmatrix} \begin{pmatrix} \tilde{\psi}_q \\ \tilde{\psi}_{q+N} \end{pmatrix}, \tag{2.148}$$

$$\text{with } \pi(q) = \frac{1}{a} (c_1 \sin(\pi q / N) + c_3 \sin(3\pi q / N)) \tag{2.149}$$

$$= \frac{1}{a} (c_1 \sin(ka) + c_3 \sin(3ka)). \tag{2.150}$$

The eigenvalues of H_{free} are

$$\pm\omega(q) = \pm\omega_q = \pm\sqrt{m^2 + \pi^2(q)} \tag{2.151}$$

and the eigenvectors read as

$$v^+(q, m) = [2\omega_q(\omega_q - \pi_q)]^{-\frac{1}{2}} \begin{pmatrix} m \\ \omega_q - \pi_q \end{pmatrix} \tag{2.152}$$

$$v^-(q, m) = [2\omega_q(\omega_q + \pi_q)]^{-\frac{1}{2}} \begin{pmatrix} -m \\ \omega_q + \pi_q \end{pmatrix}. \tag{2.153}$$

Those eigenvectors build up the transformation $S(q) = (v^+(q, m), v^-(q, m))$ under which H_{free} becomes diagonal; and as such they transform the field operators $\tilde{\psi}_q$ and $\tilde{\psi}_{q+N}$ onto the quasi-particle creation and annihilation operators:

$$\begin{pmatrix} a_q \\ b_q^\dagger \end{pmatrix} = S(q)^\dagger \begin{pmatrix} \tilde{\psi}_q \\ \tilde{\psi}_{q+N} \end{pmatrix} \tag{2.154}$$

If one now would like to improve the Hamiltonian to $\mathcal{O}(a^4)$ instead of the regular $\mathcal{O}(a^2)$ of staggered fermions, one can uniquely fix the coefficients c_1 and c_3 by equating coefficients of the series expansion of the lattice momentum π_k to the ‘coefficients’ of the continuum result $\pi_{\text{cont}}(k) = k$

$$\pi(k; a) = \frac{1}{a} (c_1 \sin(ka) + c_3 \sin(3ka)) \quad (2.155)$$

$$= k(c_1 + 3c_3) - \frac{a^2}{6} k^3 (c_1 + 27c_3) + \mathcal{O}(a^4 k^5) \quad (2.156)$$

$$\stackrel{!}{=} k + \mathcal{O}(a^4 k^5) \quad (2.157)$$

The two algebraic equations $c_1 + 3c_3 = 1$, $c_1 + 3^3 c_3 = 0$ uniquely define the coefficients to be $c_1 = 9/8$ and $c_3 = -1/24$.

Consequently, we find the dispersion relation,

$$\omega_k = \sqrt{m^2 + \pi_k^2} = \sqrt{m^2 + k^2} + \mathcal{O}(a^4 k^5), \quad (2.158)$$

to be accurate to $\mathcal{O}(a^4 k^5)$.

Now, suppose we would include a fifth derivative operator, the next highest derivative respecting the symmetries of staggered fermions, in the Hamiltonian. It is easily confirmed this would alter the lattice momentum $\pi(k)$ simply by a new addend $\frac{1}{a} c_5 \sin(5ka)$. In fact, it can be readily generalised upon including n higher derivatives, which all must be uneven as we showed in [Section 2.3](#), the lattice momentum in the free theory takes the form

$$\pi^{(n)}(k) = \frac{1}{a} \sum_{i=0}^n c_{2i+1} \sin((2i+1)ka) \quad (2.159)$$

From this analysis, we can follow a general relation of the improvement coefficients c_i given the improvement order n in the case of the free theory with staggered fermion discretisation. We find the following system of equations which determine the coefficients up to any finite order uniquely:

$$\sum_{i=0}^n c_{2i+1} (2i+1) \stackrel{!}{=} 1, \quad (2.160)$$

$$1 \leq j \leq 2n+1 : \sum_{i=0}^n c_{2i+1} (2i+1)^{2j+1} \stackrel{!}{=} 0. \quad (2.161)$$

In [Table 2.1](#) values of the coefficients up to order three in improvement are displayed.

2.4.6 Quantifying Improvements

In this section we wish to quantify the benefits of improvements. To this end, we want to quantify in some notion how ‘close’ we can get to the continuum dispersion relation upon improving the free theory.

From the explicit expression for the lattice momentum ([2.149](#)) it is evident, that for fixed a_0 one cannot find a factor α such that an improved curve agrees with an unimproved at $a = \alpha a_0$:

$$\forall \alpha : \frac{1}{a_0} \left(\frac{9}{8} \sin(ka_0) - \frac{1}{24} \sin(3ka_0) \right) \neq \frac{1}{\alpha a_0} \sin(k\alpha a_0) \quad (2.162)$$

Order	c_1	c_3	c_5	c_7
0	1	0	0	0
1	$\frac{9}{8}$	$-\frac{1}{24}$	0	0
2	$\frac{75}{64}$	$-\frac{25}{384}$	$\frac{3}{640}$	0
3	$\frac{1225}{1024}$	$-\frac{245}{3072}$	$\frac{49}{5120}$	$-\frac{5}{7168}$

Table 2.1: Improvement Coefficients for the free theory

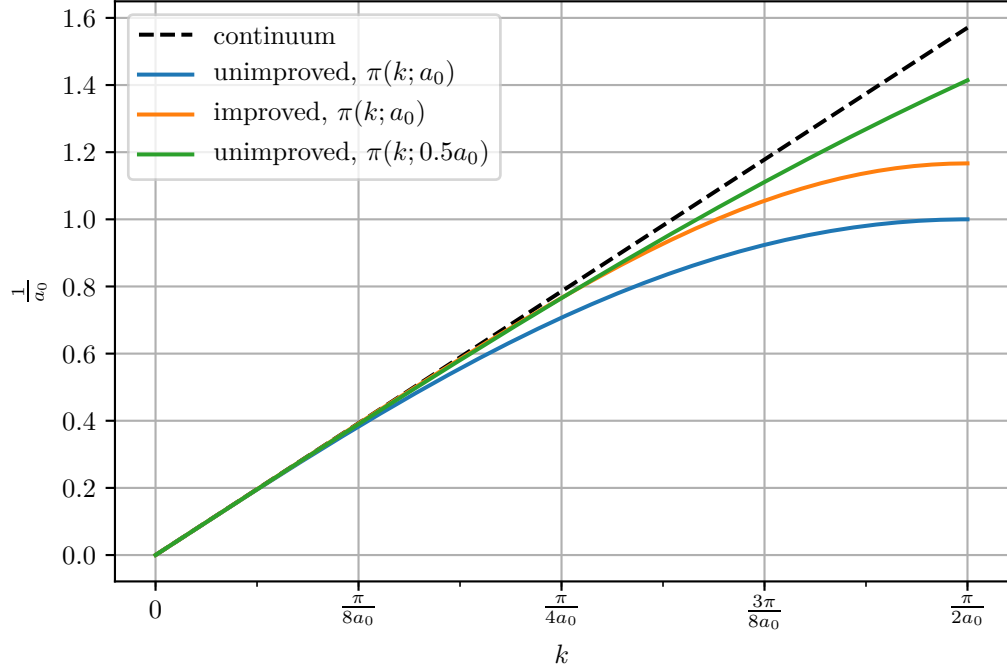


Figure 2.1: Displayed is the unimproved lattice momentum ($\pi^{(0)}(k; a_0)$) in blue, the first order improved lattice momentum in orange ($\pi^{(1)}(k; a_0)$), and the unimproved lattice momentum with half the lattice spacing w.r.t. the previous a_0 ($\pi^{(0)}(k; 0.5a_0)$). All plotted in the positive half of the Brillouin Zone (BZ). $\pi^{(1)}(k; a_0)$ follows the continuum dispersion more closely over a longer interval in BZ than $\pi^{(0)}(k; a_0)$. However, $\pi^{(0)}(k; 0.5a_0)$ is still the most advantageous when it comes to describing more accurately the momentum in the same physical momentum range.

However, one might find a rather good agreement in e.g. the interval $\left[-\frac{\pi}{4a_0}, \frac{\pi}{4a_0}\right]$. The factor α , where the improved curve and the unimproved curve coincide most closely, may then give a hint of what improvements quantitatively yield. Figure 2.1 displays such a relation of the unimproved curve with a_0 , the improved curve with a_0 , and an unimproved curve with $a = 0.5a_0$, which yields good quantitative agreement over the interval $\left[0, \frac{\pi}{4a_0}\right]$.

For further analysis, we defined a figure of merit by the following protocol: Given a small δ and starting at $k = 0$, at which k does one find a deviation of the given dispersion curve from the continuum curve which is equal or greater than δ ? This Figure of Merit is displayed in Figure 2.2. Here, we can see, just as in Figure 2.1, at

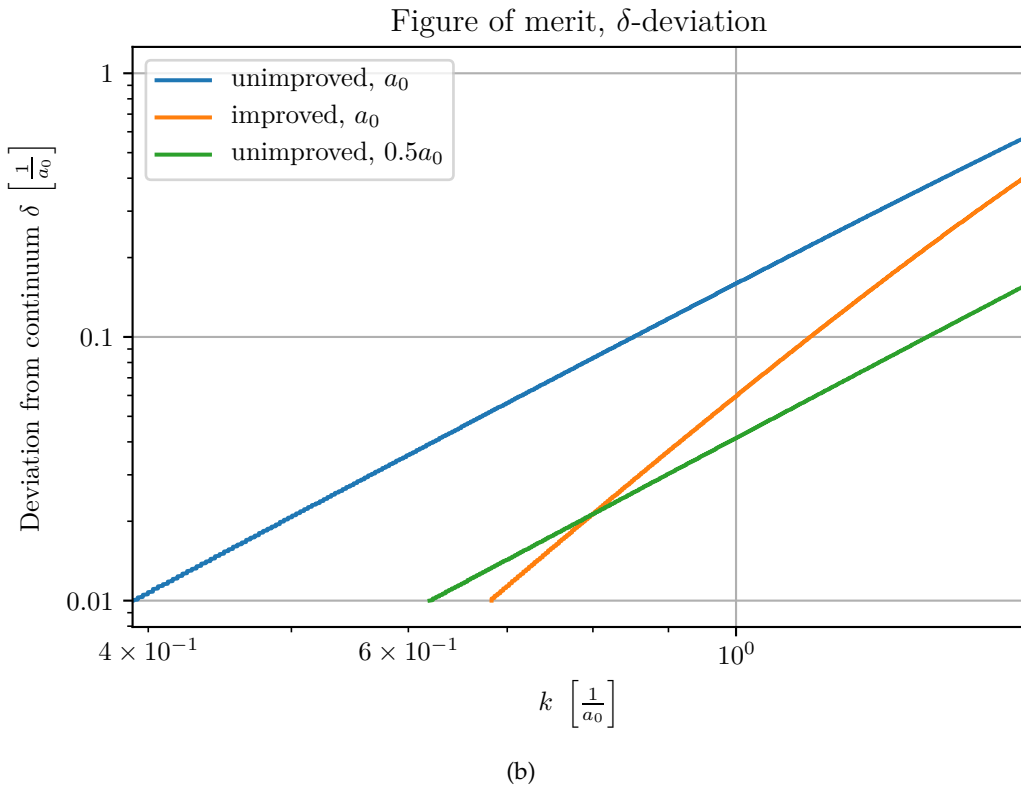
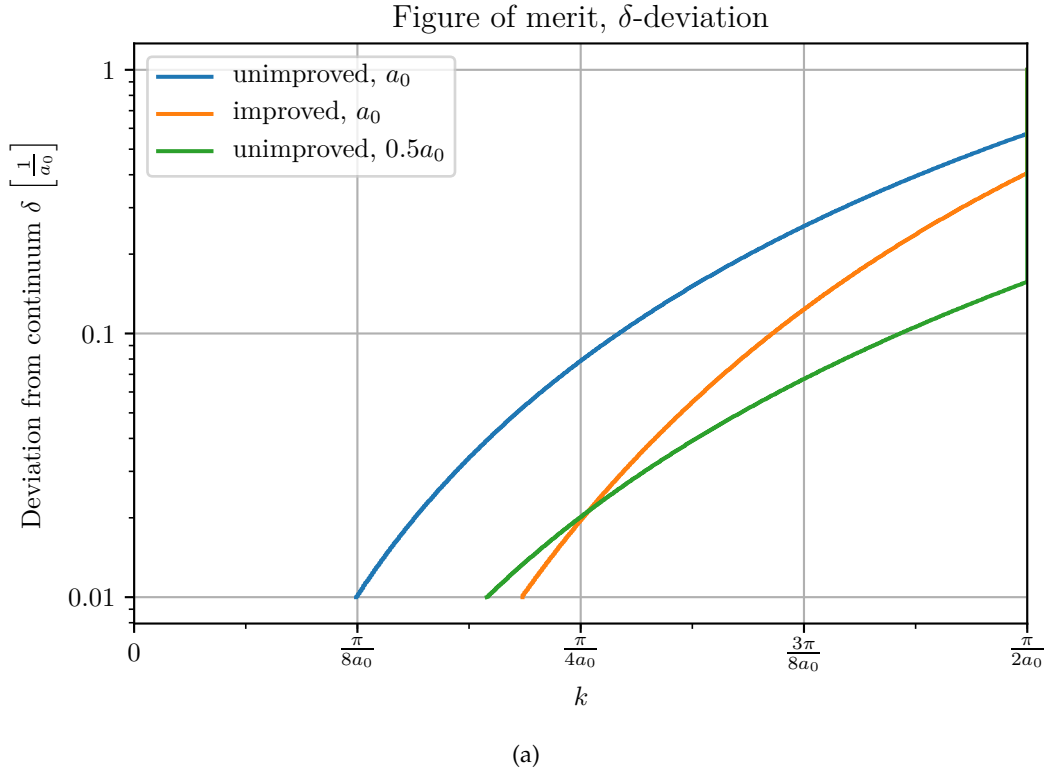


Figure 2.2: Figure of merit δ -deviation from the continuum: Given a small δ and starting at $k = 0$ when is it, that the respective lattice momentum deviates from the continuum with more than δ ? (a) lin-log plot over the positive half BZ, (b) log-log plot over the positive half BZ. We observe for an error margin of a few per cent an increase in accuracy by a factor of around 1.5.

equal a_0 the improved curve gives better agreement with the continuum as opposed to the unimproved curve. From Figure [Figure 2.2b](#) we can clearly see that the unimproved curves are parallel while the improved curve has a higher slope. Upon increasing $\alpha \rightarrow 1$ one would move the improved curve towards the unimproved curve, and vice versa.

In a regime of the order of 0.1%–2% deviation from the continuum, the improved curve yields the best results of those three curves. Beyond this, the unimproved curve with half the lattice spacing performs best with regards to this figure of merit. Consequently, if one was to restrict oneself to an error on the lattice momentum of only 0.1%–2%, only then the improved curve would surpass the unimproved one with half the lattice spacing. However, the self-restricted momentum range would then only cover half the Brillouin zone. This forgoes important numerical resources which ought not to be wasted. In comparison, if one was to allow an error of a few per cent, the best curve would be the unimproved curve with half the lattice spacing, as it follows the continuum dispersion more closely over a larger range of k . Nevertheless, the improved curve yields better performance over the improved curve given same lattice spacing. If one allows for a few per cent error margin from the continuum, we read off from [Figure 2.2](#) a good coverage in the Brillouin zone of about 1.5 larger compared to the unimproved curve. This is also evident from [Figure 2.1](#).

Therefore, we conclude that improving the lattice momentum yields very good agreement with the continuum over a little more than half the Brillouin zone (cf. [Figure 2.1](#)). However, the improvements do not change the lattice cutoff at the Brillouin zone boundary $\sim \frac{1}{a}$, and consequently, for high momenta they cannot compete against a truly reduced αa_0 .

It shall be noted, that the Schwinger effect, which we will use to benchmark our results, indeed produces particles at $p = 0$. For low momenta, as we already discussed, the improved curve has a better accuracy over the unimproved curve by some per cent points. Hence, we may be able to observe some better accuracy of the particle production rate with improved Hamiltonians, as the high momentum accuracy is not of great importance for particle production.

Lastly, we want to summarise our findings in this section by remarking that whether and how much improvements are beneficial depends on the phenomena of interest, whether it probes only low momenta or also high momenta towards the boundary of the Brillouin zone.

2.5 SCHWINGER MECHANISM IN A CONSTANT, HOMOGENEOUS ELECTRIC FIELD

In this section we wish to expand the foundations we laid in the previous section and apply those insights to the ‘interacting’ theory in the limit of a strong, constant, and homogeneous electric field. In this limit the link variables $U_n = U = e^{iaeEt}$ are treated classically. We will show the results from [Section 2.4.5](#) still hold and the improvement coefficients can be taken from the free theory. Finally, we want to present some numerical results from Classical Statistical Simulations, to give some intuition in how the Schwinger effect works with a constant field.

2.5.1 Particle Number definition

The Hamiltonian [\(2.145\)](#) with the approximation $U_n = U = e^{iaeEt}$ can then be written as [\[20\]](#)

$$\begin{aligned}
 H_{\text{lat}} &= m \sum_{n=0}^{2N-1} (-1)^n \psi_n^\dagger \psi_n + \frac{e^2 a}{2} \sum_{n=0}^{2N-1} L_n^2 \\
 &\quad - \frac{i}{2a} \sum_{n=0}^{2N-2} \left[c_1 \psi_n^\dagger e^{iaeEt} \psi_{n+1} - \text{h.c.} \right] \\
 &\quad - \frac{i}{2a} \sum_{n=0}^{2N-4} \left[c_3 \psi_n^\dagger e^{i3aeEt} \psi_{n+3} - \text{h.c.} \right], \tag{2.163}
 \end{aligned}$$

$$= \sum_{q=0}^{N-1} \begin{pmatrix} \tilde{\psi}_q^\dagger & \tilde{\psi}_{q+N}^\dagger \end{pmatrix} \begin{pmatrix} \pi(q) & m \\ m & -\pi(q) \end{pmatrix} \begin{pmatrix} \tilde{\psi}_q \\ \tilde{\psi}_{q+N} \end{pmatrix}, \tag{2.164}$$

with

$$\pi(q) = \frac{1}{a} \left[c_1 \sin\left(\frac{\pi q}{N} + aeEt\right) + c_3 \sin\left(3\left(\frac{\pi q}{N} + aeEt\right)\right) \right] \tag{2.165}$$

$$= \frac{1}{a} \left[c_1 \sin(a(k + eEt)) + c_3 \sin(3a(k + eEt)) \right]. \tag{2.166}$$

Energy will not be conserved as the Hamiltonian is explicitly time dependent. It is important to stress that the function π_q from [\(2.165\)](#) is not the same as in [\(2.149\)](#). In fact, the physical momentum from the previous section is generalised to the canonical momentum

$$k \longrightarrow k + eEt, \tag{2.167}$$

corresponding to

$$\partial \longrightarrow \partial + eA(t), \tag{2.168}$$

in the limit of $E = \partial_t A = \text{const.} \Rightarrow A(t) = Et$.

We can still diagonalise the Hamiltonian instantaneously. The derivation is straightforward and follows the diagonalisation of [Section 2.4.5](#), only taking into account the modified version of π_q . We would find for the improvement coefficients exact agreement with the ones from the previous section if we were to demand the continuum result to of the dispersion relation to be $\omega(k) = \sqrt{m^2 + (k + eEt)^2}$.

The Hamiltonian still has eigenvalues $\omega_q = \pm \sqrt{m^2 + \pi_q^2}$, and eigenvectors

$$v^+(q, m) = [2\omega_q(\omega_q - \pi_q)]^{-\frac{1}{2}} \begin{pmatrix} m \\ \omega_q - \pi_q \end{pmatrix} \quad (2.169)$$

$$v^-(q, m) = [2\omega_q(\omega_q + \pi_q)]^{-\frac{1}{2}} \begin{pmatrix} -m \\ \omega_q + \pi_q \end{pmatrix}. \quad (2.170)$$

Again, defining

$$S(q) = (v^+(q, m), v^-(q, m)) \quad (2.171)$$

$$= \begin{pmatrix} \frac{m}{\mathcal{N}_-} & -\frac{m}{\mathcal{N}_+} \\ \frac{\omega_q - \pi_q}{\mathcal{N}_-} & \frac{\omega_q + \pi_q}{\mathcal{N}_+} \end{pmatrix}, \quad (2.172)$$

with

$$\mathcal{N}_\pm = \sqrt{2\omega_q(\omega_q \pm \pi_q)}, \quad (2.173)$$

and

$$\begin{pmatrix} a_q \\ b_q^\dagger \end{pmatrix} = S(q)^\dagger \begin{pmatrix} \tilde{\psi}_q \\ \tilde{\psi}_{q+N} \end{pmatrix}, \quad (2.174)$$

the Hamiltonian becomes diagonal and reads as

$$H = \sum_{q=0}^{N-1} \omega_q (a_q^\dagger a_q + b_q^\dagger b_q - 1). \quad (2.175)$$

Consequently, we define the quasi-particle number density

$$n_q := \langle \Omega | a_q^\dagger a_q + b_q^\dagger b_q | \Omega \rangle, \quad (2.176)$$

as the expectation value of the instantaneous number operator. The state $|\Omega\rangle$ is taken to be the ground state of H with $U_n = 1$, $E_n = 0$.

Furthermore, we may conclude for the energy density

$$\varepsilon_q = \omega_q (n_q - 1), \quad (2.177)$$

$$\text{and } \mathcal{E} = \langle \Omega | H | \Omega \rangle = \sum_{q=0}^{N-1} \omega_q (n_q - 1). \quad (2.178)$$

Utilising the Bogoliubov transform (2.172), we can compute the two contributions to the particle number density n_q as

$$\begin{aligned} \langle \Omega | a_q^\dagger a_q | \Omega \rangle &= \frac{m^2}{2\omega_q(\omega_q - \pi_q)} \langle \Omega | \psi_q^\dagger \psi_q | \Omega \rangle + \frac{\omega_q - \pi_q}{2\omega_q} \langle \Omega | \psi_{q+N}^\dagger \psi_{q+N} | \Omega \rangle \\ &+ \frac{m}{2\omega_q} \left(\langle \Omega | \psi_q^\dagger \psi_{q+N} | \Omega \rangle + \langle \Omega | \psi_{q+N}^\dagger \psi_q | \Omega \rangle \right), \end{aligned} \quad (2.179)$$

and

$$\begin{aligned} \langle \Omega | b_q^\dagger b_q | \Omega \rangle &= \frac{m^2}{2\omega_q(\omega_q + \pi_q)} \langle \Omega | \psi_q \psi_q^\dagger | \Omega \rangle + \frac{\omega_q + \pi_q}{2\omega_q} \langle \Omega | \psi_{q+N} \psi_{q+N}^\dagger | \Omega \rangle \\ &\quad - \frac{m}{2\omega_q} \left(\langle \Omega | \psi_q \psi_{q+N}^\dagger | \Omega \rangle + \langle \Omega | \psi_{q+N} \psi_q^\dagger | \Omega \rangle \right), \end{aligned} \quad (2.180)$$

respectively. With this result and the definition of the statistical propagator

$$\tilde{F}_{q,p} := \langle \Omega | [\tilde{\psi}_q, \tilde{\psi}_p^\dagger] | \Omega \rangle = \frac{1}{2N} \sum_{n,m=0}^{2N-1} e^{-\frac{i\pi}{N}(qn-pm)} F_{n,m} \quad (2.181)$$

at hand, we can formulate the energy density ε_q in terms of F ,

$$\varepsilon_q = \frac{1}{2} \left(\pi_q (\tilde{F}_{q+N,q+N} - \tilde{F}_{q,q}) - m (\tilde{F}_{q+N,q} + \tilde{F}_{q,q+N}) \right). \quad (2.182)$$

Then, the particle number density distribution is given by $n_q = \frac{\varepsilon_q}{\omega_q} + 1$, and the total particle number density by

$$\frac{\mathcal{N}(t)}{Lt} = \frac{1}{Na} \sum_{q=0}^{N-1} n_q. \quad (2.183)$$

NB: This definition of the particle number counts particles as well as anti-particles. Depending on the reference, an appropriate factor of two must be included.

PARTICLE PRODUCTION RATE IN THE CONTINUUM Here, we merely want to cite the particle distribution for late times after a sudden switch-on of the constant electric field in the continuum [43],

$$n_k = \exp\left(-\frac{\pi m^2}{eE}\right) \Theta(k) \Theta(eEt - k). \quad (2.184)$$

For the particle production rate follows [43, 44]

$$\frac{\mathcal{N}(t)}{Lt} = \frac{eE}{2\pi} \exp\left(-\frac{\pi m^2}{eE}\right) = \frac{m^2 E}{\pi E_c} \exp\left(-\frac{\pi E_c}{E}\right), \quad (2.185)$$

with

$$E_c = \frac{m^2}{e}. \quad (2.186)$$

2.5.2 Fermionic Current Operator

The fermion current $j(n)$ can be computed with the help of a Maxwell equation. In $1 + 1d$ Ampère's law reads

$$\text{curl}(B) = 0 = e j + \frac{\partial E}{\partial t}. \quad (2.187)$$

Since $\theta = aeA$ and $L = \frac{E}{e}$ are canonical conjugates of each other, they obey the following commutation relation¹:

$$[L_m, U_n] = [L_m, e^{i\theta_n}] = \delta_{nm} U_n \quad (2.188)$$

¹ This is a corollary of the Baker-Campbell-Hausdorff formula, $e^{sX} Y e^{-sX} = Y + s[X, Y] \Leftrightarrow [e^{sX}, Y] = s[X, Y] e^{sX}$, when $[[X, Y], X] = 0 = [[X, Y], Y]$.

Hence, we obtain

$$\frac{\partial L}{\partial t} = -i[L, H] = -\hat{j}, \quad (2.189)$$

$$\begin{aligned} \hat{j}(n) = \frac{1}{2a} & \left[c_1 \left(\psi_n^\dagger U_n \psi_{n+1} + \text{h.c.} \right) \right. \\ & \left. + c_3 \left(\psi_n^\dagger U_n U_{n+1} U_{n+2} \psi_{n+3} + \psi_{n-1}^\dagger U_{n-1} U_n U_{n+1} \psi_{n+2} + \psi_{n-2}^\dagger U_{n-2} U_{n-1} U_n \psi_{n+1} \right. \right. \\ & \left. \left. + \text{h.c.} \right) \right]. \end{aligned} \quad (2.190)$$

This calculation is straightforward to generalise when including higher order kinetic terms.

2.5.3 Average Current & its improvement

For the average current $\sum_n j(n)$ we can compute in the homogeneous case:

$$\begin{aligned} \frac{1}{2N} \sum_{n=0}^{2N-1} \hat{j}_n &= \frac{1}{2N} \sum_{n=0}^{2N-1} \frac{1}{2a} \frac{1}{2N} \sum_{q,p=0}^{2N-1} \left[c_1 \left(\tilde{\psi}_q^\dagger U \tilde{\psi}_p e^{-\frac{i\pi n}{N}(q-p)} e^{\frac{i\pi p}{N}} + \text{h.c.} \right) \right. \\ & \left. + 3c_3 \left(\tilde{\psi}_q^\dagger U^3 \tilde{\psi}_p e^{-\frac{i\pi n}{N}(q-p)} e^{3i\frac{\pi p}{N}} + \text{h.c.} \right) \right] \end{aligned} \quad (2.191)$$

$$\begin{aligned} &= \frac{1}{2N} \frac{1}{2a} \sum_{q=0}^{N-1} \left[c_1 \left(\left(\tilde{\psi}_q^\dagger \tilde{\psi}_q + e^{i\pi} \tilde{\psi}_{q+N}^\dagger \tilde{\psi}_{q+N} \right) U e^{\frac{i\pi q}{N}} + \text{h.c.} \right) \right. \\ & \left. + 3c_3 \left(\left(\tilde{\psi}_q^\dagger \tilde{\psi}_q + e^{3i\pi} \tilde{\psi}_{q+N}^\dagger \tilde{\psi}_{q+N} \right) U^3 e^{3i\frac{\pi q}{N}} + \text{h.c.} \right) \right] \end{aligned} \quad (2.192)$$

Here, we can substitute $\tilde{\psi}_p$ and $\tilde{\psi}_{p+N}$ according to (2.174) with the quasi particle creation and annihilation operators:

$$\left\langle \tilde{\psi}_q^\dagger \tilde{\psi}_q - \tilde{\psi}_{q+N}^\dagger \tilde{\psi}_{q+N} \right\rangle = \left\langle \frac{m^2}{\mathcal{N}_-^2} a_q^\dagger a_q + \frac{m^2}{\mathcal{N}_+^2} b_q b_q^\dagger - \frac{(\omega_q - \pi_q)^2}{\mathcal{N}_-^2} a_q^\dagger a_q - \frac{(\omega_q + \pi_q)^2}{\mathcal{N}_+^2} b_q b_q^\dagger \right\rangle \quad (2.193)$$

$$= \frac{\pi_q}{\omega_q} \left\langle a_q^\dagger a_q - b_q b_q^\dagger \right\rangle. \quad (2.194)$$

This yields for the expectation value of the average current

$$\frac{1}{2N} \sum_{n=0}^{2N-1} \langle \hat{j}_n \rangle = \frac{1}{2N} \frac{1}{a} \sum_{q=0}^{N-1} \frac{\pi_q}{\omega_q} \left\langle a_q^\dagger a_q - b_q b_q^\dagger \right\rangle \quad (2.195)$$

$$\cdot \left\{ c_1 \cos\left(\frac{\pi q}{N} + aeEt\right) + 3c_3 \cos\left(3\left(\frac{\pi q}{N} + aeEt\right)\right) \right\} \quad (2.196)$$

$$\begin{aligned} &=: \frac{1}{2Na} \sum_{q=0}^{N-1} \frac{\pi_q}{\omega_q} \left\langle a_q^\dagger a_q - b_q b_q^\dagger \right\rangle \mu_q = \frac{1}{2Na} \sum_{q=0}^{N-1} \frac{\pi_q}{\omega_q} (n_q + 1) \mu_q. \end{aligned} \quad (2.197)$$

We defined the function μ_q as

$$\mu_q = c_1 \cos\left(\frac{\pi q}{N} + aeEt\right) + 3c_3 \cos\left(3\left(\frac{\pi q}{N} + aeEt\right)\right), \quad (2.198)$$

which might be written in terms of the physical momentum $k = \frac{\pi q}{Na}$ as

$$\mu_k = c_1 \cos(a(k + eEt)) + 3c_3 \cos(3a(k + eEt)). \quad (2.199)$$

Notice the addend $+1$ in (2.197) may be omitted as

$$\sum_{k=-\pi/(2a)}^{\pi/(2a)} \pi(k) \mu(k) = 0, \quad (2.200)$$

for all orders of improvements. One can see (2.197) confirmed in Figure 2.3b. There, we plotted the averaged current according to (2.197) given the particle number from classical-statistical results as well as the direct measure via the operators from (2.190) and subsequent averaging.

From Section 2.4.5 we know $c_1 = \frac{9}{8}$ and $c_3 = -\frac{1}{24}$, such that we follow

$$\mu_k = 1 + \mathcal{O}(a^4(k + eEt)^4). \quad (2.201)$$

As such, μ_k is in fact accurate to $\mathcal{O}(a^4(k + eEt)^4)$ as opposed to $\mathcal{O}(a^2(k + eEt)^2)$ without the next-to-leading order improvement. This is because we know μ_k approaches 1 in the continuum, as the continuum expression for the time-dependent part of the current for late times reads as² [43]

$$j = \int \frac{dp}{2\pi} v(p) n_p = \int \frac{dp}{\pi} \frac{p}{\omega_k} n_p. \quad (2.202)$$

The previous analysis is valid up to any order in improvement. In fact, one can show that for the system of equations from (2.160)f. μ_k is going to have ever less lattice artefacts just like its counterpart π_k . To see this, consider a given order of improvement n . The function $\mu(k)$ then changes according to,

$$\mu(k) = \sum_{i=0}^{2n+1} (2i+1) c_{2i+1} \cos((2i+1)a(k + eEt)). \quad (2.203)$$

Indeed, demanding for a given order of improvement n

$$\sum_{i=1}^{2n+1} (2i+1) \cdot c_{2i+1} \cos((2i+1) \cdot a(k + eEt)) \stackrel{!}{=} 1 + \mathcal{O}(a^{2n+2}(k + eEt)^{2n+2}) \quad (2.204)$$

gives the exact same conditions for the c_i :

$$\sum_{i=0}^n (2i+1) \cdot c_{2i+1} = 1, \quad (2.205)$$

$$1 \leq j \leq 2n+1 : \sum_{i=0}^n (2i+1)(2i+1)^{2j} \cdot c_{2i+1} = 0. \quad (2.206)$$

Thus, upon including irrelevant kinetic operators to improve the Hamiltonian we are to improve the current as well as the dispersion relation. This confirms our earlier claim improving with kinetic operators yields improvement in kinetic observables.

² We differ from the refs. by a factor of two as Tanji defines $n_p = \langle a_p^\dagger a_p \rangle$ (cf. Equation 2.176). For late times, the time-independent part of the current arises from the sudden switch-on quench. It merely gives an offset to the current at late times, i.e. after the quench.

Crucially, we see from (2.201) that improvement for the current means not only more accuracy in orders of a but also in orders of t ! This is due to promoting $k \rightarrow k + eEt$ in the presence of a constant, homogeneous field. Consequently, we expect the current to be more accurate over a longer period of time.

Reflecting on (2.182) and $n_k = \epsilon_k/\omega_k + 1$, we hope this argument should also extend to the particle number.

CONTINUUM ESTIMATE FOR THE CURRENT Together with (2.184) we can estimate the continuum result of the current for late times to be:

$$j = 2 \int \frac{dk}{2\pi} v n_k = 2 e^{-\frac{\pi m^2}{eE}} \int_0^{eEt} \frac{dk}{2\pi} \frac{k}{\sqrt{m^2 + k^2}} \quad (2.207)$$

$$\stackrel{tm \gg 1}{\simeq} \frac{1}{\pi} e^{-\frac{\pi m^2}{eE}} eEt. \quad (2.208)$$

2.5.4 Periodicity and Cutoff

From the explicit time dependence of the link $U = e^{iaeEt}$ in the Hamiltonian, it becomes evident that the system must obey some periodicity with frequency $\sim aeE$. From the continuum result (2.184) we expect particles to be produced homogeneously in space and at $p = 0$ in the BZ. The constant field will then accelerate the particle pairs in opposite directions respective to their charge. Eventually, these particles will gain so much momentum they run into the lattice cutoff $\frac{\pi}{2a}$. This can be estimated by the continuum expansion rate of the particle distribution in momentum space:

$$eEt_{\max.} \stackrel{!}{=} \frac{\pi}{2a} \quad (2.209)$$

from which we can follow

$$\Leftrightarrow t_{\max.} m = \frac{\pi m^2}{2(am)eE} = \frac{\pi}{2(am)E/E_c} = \frac{\pi N}{2(Lm)} \quad (2.210)$$

This maximal cutoff in time can also be derived from (2.197), as we have, simplifying for

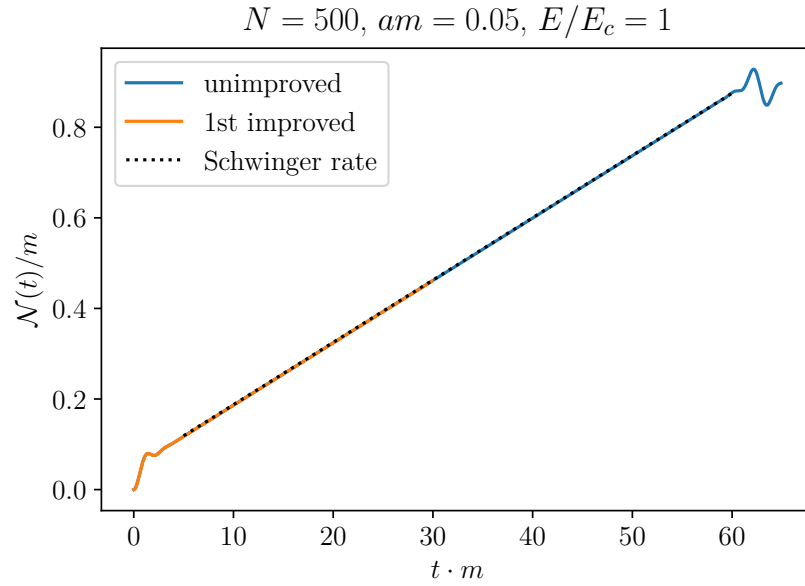
This cutoff in time is inherently programmed into the theory as long as we do not reduce the production rate via back reactions onto the electric field. This effect, however, requires a full quantum treatment of the gauge sector, which we cannot offer within Exact Diagonalisation and periodic boundary conditions. This will become clearer in the next chapter.

Furthermore, the maximum time estimated by (2.210) marks an cutoff for all kinetic observables like the current. When particles overstep the cutoff in the Brillouin zone the lattice recognises them as particles travelling in the opposite direction. At the very latest here, the description of their kinematics must be rendered useless.

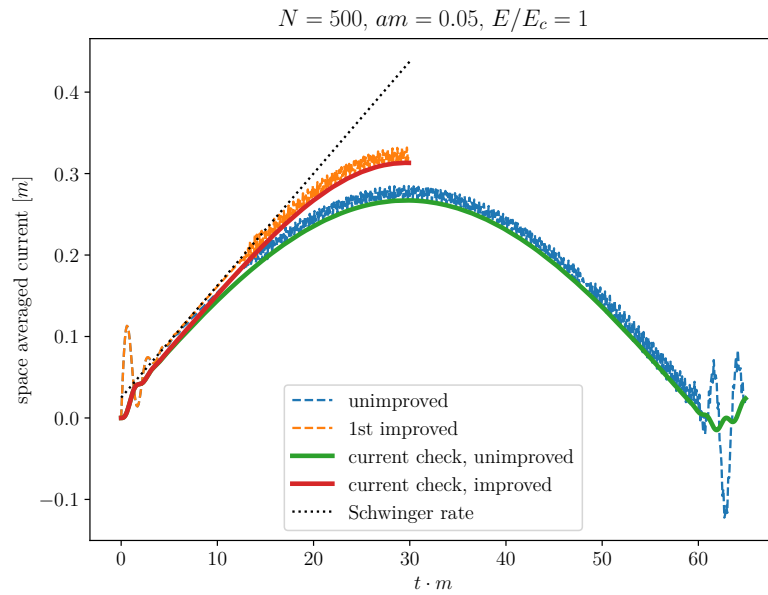
However, the particle number merely counts the number of particles within the Brillouin zone. And as already mentioned, being accelerated over the Brillouin zone edge results only in a misinterpreted momentum. Particles can only 'leave' the BZ via annihilation processes. Since the Schwinger mechanism creates particle pairs at $p = 0$ in the BZ and accelerates them both in the same direction depending on E , annihilation does only happen when the particle distribution is pushed over the BZ edge, comes around at negative momenta and meets itself at $p = 0$. Consequently, the 'cutoff' in time for the particle production rate is given by $2t_{\max.}$

2.5.5 *Illustration*

We wish to illustrate above thoughts with plots from a classical-statistical simulation (without back reaction) in order to facilitate the intuition as to how the Schwinger mechanism works on the lattice in the limit of a constant, homogeneous background field. To this end, we show results of a classical-statistical simulation with $N = 500$, $am = 0.05$ and $E/E_c = 1.0$. We plot the particle production rate and the corresponding current in [Figure 2.3](#) and use [Equation 2.197](#) to infer a second curve for the current, which almost perfectly agrees with the direct measure on the lattice after [\(2.190\)](#) in [\(b\)](#). We demonstrated above that [\(2.197\)](#) is in fact accurate to $\mathcal{O}(a^{2n+2}(k + eEt)^{2n+2})$ for improvement order n . This means particularly, for any finite cutoff we will find the current to be more accurate for longer times comparing improved and unimproved. This is to be observed in [Figure 2.3b](#) as the improved current appears to be more accurate for a 1.5 times longer period of time. This factor in accuracy is reminiscent the previous section at [Figure 2.1](#) and [Figure 2.2](#), respectively, if one allows for a reasonable error margin of a few per cent. However, at such large system sizes and small lattice spacings, the particle production rate already converged in the simulated time scales to its continuum value. Any benefit of improvements are thus unnoticeable. The investigation whether we see such benefits below such large system sizes and small lattice spacings will be discussed in [Chapter 5](#). In [Appendix A](#) one may view the particle number distribution for different times and observe it overstepping the Brillouin zone boundary to reemerge on the other side until it interferes with itself.



(a) Particle Number



(b) Averaged Current

Figure 2.3: Displayed is a single run without any improvement and with first order improvement, respectively. For demonstration we ran the simulation of the unimproved system until $2t_{max}m = 20\pi \simeq 63$, while the improved simulation ran only up to t_{max} . (a) The particle number displays continuum behaviour almost up to $2t_{max}m$. Only then lattice artefacts find their way into the observable. (b) In blue and orange is plotted the space averaged current from the local currents defined by (2.190) for the unimproved and improved system, respectively. We used Equation 2.197 and the particle number from (a) to draw the green and red curves, respectively. They agree almost perfectly; only during the quench we observe a difference. The improved current follows the continuum estimate more closely for a period about 1.5 times larger than for the unimproved current and both currents find their maximum at $t_{max}m$. This confirms Equation 2.197. One can observe at the unimproved current that particles pushed over the BZ edge are being recognised as backwards travelling which counters the growth of the current. For further plots, see Appendix A.

METHODS

In this thesis we employ two methods to investigate the physics of QED in $1 + 1d$. This chapter is dedicated to introducing these two. On the one hand we have Exact Diagonalisation – a long-established method [45, 46] within condensed matter physics / quantum many body physics, and the newly application of the very same to simulating real time dynamics of lattice gauge theories [47, 48]. On the other hand we will investigate the approach to the continuum limit also with Classical Statistical Methods [49], which already served as a benchmark to real time dynamics in the Schwinger Model at strong fields [20, 50, 51].

We implemented both methods such that they simulate the physics of the Schwinger model with Hamiltonian

$$\begin{aligned}
 H = & m \sum_{n=0}^{2N-1} (-1)^n \psi_n^\dagger \psi_n + \frac{a}{2} \sum_{n=0}^{2N-1} E_n^2 \\
 & - \frac{i}{2a} \sum_{n=0}^{2N-1} \left[c_1 \psi_n^\dagger U_n \psi_{n+1} - \text{h.c.} \right] \\
 & - \frac{i}{2a} \sum_{n=0}^{2N-1} \left[c_3 \psi_n^\dagger U_n U_{n+1} U_{n+2} \psi_{n+3} - \text{h.c.} \right] \\
 & - \frac{i}{2a} \sum_{n=0}^{2N-1} \left[c_5 \psi_n^\dagger U_n U_{n+1} U_{n+2} U_{n+3} U_{n+4} \psi_{n+5} - \text{h.c.} \right] \tag{3.1}
 \end{aligned}$$

and improvement coefficients chosen from Table 2.1 up to second order of improvement.

For the sake of brevity and readability we shall from now on write the Hamiltonian only to first order in improvement and omit the second order improvement term. It is implied we also have an additional irrelevant operator. However, any calculation which follows goes through with the additional operator. We conclude it suffices to write one improvement order vicariously for both of them.

3.1 EXACT DIAGONALISATION

This section wishes to explain the methodology of Exact Diagonalisation (ED) and the framework in which it is used to simulate real-time dynamics of lattice QED in $1 + 1d$.

The central idea around Exact Diagonalisation is to numerically work with a (finite dimensional) matrix representation of a quantum mechanical operator. These would build up a matrix representation of the Hamiltonian corresponding to the system of interest.

Through C-symmetry we can restrict the full Hilbert space of N fermions of naive size $\dim(\mathcal{H}) = 2^{2N}$ to be only of size $\dim(\mathcal{H}) = \binom{2N}{N}$. This is because we will always want to have an initial state free of total charge. And as we argued in Section 2.1.0.2, time evolution commutes with the Gauß operator such that one never leaves the subspace of zero total charge.

3.1.1 Solving Gauss law with periodic boundary conditions

An essential requirement for employing ED is the finiteness of the Hilbert space one wishes to simulate. Gauge theories describe the fundamental interaction of fermionic matter fields with bosonic gauge fields. Bosonic degrees of freedom, however, always have an infinite Hilbert space of states. This poses a fundamental problem of how to handle gauge theories with ED. Previously, there were so called ‘encoding’ techniques employed [52], which relied on open boundary conditions. Within this thesis we will however demand periodic boundary conditions. A short review of the effects of open boundary conditions is enclosed in [Appendix D](#).

Following Refs [53], we take a similar approach to the encoding technique in [52], adapted for periodic boundary conditions.

We shall consider

$$H = H_F + H_E, \quad H_E = \frac{a}{2} \sum_n^{2N-1} E_n^2, \quad (3.2)$$

as well as Gauß’s law

$$E_n - E_{n-1} = Q_n, \quad (3.3)$$

and read it as an operator equation when acting on a state in the physical subspace.

In the approach of [53] one splits the electric field into the spatial average part and a spatial varying part defined like,

$$E_n = E + \delta E_n, \quad (3.4)$$

$$\sum_{n=0}^{2N-1} E_n = \bar{E}, \quad (3.5)$$

$$\sum_{n=0}^{2N-1} \delta E_n = 0. \quad (3.6)$$

Thus,

$$\frac{1}{2} \sum_{n=0}^{2N-1} \left(\bar{E}^2 + 2\bar{E}\delta E_n + (\delta E_n)^2 \right) = N\bar{E}^2 + \frac{1}{2} \sum_n (\delta E_n)^2. \quad (3.7)$$

Ultimately, one is able to express $\sum_n (\delta E_n)^2$ only in terms of charge operators Q_n which are bilinears in the fermionic fields while their exact form varies from different fermion discretisation. For staggered fermions the charge operator reads as [20]

$$Q_n = \psi_n^\dagger \psi_n + \frac{1}{2} ((-1)^n - 1). \quad (3.8)$$

One finds [53]

$$\begin{aligned} \sum_{n=0}^{2N-1} (\delta E_n)^2 = -e^2 \frac{2N-3}{2(2N-2)} \sum_{n=0}^{2N-1} \left[\sum_{d=0}^N \left(d + \frac{d^2 - 3d + 2}{2N-3} \right) Q_n (Q_{n+d} + Q_{n-d}) \right. \\ \left. + Q_n (Q_{n+1} + Q_{n-1}) + \frac{4N^2 - 8}{4(2N-3)} Q_n Q_{n+N} \right], \end{aligned} \quad (3.9)$$

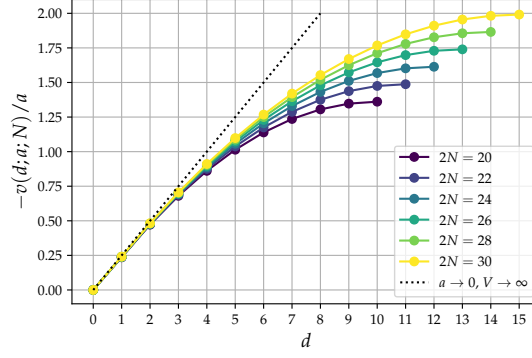


Figure 3.1: Displayed is the potential $v(d; a; N)$ for different values of system size $2N$. One can see the potential to yield ever more linear behaviour for larger N . The continuum and infinite volume curve is plotted as a dotted line.

given the restriction on the physical subspace where $G_n = 0 = E_n - E_{n-1} - eQ_n$. This is only possible because of the periodic boundary conditions $Q_N = Q_0$, $E_N = E_0$ as well as the constraint (3.6) [53].

One might define the potential $v(d; a)$ as

$$v(d; a) = -\frac{a}{4} \frac{2N-3}{2N-2} \cdot \begin{cases} d, & d = 0, 1 \\ d + \frac{d^2 - 3d + 2}{3 - 2N}, & 2 \leq d \leq N-1 \\ \frac{4N^2 - 8}{8(2N-3)}, & d = N \end{cases} \quad (3.10)$$

We gather

$$H_E = \frac{2Na}{2} \bar{E}^2 + e^2 \sum_{n=0}^{2N-1} \sum_{d=0}^N v(d; a) Q_n (Q_{n+d} + Q_{n-d}). \quad (3.11)$$

Let us define $L = 2Na$ and $|x| = da$. Then, this potential has the limits

$$\lim_{2N \rightarrow \infty} v(d; a) \rightarrow -\frac{1}{4} ad, \quad d < \infty, \quad (3.12)$$

$$\lim_{a \rightarrow 0} v(d; a) \rightarrow -\frac{1}{4} \left(|x| - \frac{x^2}{L} \right), \quad (3.13)$$

$$\lim_{a \rightarrow 0} \lim_{2N \rightarrow \infty} v(d; a) = \lim_{2N \rightarrow \infty} \lim_{a \rightarrow 0} v(d; a) \rightarrow -\frac{1}{4} |x|. \quad (3.14)$$

For illustrative purposes we plotted the potential in Figure 3.1. Hence, in the limit of $N \rightarrow \infty$, $a \rightarrow 0$ we find the same expression as in Equation 2.30,

$$H_G = -\frac{e^2}{4} \int dx dy \rho(x) |x - y| \rho(y), \quad (3.15)$$

with $Q_n \rightarrow \rho(x)$.

Similarly to the residual gauge transformation in Equation 2.31 we shall perform the analogous transformation on the lattice:

$$\psi_n = \prod_{l < n} U_l^\dagger \psi'_n \quad (3.16)$$

However, with periodic boundary conditions, we have a persistent ‘boundary’ term:

$$\begin{aligned}
H = & -\frac{i}{2a}c_1 \sum_{n=0}^{2N-2} \left(\psi_n^\dagger \psi'_{n+1} + \text{h.c.} \right) - \frac{i}{2a}c_3 \sum_{n=2N-2}^{2N-4} \left(\psi_n^\dagger \psi'_{n+3} + \text{h.c.} \right) \\
& - \frac{i}{2a}c_1 \psi_{2N-1}^\dagger \left(\prod_{n=0}^{2N-1} U_n \right) \psi'_0 - \frac{i}{2a}c_3 \psi_{2N-3}^\dagger \left(\prod_{n=0}^{2N-1} U_n \right) \psi'_0 + \text{h.c.} \\
& + m \sum_{n=0}^{2N-1} (-1)^n \psi_n^\dagger \psi'_n \\
& + \frac{2Na}{2} \bar{E}^2 + e^2 \sum_{n=0}^{2N-1} \sum_{d=0}^N v(d; a) Q_n (Q_{n+d} + Q_{n-d}) .
\end{aligned} \tag{3.17}$$

We have

$$\mathcal{E} := \sum_{n=0}^{2N-1} E_n = 2N\bar{E} , \tag{3.18}$$

$$\mathcal{U} := \prod_{n=0}^{2N-1} U_n , \tag{3.19}$$

$$[\mathcal{E}, \mathcal{U}] = e\mathcal{U} , \tag{3.20}$$

$$\mathcal{U} = e^{iae \int dt \sum_n E_n} = e^{iae2N \int dt \bar{E}} . \tag{3.21}$$

Thus, these two persistent ‘boundary’ variables (\mathcal{E} , \mathcal{U}) are true quantum degrees of freedom, which find no analogy in the continuum and infinite volume limit.

This (boundary) degree of freedom has unfortunately an infinite Hilbert space. To render the Hilbert space finite, we shall omit the quantum nature of this DoF and suppose the electric background field is strong and constant, such that the quantum corrections can be neglected, much similar to the classical statistical approximation [49, 51]. This, however, means we are unable to observe a back reaction from the fermion current onto the electric field.

Consequently, we approximate

$$\mathcal{U} \simeq e^{iae2N\bar{E}t} . \tag{3.22}$$

It must be noted that the residual gauge transformation (3.16) renders the ‘dressed’ statistical propagator $F'_{n,m} = \langle [\psi'_n, \psi_m^\dagger] \rangle$ gauge invariant. Consequently, the definition for the particle number from Section 2.5.1 with $F'_{n,m}$ will be gauge invariant, too.

RETRIEVING THE ELECTRIC FIELD As we implemented Gauß’s law in the physical Hilbert space to eliminate the electric field from our Hamiltonian, we may just invert this to recover the state of the local electric field variation δE_n in terms of the charge operator. To this end, consider Gauß’s law $E_n - E_{n-1} = eQ_n$ from which we can deduce

$$\delta E_n = \delta E_0 + e \sum_{i=1}^n Q_i . \tag{3.23}$$

Together with (3.6) we can constrain above equation to obtain

$$0 = \sum_{n=0}^{2N-1} \delta E_n = 2N \delta E_0 + e \sum_{n=1}^{2N-1} \sum_{i=1}^n Q_i = 2N \delta E_0 + e \sum_{i=1}^{2N-1} (2N - i) Q_i, \quad (3.24)$$

$$\delta E_0 = -\frac{e}{2N} \sum_{i=1}^{2N-1} (2N - i) Q_i. \quad (3.25)$$

From (3.25) onwards one can apply Gauß's law iteratively to obtain the state of every local field variation δE_n .

3.1.2 Numerical simulation

Before we give the explicit form of the Hamiltonian we wish to simulate on the lattice with Exact Diagonalisation, we will perform one last transformation. As we approximate the product over all link variables as a c-number $\mathcal{U} = \exp(iae2N\bar{E}t)$ we shall 'redistribute' this function over all DoF, according to the unitary transformation

$$\psi'_n = \prod_{l < n}^{2N} \sqrt{\mathcal{U}} \psi''_n = \mathcal{U}^{\frac{1}{2N}} \psi''_n =: \bar{\mathcal{U}}^n \psi''_n, \quad (3.26)$$

with

$$\bar{\mathcal{U}} = e^{iae\bar{E}t}. \quad (3.27)$$

Finally, we can cast the Hamiltonian from (3.17) into the following form:

$$\begin{aligned} H = & -\frac{i}{2a} c_1 \sum_{n=0}^{2N-1} \left(\psi''_n{}^\dagger \bar{\mathcal{U}} \psi''_{n+1} + \text{h.c.} \right) - \frac{i}{2a} c_3 \sum_{n=0}^{2N-1} \left(\psi''_n{}^\dagger \bar{\mathcal{U}}^3 \psi''_{n+3} + \text{h.c.} \right) \\ & + m \sum_{n=0}^{2N-1} (-1)^n \psi''_n{}^\dagger \psi''_n \\ & - e^2 \sum_{n=0}^{2N-1} \sum_{d=0}^N v(d; a) Q''_n (Q''_{n+d} + Q''_{n-d}). \end{aligned} \quad (3.28)$$

The analogy to the form of the Hamiltonian of Section 2.5 is now more obvious. The crucial difference, however, is that we have in Section 2.5 a constant homogeneous electric field, while in this section we have the approximation of a constant *background* field. This is expressed by the additional non-local quartic interaction term which H_E includes. However, retrieving a definition of a particle number from above Hamiltonian, we must diagonalise it. To this end, we neglect the electric part as it is quartic in fermion fields. Consequently, the particle number as defined in Section 2.5.1 can be applied. Merely the current changes into a rotating frame according to

As already mentioned, the Hamiltonian (3.28) is quartic in the fermion fields. To diagonalise it, we have to resort to numerical methods.

The numerical implementation of (3.28) is performed with the *QuSpin* package for the Python programming language [54].

The initial state is obtained from (3.28) with $\bar{\mathcal{U}} = 1$ and $\bar{E} = 0$ by diagonalisation via the Implicitly Restarted Lanczos Method to find eigenvalues and eigenvectors [54, 55]. It is the state corresponding to the lowest eigenvalue. For better numerical convergence, we always retrieve ~ 10 of the algebraically lowest eigenstates and eigenvalues,

respectively.

Time evolution is governed by the Schrödinger equation. It is solved with the explicit, adaptive Runge-Kutta method of order $\mathcal{O}(4(5))$ due to Dormand and Prince.

Operators corresponding to observables like the current j_n and $F_{n,m}$ are initialised as matrices and applied to the respective state at some time t in order to obtain the expectation value.

3.2 CLASSICAL STATISTICAL SIMULATION

In this part of the chapter we introduce the Classical Statistical Approximation briefly, discuss its limitations and derive what changes with respect to the Improvements we are implementing.

3.2.1 Introduction

The Classical Statistical Approximation is based on the path integral approach. The central idea of this approximation is to map the full quantum theory onto a classical-statistical ensemble, which is achieved by a semi-classical expansion around the initial state [49, 51]. This means in detail that one solves classical equations of motion and samples over fluctuating initial values in order to obtain non-perturbative approximations for real-time quantum observables. For a more detailed introduction we refer the reader to [49].

3.2.2 Validity

First, we shall denote the classical electric field as \bar{E} and the quantum electric field as \tilde{E} . Then the $U(1)$ gauge part of the action is invariant under a rescaling of the fields [49]:

$$\bar{E} = \bar{E}' / e, \quad (3.29)$$

$$\tilde{E} = e\tilde{E}'. \quad (3.30)$$

Diagrammatically, the classical statistical approximation involves only contributions with one quantum field \tilde{E}' , any higher contribution is neglected. Whence, the classical statistical approximation is exact to $\mathcal{O}(e^2)$, while contributions of two or more quantum fields \tilde{E}' are neglected. Or equivalently, contributions with $\mathcal{O}(e^4)$ and higher are omitted [49].

Thus, the classical statistical approximation is only valid for small couplings.

3.2.3 Equations of Motion

Within the classical statistical approximation, the state is fully parameterised by the statistical propagator $F_{n,m} = \langle [\psi_n, \psi_m^\dagger] \rangle$, the link variable U_n and the electric field E_n .

We want to abbreviate (3.1) as

$$H = H_F + H_G \quad (3.31)$$

with

$$H_F = \sum_{n,m} \psi_n^\dagger h_{n,m}^F \psi_m, \quad (3.32)$$

$$\begin{aligned} h_{n,m}^F = & -\frac{i}{2a} c_1 \left(U_n \delta_{m,n+1} - U_n^\dagger \delta_{m,n-1} \right) \\ & -\frac{i}{2a} c_3 \left(U_n U_{n+1} U_{n+2} \delta_{m,n+3} - U_n^\dagger U_{n+1}^\dagger U_{n+2}^\dagger \delta_{m,n-3} \right) \\ & + (-1)^n m \delta_{m,n}. \end{aligned} \quad (3.33)$$

In [Section 2.5.2](#) we present the calculation of the fermionic current j_n when including improvement. It is now straightforward to express the operators for j_n in terms of F_{nm} and U_n . The detailed computation shall be omitted and the result stated.

The equations of motion are [\[50\]](#)

$$\begin{aligned} \partial_t E_n = \frac{e}{2a} \{ & c_1 \Re (F_{n+1,n} U_n) \\ & + c_3 \Re (F_{n+3,n} U_n U_{n+1} U_{n+2} + F_{n+2,n-1} U_{n-1} U_n U_{n+1} + F_{n+1,n-2} U_{n-2} U_{n-1} U_n) \}, \end{aligned} \quad (3.34)$$

$$\partial_t U_n = iae E_n U_n, \quad (3.35)$$

$$\partial_t F_{n,m} = -i \sum_j \left(h_{n,j}^F F_{j,m} - F_{n,j} h_{j,m}^F \right). \quad (3.36)$$

As we explained in [Section 3.1](#), the Exact Diagonalisation method is not fit to observe back reactions from the current onto the electric field. We therefore set the equation of motion

$$\partial_t E_n = 0, \quad (3.37)$$

to better compare results between the two methods.

The equations of motion are again solved with an adaptive Runge-Kutta algorithm of order 4(5) due to Dormand and Prince.

3.2.4 Initial conditions

The state of the system is prepared in the fermionic vacuum with $U_n = 1$, $E_n = 0$. The initial conditions for

$$F_{n,m} = \langle 0 | [\psi_n, \psi_m^\dagger] | 0 \rangle = \sum_{q,p=0}^{2N-1} \langle 0 | [\tilde{\psi}_q, \tilde{\psi}_p^\dagger] | 0 \rangle e^{i\frac{\pi}{N}(qn-pm)} \quad (3.38)$$

are computed by diagonalising H_F like in [Section 2.4.5](#). The exact calculation is straightforward and shall be omitted. The result reads as

$$F_{n,m} = \frac{1}{2N} \sum_{q=0}^{N-1} e^{i\frac{\pi q}{N}(n-m)} \left[\frac{\pi q}{\omega_q} (1 + (-1)^{n+m}) + \frac{m}{\omega_q} ((-1)^n + (-1)^m) \right]. \quad (3.39)$$

Naturally, with different improvement order the functions π_q and ω_q are altered and the initial state changes accordingly.

Because the dynamics is dominated by the strong electric field, we will omit the statistical sampling over the initial conditions and only opt for a good approximation by single runs as was done in Refs. [\[42, 50, 51\]](#).

In this chapter we will briefly review some of the most relevant concepts to quantum computing with trapped ions. In particular, we will discuss the 4-qubit quantum gate corresponding to the irrelevant kinetic first order improvement discussed in [Section 2.4.5](#).

The concept of universal quantum computing was significantly propelled after David Deutsch published his 1985 landmark paper [15] in which he describes the notion of a quantum Turing machine. That is to say, Deutsch describes the formal requirements of manipulation on quantum states to successfully be able to compute all computable, in particular finite, quantum algorithms. The required manipulations are called quantum gates in analogy to their classical counterpart—binary logic gates. Particularly, he argues one only requires single-qubit gates as well as one specific two-qubit gate [15, 18] to have a so-called complete set of gates.

In the digital approach to quantum simulation the time evolution operator $U(t, t_0) = T \exp\left\{-i \int_{t_0}^t H(t') dt'\right\}$ is approximate by the Lie-Trotter product formula,

$$e^{A+B} = \lim_{N \rightarrow \infty} \left(e^{A/N} e^{B/N} \right)^N, \quad (4.1)$$

and as such split into a sequence of successive application of different factors corresponding to different terms in the Hamiltonian. This gives an error of higher order in Δt . As

Consequently, we first cite the Hamiltonian of cold ions trapped on a string, after which we review the single-qubit gate as well as the two-qubit gate after Mølmer and Sørensen [56]. This review is closely oriented towards Refs. [18, 57].

Finally, we compute the specific gate sequence corresponding to the 4-qubit interaction involved in the first order improvement term, as it is the only new term compared to the unimproved Hamiltonian, for which the corresponding quantum gate sequences are already known from Refs. [23].

4.1 HAMILTONIAN OF TRAPPED IONS

The relevant degrees of freedom describing the physics of ultra cold ions trapped in a string are often the two-level system of a single ion and a single mode of the collection of harmonic oscillators as the motional degrees of freedom—the centre-of-mass mode [18].

The Hamiltonian of trapped ions is given by [18, 56]

$$H_{\text{int}} = \Omega \sum_{n=0}^{N-1} \left\{ \sigma_n^+ e^{-i(\Delta t - \phi)} + \sigma_n^- e^{i(\Delta t - \phi)} + i\eta \left(\sigma^+ e^{-i(\Delta t - \phi)} - \sigma^- e^{i(\Delta t - \phi)} \right) \left(a e^{-i\omega t} + a^\dagger e^{i\omega t} \right) \right\}, \quad (4.2)$$

where Ω is the Rabi frequency, σ^\pm the qubit raising / lowering operators, a and a^\dagger the phonon annihilation and creation operators, respectively. Furthermore, ϕ is the phase of the field with respect to the qubit polarisation, Δ is the laser-atom detuning, and ω_t is the trap frequency. This Hamiltonian is a result of some approximations including the rotating wave approximation which assumes both laser detuning Δ and Rabi frequency Ω to be much smaller than any other optical relevant frequency.

4.2 SINGLE-QUBIT GATE

Given the Hamiltonian (4.2), single qubit operations are simply rotations on the Bloch sphere described by

$$R_i(\theta, \phi) = \exp\left\{i\frac{\theta}{2}\left(e^{i\phi}\sigma_i^+ + e^{-i\phi}\sigma_i^-\right)\right\} \quad (4.3)$$

$$= \mathbb{1}_i \cos\left(\frac{\theta}{2}\right) + i\left[\sigma_i^x \cos(\phi) - \sigma_i^y \sin(\phi)\right] \sin\left(\frac{\theta}{2}\right), \quad (4.4)$$

where ϕ specifies the azimuthal angle of the axis of rotation and θ describes the amount of rotation. Rotations around the z-axis are either decomposable in rotations around the x and y axis or it might be realised via far detuned laser beam which shifts the energies due to an AC-Stark effect [18].

Experimentally, θ is given by the pulse area Ωt of the Rabi frequency and the time of the pulse, and ϕ is given by the phase of the field.

4.3 TWO-QUBIT GATE

Historically, the first two-qubit gate experimentally realisable was the proposal of Cirac and Zoller [58]. However, this proposal bears some weakness in its robustness and requires direct addressing of the individual qubits.

Instead, we review the two-qubit gate proposed by Mølmer and Sørensen [56] (MS gate) in which all qubits are irradiated by a dichromatic laser field. The two frequencies are symmetrically close around the qubit transition frequency ($\omega_0 \pm (\omega_{eg} + \Delta)$). The detuning is chosen such that an effective second-order coupling between pairs of ions is generated by off-resonantly coupling the blue and red phonon side bands [57]. The MS gate is particularly favourable as it not necessarily requires the ions to be in the motional ground state [18, 56, 57], and it addresses the qubits collectively and drives spin flipping of the desired qubits. Figure 4.1 shows the driven transitions $|n, gg\rangle \leftrightarrow |n, ee\rangle$ and $|n, eg\rangle \leftrightarrow |n, ge\rangle$ via the intermediate states indicated with dashed lines. The former transition is the only energy conserving transition given above mentioned detuning. The Rabi frequency $\tilde{\Omega}$ of this transition can be computed using second order perturbation theory and is given by [56]

$$\tilde{\Omega} = -\frac{(\Omega\eta)^2}{2(\nu - \Delta)}, \quad (4.5)$$

where ν denotes the phonon oscillation frequency. Remarkably, (4.5) does not depend on the phonon number n . This is due to the symmetric path illustrated in Figure 4.1 and the destructive interference that comes with it due to the different sign in the detuning [56].

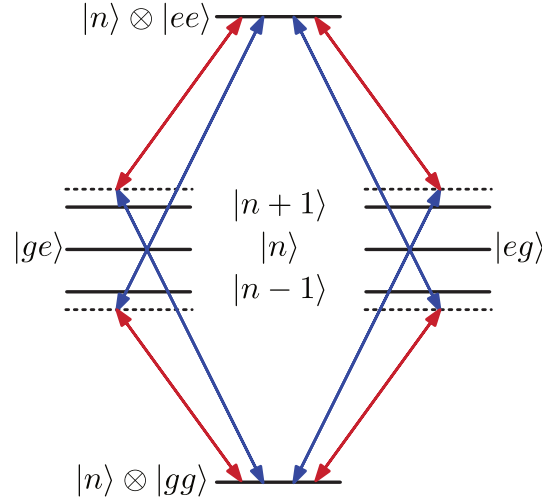


Figure 4.1: Illustration of the energy levels involved in the two-qubit Mølmer-Sørensen (MS) gate. The slightly blue and red detuned laser beams drive the system via the virtual levels marked by dashed lines between the states $|n\rangle \otimes |gg\rangle$ and $|n\rangle \otimes |ee\rangle$. $|n\rangle$ marks the state with phonon number n and $|g\rangle, |e\rangle$, the ground and excited state, respectively. This figure applies to cases where the detuning is much smaller than the Rabi frequency. Then, the Rabi frequency is in fact independent of the phonon number n as the influence destructively interferes due to the symmetric paths and the opposite sign of the detuning. This allows the application of the MS gate without cooling to motional ground state.

Furthermore, the transition $|n, eg\rangle \leftrightarrow |n, ge\rangle$ can be realised by a so-called photon echo trick: the detuning is at a suitable time inverted such that the exchange of the excited quantum in the two qubits can be realised [56]. The Rabi frequency of this transition is of identical magnitude as (4.5) but with opposite sign.

Consequently, by applying the MS gate to two qubits of one's liking the transition they undergo read like

$$|gg\rangle \rightarrow \cos\left(\frac{\tilde{\Omega}t}{2}\right) |gg\rangle + i \sin\left(\frac{\tilde{\Omega}t}{2}\right) |ee\rangle, \quad (4.6)$$

$$|ee\rangle \rightarrow \cos\left(\frac{\tilde{\Omega}t}{2}\right) |ee\rangle + i \sin\left(\frac{\tilde{\Omega}t}{2}\right) |gg\rangle, \quad (4.7)$$

$$|ge\rangle \rightarrow \cos\left(\frac{\tilde{\Omega}t}{2}\right) |ge\rangle - i \sin\left(\frac{\tilde{\Omega}t}{2}\right) |eg\rangle, \quad (4.8)$$

$$|eg\rangle \rightarrow \cos\left(\frac{\tilde{\Omega}t}{2}\right) |eg\rangle - i \sin\left(\frac{\tilde{\Omega}t}{2}\right) |ge\rangle. \quad (4.9)$$

Varying the pulse area $\tilde{\Omega}t$ thus tunes the amount of entanglement and reaches for $\tilde{\Omega}t = \pi/2$ its maximum.

4.4 4-QUBIT GATE

For the basic four-qubit gate we specialise the multi-qubit MS gate as described in [57]. Underling the multi-qubit MS gate is the collective spin $S^{x,y} = \sum_{i=0}^n \sigma_i^{x,y}$ over all ions involved in the gate; including the 0th (ancilla) qubit.

The MS gate operation is then described by [57]

$$U_{MS}(\theta, \phi) = \exp\left\{-i\frac{\theta}{4} [\cos(\phi)S^x + \sin(\phi)S^y]\right\}, \quad (4.10)$$

where θ is the main control parameter for which it is at $\theta = \pi/2$ maximally entangling while ϕ is again the phase of the field tuning a σ^x -type gate ($\phi = 0$) and a σ^y -type gate ($\phi = \pi/2$).

We wish to simulate a coherent time step of a specific 4-qubit interaction term,

$$\simeq e^{-iH_\alpha\tau}, \quad (4.11)$$

$$\text{with } H_\alpha = \omega_\alpha \sigma_1^x \sigma_2^x \sigma_3^x \sigma_4^x. \quad (4.12)$$

Although it is in principle possible to solely rely on single and two-qubit gates—as we already mentioned Deutsch proved [15]—Refs [57] resorts to a gate sequence involving the 4-qubit MS gate. This sequence is a series of three gate operations: a maximally entangling 4-qubit MS gate, a single-qubit rotation on the ancilla qubit, and another inverse maximally entangling 4-qubit MS gate.

This evolution is given by [57]

$$U_{H_\alpha} = U_{MS}\left(-\frac{\pi}{2}, 0\right) R_{anc}^z(\phi) U_{MS}\left(\frac{\pi}{2}, 0\right) \quad (4.13)$$

$$= \exp\left\{i\frac{\pi}{4} S^x \sigma_0^x\right\} \exp\{i\phi \sigma_0^z\} \exp\left\{-i\frac{\pi}{4} S^x \sigma_0^x\right\} \quad (4.14)$$

$$= \exp\left\{i\phi \left[\cos\left(\frac{\pi}{2} \sum_{i=1}^4 \sigma_i^x\right) \sigma_0^z + \sin\left(\frac{\pi}{2} \sum_{i=1}^4 \sigma_i^x\right) \sigma_0^y\right]\right\}. \quad (4.15)$$

Crucially, the collective spin in the cosine and sine do not include the spin of the ancilla qubit which factors out of the trigonometric function. Furthermore, for 4-qubits we have the identities

$$\cos\left(\frac{\pi}{2} \sum_{i=1}^4 \sigma_i^x\right) = \prod_{i=1}^4 \sigma_i^x = \frac{H_\alpha}{\omega_\alpha}, \quad (4.16)$$

$$\sin\left(\frac{\pi}{2} \sum_{i=1}^4 \sigma_i^x\right) = \prod_{i=1}^4 \sigma_i^x = \frac{H_\alpha}{\omega_\alpha}, \quad (4.17)$$

with which we conclude

$$U_{H_\alpha} = \exp\left\{i\frac{\phi}{\omega_\alpha} H_\alpha\right\} \exp\{i\phi \sigma_0^z\}. \quad (4.18)$$

Thus, the dynamics of the ancilla qubit completely factors out and as a consequence we can in principle use any of the participating qubits as the ancilla qubit.

4.5 4-QUBIT GATE SEQUENCE OF 1ST IMPROVEMENT

Here, we want to employ the knowledge of simulating coherently 4-body interactions and compute the gate sequence for the 4-qubit interaction corresponding to the 1st order improvement term expressed in spin DoF in [Section B.2](#).

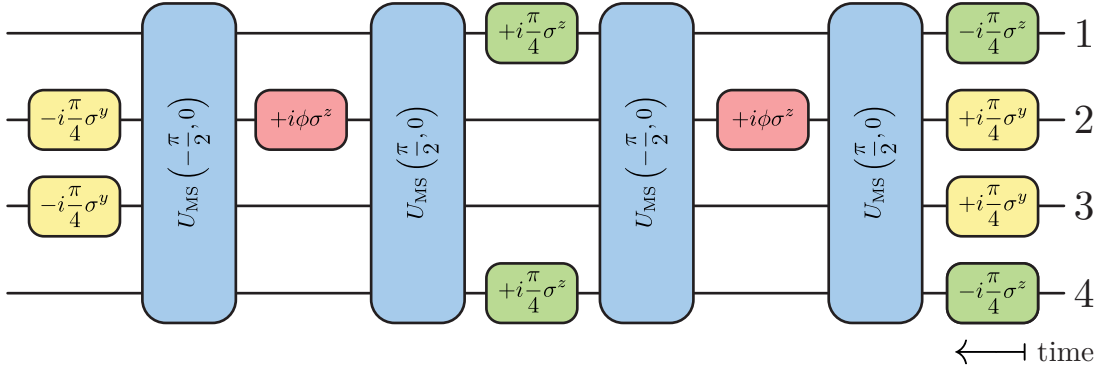


Figure 4.2: Graphical representation of the gate sequence to simulate the 4-body qubit interaction due to the 1st improvement. Read from right to left. The ancilla qubit operation is coloured red, the rotation around the z -axis is coloured green, the rotation around the y -axis is coloured yellow, and the 4-qubit MS gate is coloured blue.

To this end, we shall first compute the interaction term only in terms of $\sigma^{x,y,z}$:

$$\begin{aligned} & \exp\{-i\phi (\sigma_1^+ \sigma_2^z \sigma_3^z \sigma_4^- + \text{h.c.})\} \\ &= \exp\left\{-i\frac{\phi}{4} (\sigma_1^x \sigma_2^z \sigma_3^z \sigma_4^x + \sigma_1^y \sigma_2^z \sigma_3^z \sigma_4^y + i\sigma_1^y \sigma_2^z \sigma_3^z \sigma_4^x - i\sigma_1^x \sigma_2^z \sigma_3^z \sigma_4^y \right. \\ & \quad \left. + \sigma_4^x \sigma_3^z \sigma_2^z \sigma_1^x + \sigma_4^y \sigma_3^z \sigma_2^z \sigma_1^y + i\sigma_4^y \sigma_3^z \sigma_2^z \sigma_1^x - i\sigma_4^x \sigma_3^z \sigma_2^z \sigma_1^y)\right\} \end{aligned} \quad (4.19)$$

$$= \exp\left\{-i\frac{\phi}{2} (\sigma_1^x \sigma_2^z \sigma_3^z \sigma_4^x + \sigma_1^y \sigma_2^z \sigma_3^z \sigma_4^y)\right\} \quad (4.20)$$

$$= \exp\left\{-i\frac{\phi}{2} (\sigma_1^x \sigma_2^z \sigma_3^z \sigma_4^x)\right\} \exp\left\{-i\frac{\phi}{2} (\sigma_1^y \sigma_2^z \sigma_3^z \sigma_4^y)\right\} \exp\{\mathcal{O}(\phi^2)\} \quad (4.21)$$

Subsequently, we must perform several single-qubit rotations from (4.3) to map (4.22) into the interaction H_α we discussed in the previous section. We want to denote qubit rotations as

$$R_i^{x,y,z}(\pm\theta) = \exp\left\{\mp i\frac{\theta}{2} \sigma_i^{x,y,z}\right\}. \quad (4.22)$$

Then, we obtain for

$$\exp\{-i\phi (\sigma_1^+ \sigma_2^z \sigma_3^z \sigma_4^- + \text{h.c.})\} \quad (4.23)$$

$$= R_3^y\left(\frac{\pi}{2}\right) R_2^y\left(\frac{\pi}{2}\right) U_{MS}\left(-\frac{\pi}{2}, 0\right) R_2^z(-2\phi) U_{MS}\left(\frac{\pi}{2}, 0\right) \quad (4.24)$$

$$\cdot R_1^z\left(-\frac{\pi}{2}\right) R_4^z\left(-\frac{\pi}{2}\right) U_{MS}\left(-\frac{\pi}{2}, 0\right) R_2^z(-2\phi) U_{MS}\left(\frac{\pi}{2}, 0\right) \quad (4.25)$$

$$\cdot R_4^z\left(\frac{\pi}{2}\right) R_3^y\left(-\frac{\pi}{2}\right) R_2^y\left(-\frac{\pi}{2}\right) R_1^z\left(\frac{\pi}{2}\right) \quad (4.26)$$

A graphic representation of the result is displayed in Figure 4.2.

RESULTS: UV CONVERGENCE WITH LATTICE IMPROVEMENTS

Within this chapter we present the result of numerical simulations with exact diagonalisation and classical-statistical methods, respectively.

First, we must beg your pardon as we abandoned the previously set notation of referring with $2N$ to the total number of lattice sites; within this chapter and the next we shall denote the total number of lattice sites, particularly in descriptions of plots, et cetera, with N .

5.1 APPROACHING THE CONTINUUM – EXACT DIAGONALISATION

What follows are the results of Exact Diagonalisation Simulations to gain insight into the effects of improvements on small lattices. The Exact diagonalisation was performed without solving Gauß's law and expressing the electric field in terms of fermionic charge operators. Instead, we have a constant *homogeneous* electric field.

We sampled for one critical field ($E = 1m^2/e$), $e/m = 0.1$, and different volumina ($Lm = 4, 5, 6$) the UV-convergence of the particle production rate by increasing $N = 10$ to $N = 20$ in order to find some lowest N at which one is with the improved curves still in acceptable margins within the theoretical prediction while the unimproved curve is significantly off. The results for $Lm = 6$ can be inspected in [Figure 5.1](#), while the series for $Lm = 5$ and $Lm = 4$ are outsourced to [Appendix C](#) at [Figure C.1](#) and [Figure C.2](#), respectively.

Contrasting improved versus unimproved, in neither of those series is any enhancement regarding the UV convergence of the particle production rate obviously to be observed.

Since these series of convergence were not indicative and the maximum capacity of available computing power is only a few sites larger, we resort in the next section on classical statistical simulations to observe an approach to the continuum, in which we wish to observe the advantages of lattice improvements.

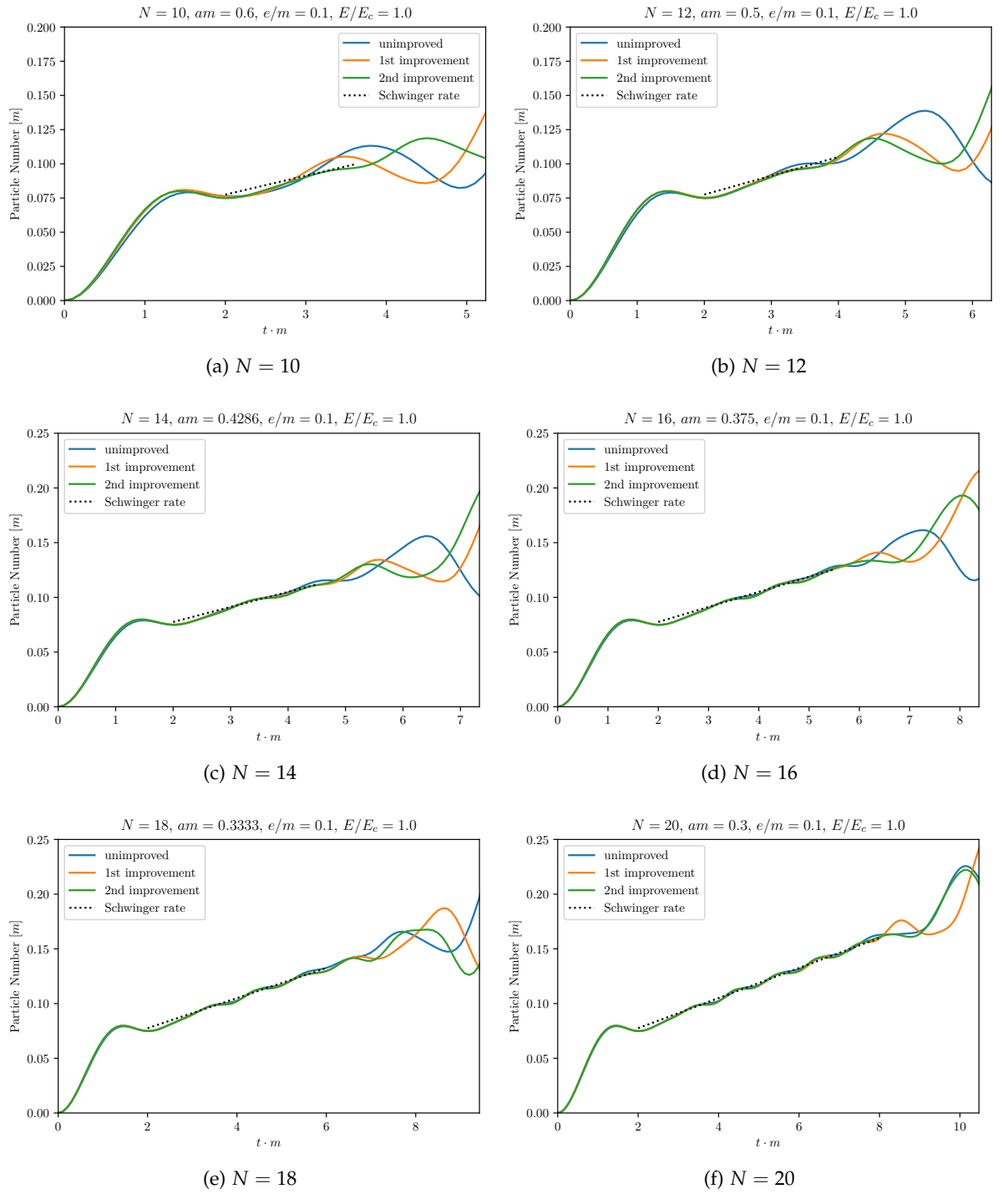


Figure 5.1: UV convergence series with $Lm = 6$, $E/E_c = 1$, $e/m = 0.1$. The largest time plotted is at each instance $2t_{max}m = \frac{\pi}{am-1}$. For reference we indicated the analytic prediction for late times with a black dotted line. The benefits of improvements are hardly distinguishable. For this set of parameters, there is no obvious advantage with improvements over the unimproved theory. System sizes with significantly larger N , i.e. smaller am , and thereby a larger t_{max} cannot be realised within this method.

5.2 APPROACHING THE CONTINUUM – CLASSICAL STATISTICAL SIMULATION

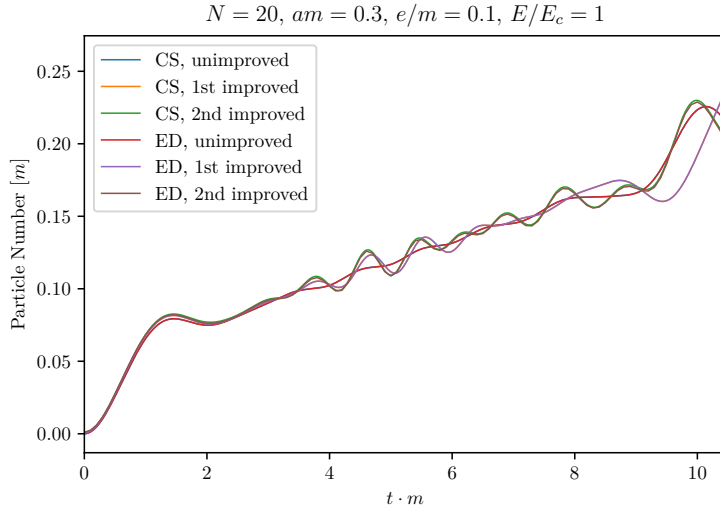


Figure 5.2: Comparison: Classical Statistical (CS) and Exact Diagonalisation (ED). Both simulations did not realise back reaction from the current onto the electric field. In the ED simulation we did not express the electric fields via Gauss law as charge operators. We observe near perfect agreement between the two methods. Only because the simulation of the second order improvement for ED (brown) is realised with double time step size, we can make out the second order improved curve of CS (green) merely at the troughs and peaks of said curve. Everywhere else, we observe perfect alignment such that only the three curves of ED are visible. We shall disregard the differences as insignificant.

As discussed in [Section 3.2](#), we employ the classical statistical simulation without back reactions of the currents to the electric field. Recall that in this scenario we are unable to observe plasma oscillations. Instead, we want to focus on the particle production rate as a reference observable in the continuum.

Moreover, in the previous simulations from [Section 5.1](#), we did not use Gauss law to express the electric field in terms of fermionic bilinears, and we thus expect the two methods to agree perfectly with each other. This is because the classical statistical simulation treats the fermionic degrees of freedom exactly while it approximates the gauge degree of freedom. When we are now additionally neglecting the back reaction of currents onto the electric field, the equation of motion (EoM) of E_n is trivial and as such the EoM of U is as well (cf. (3.34)ff.). Indeed, we find perfect agreement between the two methods (cf. [Figure 5.2](#)).

Appreciating this, we wish to expand the UV convergence series of the particle production rate from ED simulations to ever smaller lattice spacings corresponding with the aid of classical-statistical simulations.

We will proceed the investigation with refined data analysis and fit for every run a linear function in a suitable time window at sufficiently late times such that quench dynamics already faded and until approximately $1.5t_{max}$ for the respective run. The time window boundary will be varied with $\Delta t \approx 0.5tm$ such that we have a total of seven differently large time windows. The linear fit for the unimproved curved is displayed as a red dashed line in the plot series of single runs. Fitting linear functions

over seven different time windows, the average is taken as the data point for the respective run while the fit error and the standard deviation of different fits for the same run is quadratically added to the respective error estimate. In the following figures we plot the respective fitted slope normalised to the continuum prediction from (2.185). In all figures are plotted on the lower horizontal axis the inverse of the lattice spacing $1/am$, while on the higher horizontal axis the *total* number of lattice sites is plotted (only even numbers are realised in simulation).

In this section we employ statistics over view simple fit procedures to extract faithfully a linear growth rate. We cover a wide range of parameters for E/E_c and Lm in which we always sample from low cutoff and small system size, such that the linear growth in particle production is hardly observable, to clearly converged system size and large cutoff, such that $2t_{max}$ is long enough to retrieve a truthful averaged fit. We observe clear benefits, that is showing significantly better accuracy over the unimproved curve, in certain parameter regimes of view, i.e. one digit, per cent points upon improving our theory. Considering the parameters we realised, improvements are particularly beneficial for the particle production rate when the electric field strength is between 1 or 2 critical field strengths. Higher critical field strengths render the benefits insignificant. Parameters, we realised, displaying most benefits from improvements include $Lm = 7$ and $E/E_c = 1$ (Figure 5.3c), $Lm = 7$ and $E/E_c = 1.5$ (Figure 5.4b), as well as $Lm = 5.5$ and $E/E_c = 2$ (Figure 5.5c).

We can make out three general trends. 1.) Large relative errors reflect on significant finite-size effects in the form of volume oscillations. Then, varying the fitting window significantly alters the slope of the fit which is reflected in the large standard deviation (see e.g. Figure 5.3c). 2.) Given a field strength we observe an increase with accuracy with an decrease in volume. This reflects on the smaller lattice spacing which in turn renders $2t_{max}$ sufficiently larges such that we can fit linear functions and truthfully excerpt a linear growth unaffected by possibly present finite-size effects (see e.g. Figure C.5). 3.) The advantages of improvements over the unimproved system decrease with an increase in field strength (see e.g. Figure 5.3c vs Figure 5.7c).

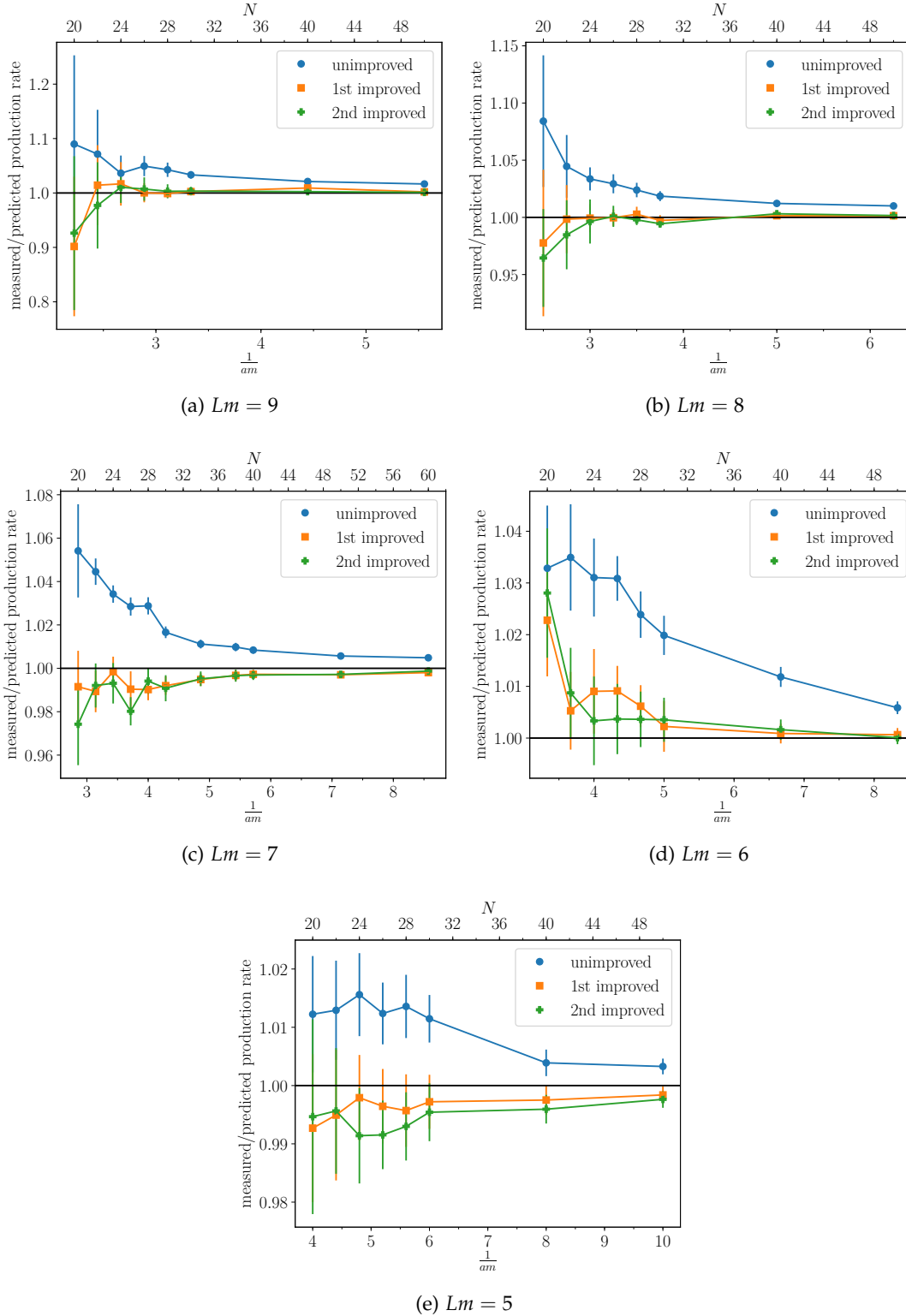


Figure 5.3: UV convergence series with $E/E_c = 1$, $e/m = 0.1$. First and last run for respective volume are enclosed in Figure C.2. For this series, the relative error (precision) of data points is minimal (maximal) at $Lm = 7$, while the overall accuracy of all points in a run is increasing with decreasing volume. The former reflects the balance between finite-size effects in form of volume oscillations, and small enough lattice spacing such that $2t_{max} = \frac{\pi}{amE/E_c}$ is large enough to observe linear growth in particle number (cf. Figure C.2). Lattice improvements are most beneficial for $Lm = 7$.

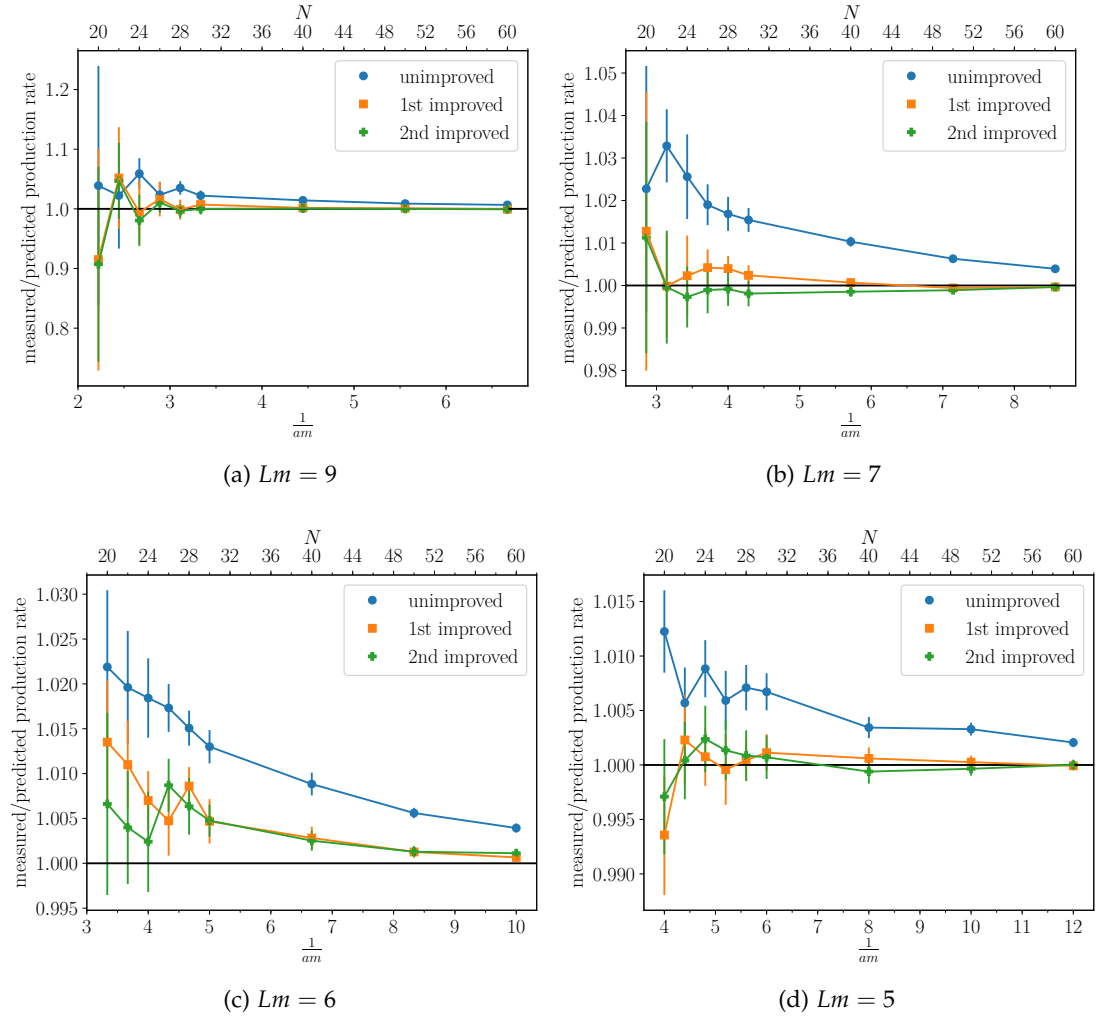


Figure 5.4: UV convergence series with $E/E_c = 1.5$, $e/m = 0.1$. First and last run for respective volume are displayed in Figure C.2. The relative error (precision) is increasing (decreasing) with decreasing physical volume. The overall accuracy increases with an decrease in volume. The overall increase in precision reflects the smaller lattice spacings such that $2t_{max}$ become large enough to observe linear growth in particle number. The most beneficial setup for improvements is $Lm = 7$ given $E/E_c = 1.5$.

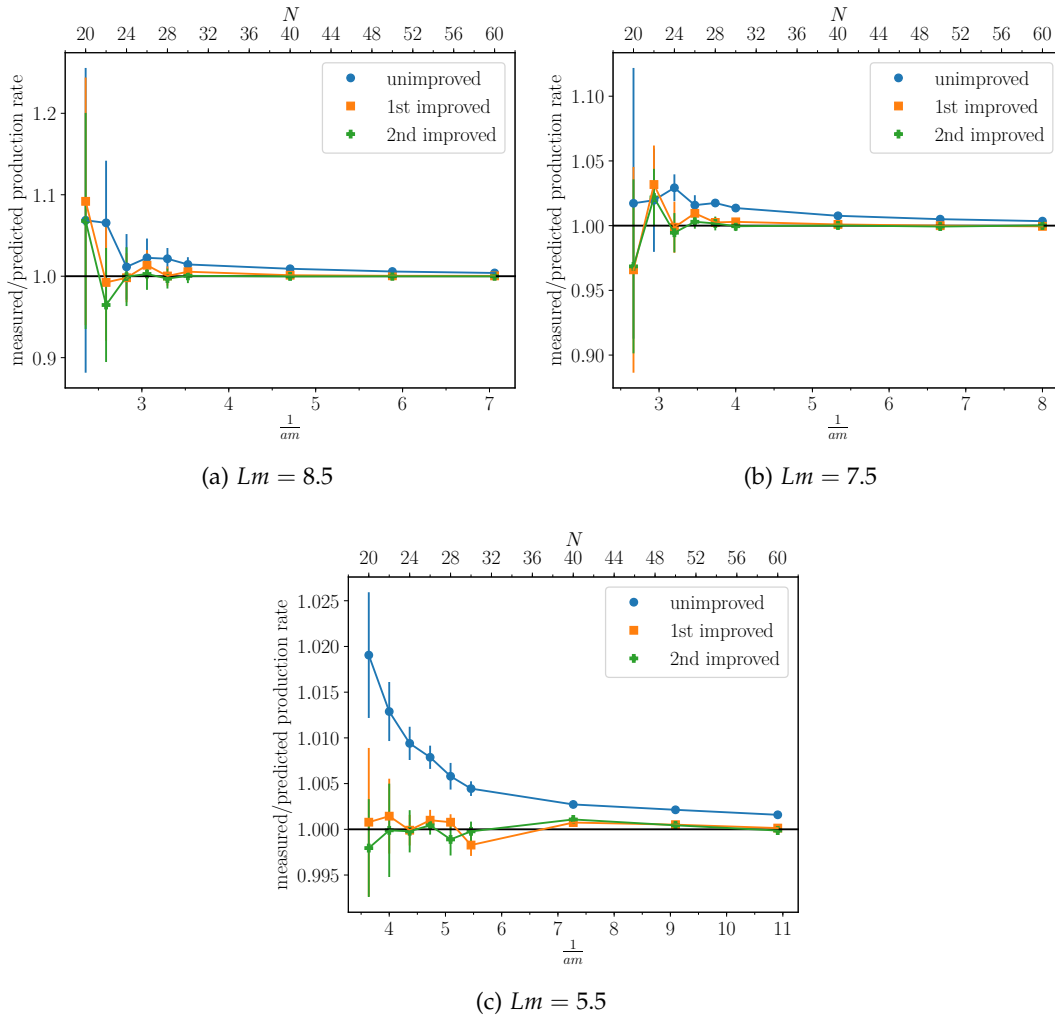


Figure 5.5: UV convergence series with $E/E_c = 2$, $e/m = 0.1$. First and last run for respective volume are displayed in Figure C.3. At $Lm = 8.5$ and $Lm = 7.5$ the simulations suffer from too small $2t_{max}$ and consequently a linear fit is infeasible (cf. Figure C.3). Only at $Lm = 5.5$ $2t_{max}$ is large enough to accurately fit a linear function. Here, the benefits of improvements are in relative terms significant, while the overall precision is already for the unimproved system as good as few per cent.

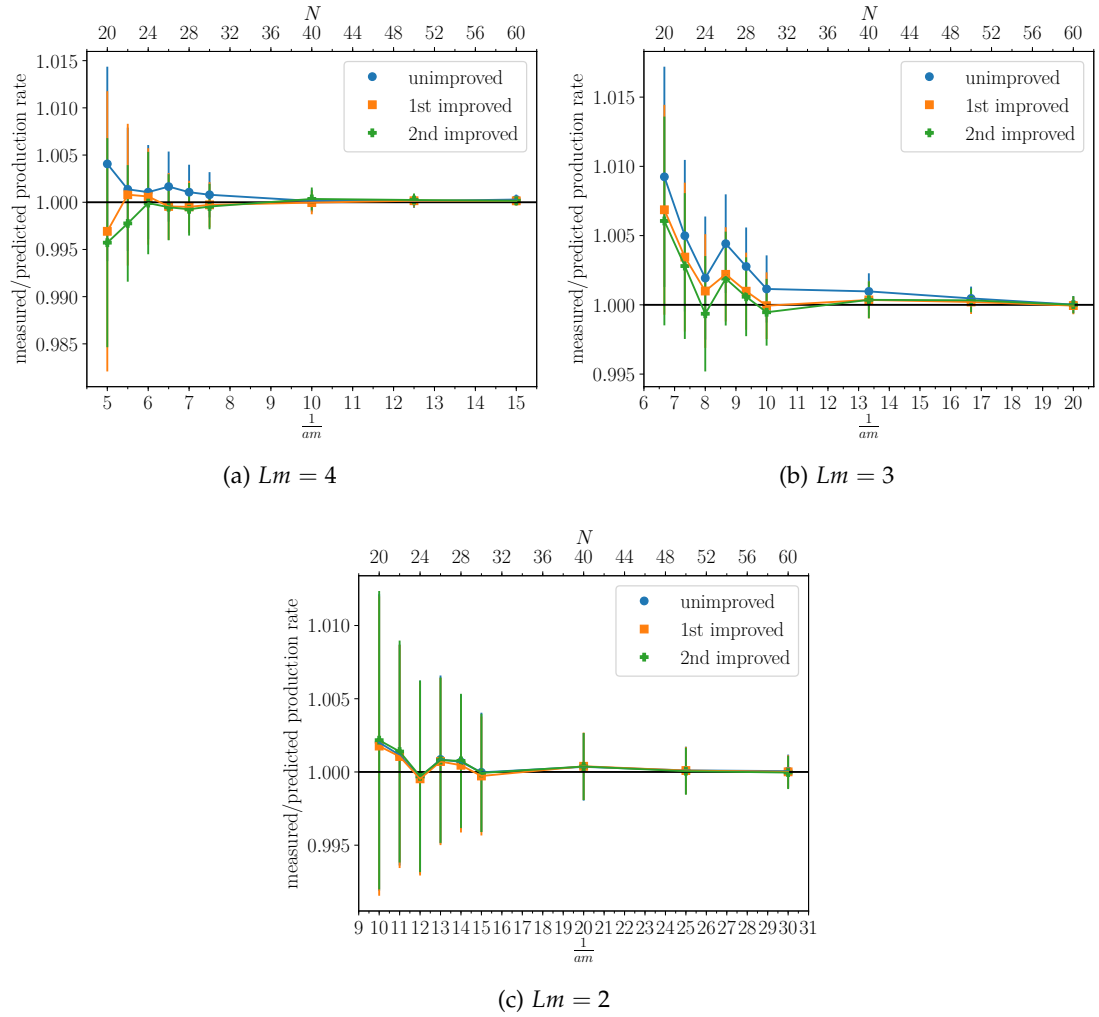


Figure 5.6: UV convergence series with $E/E_c = 5$, $e/m = 0.1$. First and last run for respective volume are displayed in Figure C.4. Precision at $E/E_c = 5$ suffers from the large finite-size effects through volume oscillation rendering a linear fit infeasible (cf. Figure C.4), while the overall accuracy is retained through the symmetric variation of the fitting window. The benefits of improvement are almost insignificant.

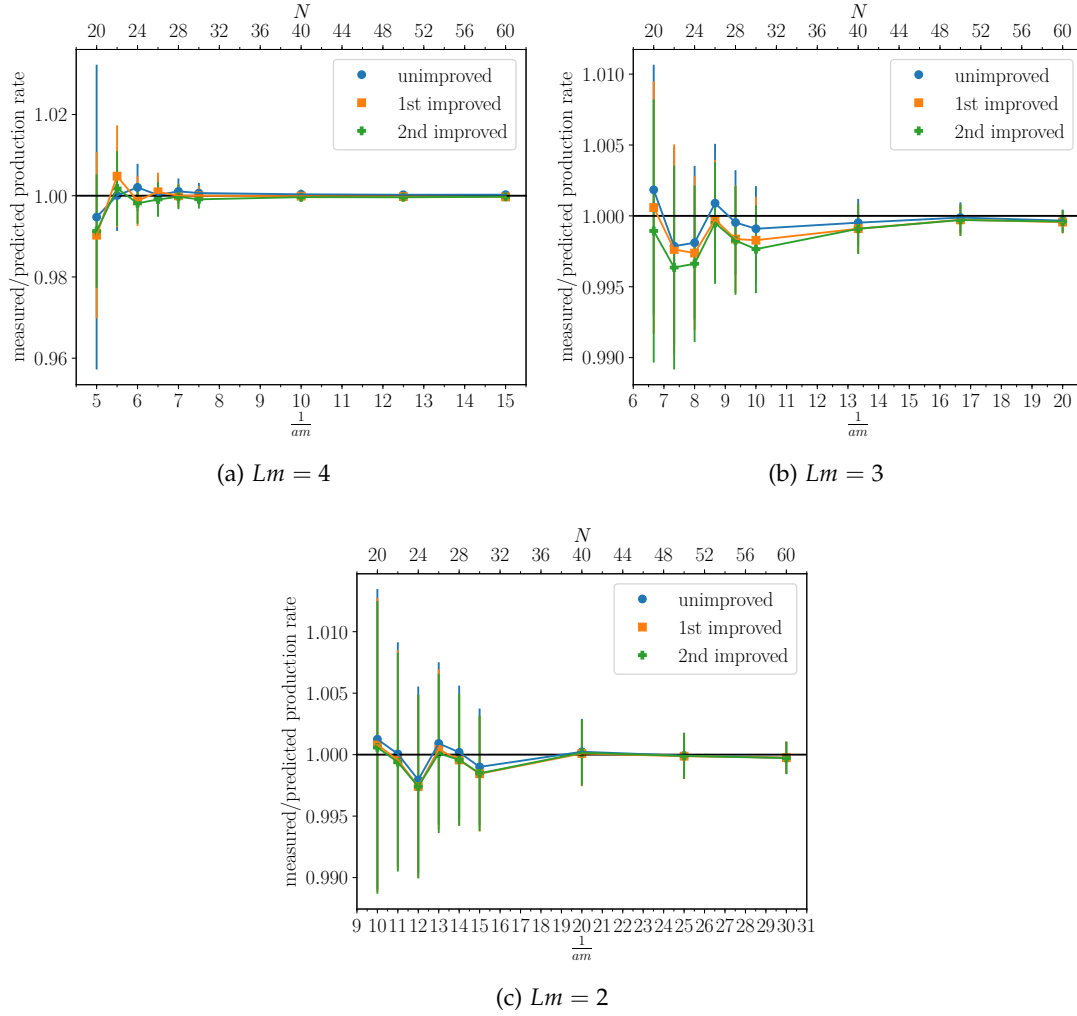


Figure 5.7: UV convergence series with $E/E_c = 7$, $e/m = 0.1$. First and last run for respective volume are displayed in Figure C.5. Similar to the case of $E/E_c = 5$, here too, we find large relative errors for the two smaller volumina due to finite-size effects in form of volume oscillations. The overall accuracy is retained through symmetrically varying the fitting window. Only the runs for $Lm = 4$ at medium and large system size show accurately and precisely continuum behaviour. There, however, no significant benefits of lattice improvements is to be observed. Reflecting on (2.210), it becomes evident, that ever larger field strength need ever smaller lattice spacing in order to obtain a time window in which one can observe linear growth.

RESULTS: EXACT DIAGONALISATION SIMULATION OF STRONGLY COUPLED QED

6.1 STRONGLY COUPLED QED AT $Lm = 7$ AND $E/E_c = 1.5$

In this chapter we present the results obtained from using the unbiased exact diagonalisation approach to simulate strongly coupled QED in $1 + 1d$. Our main interest is the particle production rate in the Schwinger mechanism and how it is affected by strong coupling.

Reflecting on the findings in the previous chapter, we opted for the parameter set $Lm = 7$ and $E/E_c = 1.5$ (cf. [Figure 5.4b](#)) since this configuration displays clear benefits of lattice improvements as opposed to $Lm = 7$ and $E/E_c = 2$ (cf. [Figure 5.5b](#)) while still yielding overall better precision compared to $Lm = 7$ and $E/E_c = 1$ (cf. [Figure 5.3c](#)). Furthermore, the parameters $Lm = 7$, $E/E_c = 1.5$ and $Lm = 5.5$, $E/E_c = 2.0$ yield very similar results in terms of precision, overall accuracy and advantages of lattice improvements. We decided in favour of the former as the maximal time $2t_{max}$ is 1.5 times higher at the former, allowing for a longer time window to observe the Schwinger mechanism—or what it might turn into—at strong couplings.

In our numerical simulations we encountered significantly different results for different system sizes. We want to resort to the fact that the Schwinger model in the massless limit features spontaneous symmetry breaking as the vacuum expectation value (VEV) of the chiral order parameter is $\langle \bar{\psi}\psi \rangle_0$ non-vanishing according to (2.48), in order to discard some of the results we encountered numerically, as we will discuss now. On the staggered lattice [Equation 2.48](#) translates to [59]

$$\langle \bar{\psi}\psi \rangle = \frac{1}{2} \left(\psi_{2n}^\dagger \psi_{2n} - \psi_{2n+1}^\dagger \psi_{2n+1} \right) = -\frac{c}{\sqrt{\pi}}. \quad (6.1)$$

Additionally, recall the Brillouin zone of staggered fermions with N sites has only $N/2$ modes (cf. [Section 2.3](#)). The total number of lattice sites thus has to be even. Henceforth, we shall call the number of total lattice sites N ‘even’ iff it is divisible by 4, and we shall call it ‘odd’ iff it is only divisible by 2, thus reflecting on the fact that for ‘odd’ number of sites the Brillouin zone actually contains an odd amount of modes, and vice versa. Furthermore, observe the Hamiltonian (3.28) we implemented retrieves axial symmetry in the limit of $e/m \rightarrow \infty$. To see this, note the action of γ_5 on the discretised spinor rebuilt via the relabelling (2.96) and the representation according to (2.3) is equivalent to a translation of one site given periodic boundary conditions [60]. The (massive) Hamiltonian (3.28) displays no invariance under translation by one site as the mass term is odd under this transformation,

$$m \sum_n (-1)^n \psi_{n+1}^\dagger \psi_{n+1} = -m \sum_n (-1)^n \psi_n^\dagger \psi_n, \quad (6.2)$$

but not the (non-local) sum of charge operators,

$$\sum_{n,m} Q_{n+1} v(n+1-m-1) Q_{m+1} = + \sum_{n,m} Q_n v(n-m) Q_m. \quad (6.3)$$

Thus, in the zero mass limit the Hamiltonian (3.28) displays axial symmetry. A truthful simulation of the continuum theory on the lattice with staggered fermions should thus display spontaneously broken symmetry in form of the non-vanishing VEV (6.1) and ideally approach the continuum expectation given in our parameter set as $-c/\sqrt{\pi}$.

Yet, we find this symmetry to be only spontaneously broken in the limit $e/m \rightarrow \infty$ in the case of ‘odd’ lattice sizes, as can be seen in Figure 6.1. For ‘odd’ system sizes we recover a non-vanishing VEV of the chiral order parameter $\langle \bar{\psi}\psi \rangle$ very close to the continuum expectation. For the ‘even’ case, however, the chiral order parameter vanishes in the strong coupling limit.

We find further disagreement between ‘even’ and ‘odd’ system sizes upon inspecting the particle number distribution in the Brillouin zone for the vacuum (cf. Figure 6.2). Here, we find the zero mode of ‘odd’ systems after some threshold $e/m = 1.5$ to be fill maximally with 2 particles, whereas the ‘even’ systems keep the zero mode unoccupied. This substantiates the assumption that the numerical simulation for ‘odd’ and ‘even’ system sizes realises different vacuum states.

The fact that only in the case of ‘odd’ system size we do *not* obtain the wrong VEV for the chiral condensate with regards to the continuum theory leads us to believe we must disregard the simulations of ‘even’ system sizes as artefacts of our discretisation, although we have at present no satisfying *ab initio* answer as to why this should be the case.

Having settled for the correct initial state on ‘odd’ system sizes, we want to inspect the dynamics of the very same. Consequently, we display the particle production rate for strongly coupled QED at ‘odd’ system sizes in Figure 6.4. For the sake of transparency, we enclose the plots for ‘even’ system sizes in Appendix E. We find the particle production rate to increase within small and medium coupling strengths ($e/m \leq 1$). This is in accordance with a naive first-order correction to the particle production rate in the continuum (2.185), which we want to outline here.

The self-energy of the massive Schwinger model in the so-called quenched rainbow approximation is given to infinite order by [61]

$$\Sigma(q^2) = -\frac{e^2}{2\pi m} + \{\text{terms vanishing with } q \rightarrow 0\}, \quad (6.4)$$

implying for the renormalised physical mass m_{phy} of the fermion to depend on the bare mass m and the coupling e as

$$m_{phy} = m - \frac{e^2}{2\pi m}. \quad (6.5)$$

Note the coupling in $1 + 1d$ QED is not renormalised since the photon self-energy (vacuum polarisation) vanishes identically for $q \rightarrow 0$ [61] and the theory is superrenormalisable [27, 44]. If one was to plug into (2.185) this physical mass and demand to measure the electric field in ‘unrenormalised’ critical field strengths,

$$E = \epsilon \frac{m^2}{e}, \quad (6.6)$$

then the particle production rate would be modified like

$$\frac{\mathcal{N}^{\text{mod.}}}{Lt} = \frac{eE}{2\pi} \exp\left\{-\frac{\pi m_{phy}^2}{eE}\right\} = m^2 \frac{\epsilon}{2\pi} \exp\left\{-\frac{\pi}{\epsilon} \left(1 - \frac{1}{2\pi} \left(\frac{e}{m}\right)^2\right)^2\right\}, \quad (6.7)$$

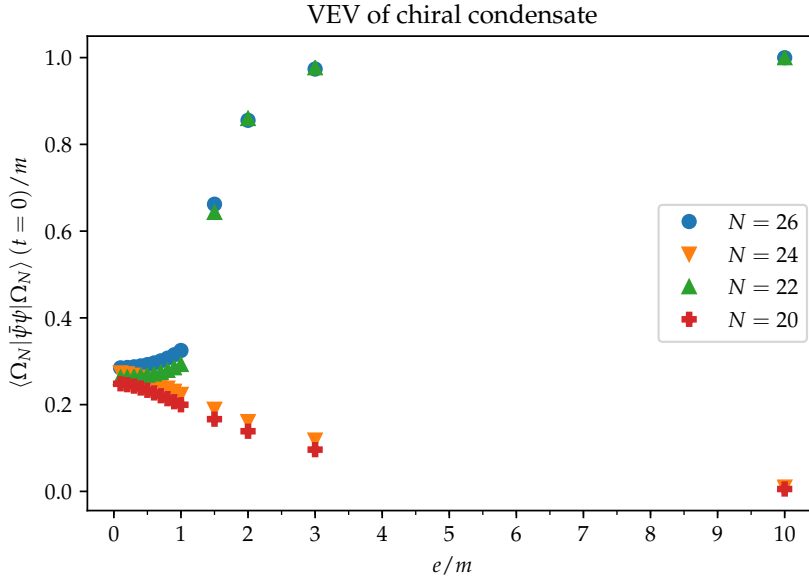
which yields for small couplings a larger production rate, which is in qualitative accordance with our findings in simulations of ‘odd’ system sizes. This corroborates our choice of disregarding ‘even’ system sizes as they display lower production rates for small to medium couplings compared to the original Schwinger formula (cf. [Figure E.1](#)). The numerical simulations can however not accurately reproduce this naive first-order correction quantitatively for small couplings, as can be observed in [Figure 6.6](#). This naive first-order approximation by no means has to serve as a quantitative reference since renormalisation on the finite lattice must also be dependent on the lattice spacing and the physical volume. However, as we are with $am \simeq 0.27$ and $Lm = 7$ on a rather coarse lattice we shall treat this naive first-order correction as a qualitative reference whose demands we meet. Lastly we want to emphasise that the 2nd order improvement yields quantitatively very similar results for small and medium couplings as can be inspected in [Figure 6.4a](#). Only for large couplings they differ. As we derived the improvement coefficients for the free theory, we cannot argue they should yield quantitative similar results for strong coupling, although we can say that the improvement coefficients, in general, tend to decrease by one order of magnitude comparing two ‘neighbouring’ coefficients (cf. [Table 2.1](#)). Thus, it can be argued any quantitative disagreement must be related to a significant change in the relevant degrees of freedom of the system.

The particle number shows clear worsening regarding the UV-convergence, that is keeping Lm fixed and increasing N , with stronger couplings (cf. [Figure 6.5](#) as well as [Figure 6.5](#)). Furthermore, it displays a stark quantitative change from $e/m = 1$ to $e/m = 1.5$ thus reflecting on the phase transition from the unbroken phase to the spontaneously broken phase (cf. [Figure 6.1](#)). This, however, should be of no surprise. The particle number is an observable derived from the free theory, and by virtue of perturbation theory expanded onto a weakly interacting theory. By no means should this also apply to the strong interacting case. Displaying a stark shift from $e/m = 1$ to $e/m = 1.5$ and growing with couplings beyond that, the particle number of the vacuum state reflects on the inadequacy of the concept we attach to the observable we call particle number at such high couplings.

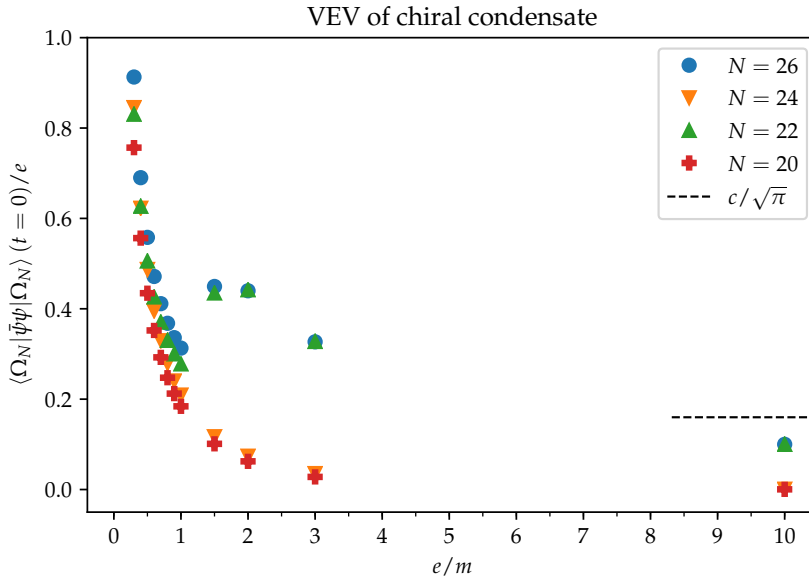
Furthermore, the total energy $\langle H \rangle$ and the electric field energy $\langle H_E \rangle$ are displayed [Figure 6.7](#). Inspecting the electric field energy content for small to medium couplings ([Figure 6.7c](#)) we may consider the initial drop in energy in the field as a result of the quench, since the time window corresponds also to the settling of the particle production rate to the linear growth of late times (cf. [Figure 6.3a](#)). This, however, cannot be confirmed within our results from simulation as such late times we were currently inaccessible. The dynamics at large couplings should be dominated by the massive free bosonic field. We thus expect the energy content to be dominated by the part of the Hamiltonian describing the electric field content, as we have seen in [Section 2.1](#). We find the total energy to be dominated by the electric field energy at couplings ≥ 2 . There, both energies show poor UV-convergence. Considering the dynamics at large couplings, we thus want to suggest the quantitative results must be taken with a grain of salt. Generally speaking, we expect the system in the massless or ultra-strong coupling limit to have massive bosonic excitations with mass $\propto e$. Consequently, the continuum limit of this theory is given by $\#a \cdot e \rightarrow 0$ with some numerical prefactor. Thus, we cannot arbitrarily take e/m high when we keep am constant.

In this chapter we presented our findings on strong coupling QED simulated on a staggered lattice with $Lm = 7$ and $E/E_c = 1.5$. We found contradictory results for ‘even’ and ‘odd’ system sizes and disregarded the former by virtue of knowing the vacuum expectation value of the chiral order parameter $\langle \bar{\psi}\psi \rangle_0$ must not vanish in the continuum theory for $E/E_c = 1.5$. Having settled for ‘odd’ system sizes, we found the particle production rate to grow with small to medium coupling strengths ($e/m \leq 1$). Furthermore, we emphasised our results for the dynamics of strong coupling QED are not to be taken quantitative as they show no UV-convergence yet.

While papers studying spontaneous symmetry breaking of the Schwinger model on finite lattices with *massless* staggered fermions include Refs. [29, 60, 62, 63], we are unaware of any reference reproducing our finding that coming from the *massive* theory and approaching the infinite coupling limit requires an ‘odd’, that is only divisible by 4 not 2, number of lattice sites in order to observe spontaneous symmetry breaking on a staggered lattice.



(a) VEV in units of mass



(b) VEV in units of coupling

Figure 6.1: The vacuum of the massive Schwinger model for ‘odd’ N does *not* retrieve translation invariance as $\lim_{e/m \rightarrow \infty} \langle \bar{\psi}\psi \rangle \neq 0$ although at similar cutoff $am \simeq 0.27, 0.29$ the vacuum of the system with ‘even’ N arrives numerically at 0. (a) VEV measured in m . For small couplings the two cases of ‘odd’ and ‘even’ are displaying similar behaviour in the VEV measured in m as well as in particle number (cf. Figure 6.2) Only between $e/m = 1$ and $e/m = 1.5$ a significant quantitative disagreement shows up. (b) VEV measured in e . Starting with $m \neq 0$ and continuously decreasing m/e , only ‘odd’ system sizes seem to qualitatively simulate the non-zero VEV of the spontaneously symmetry broken continuum theory (cf. (2.48)), neglecting a sign.

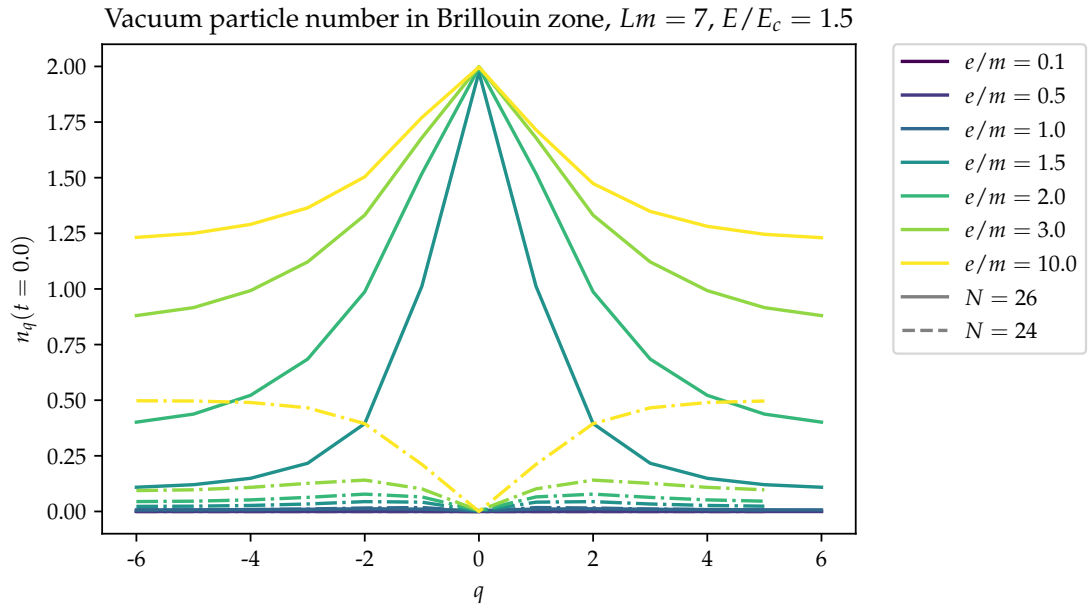


Figure 6.2: Large quantitative disagreement between ‘odd’ and ‘even’ sites show up between $e/m = 1$ and $e/m = 1.5$. The initial particle number at the zero mode is for ‘odd’ $N = 26$ at $e/m \geq 1.5$ at the highest possible value of 2, while for ‘even’ $N = 24$ it vanishes throughout the tested range of e/m .

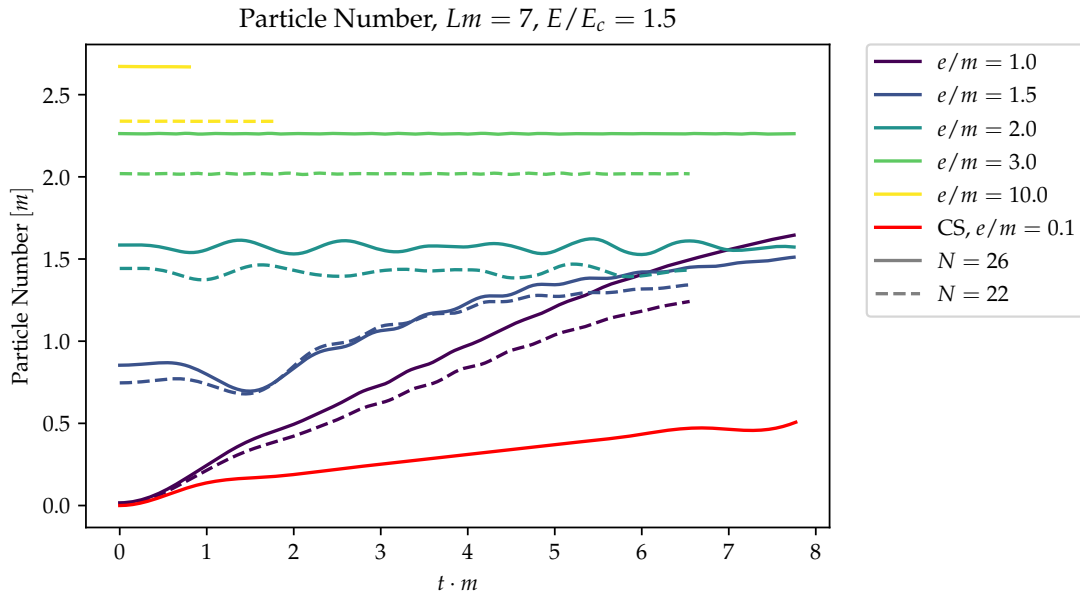
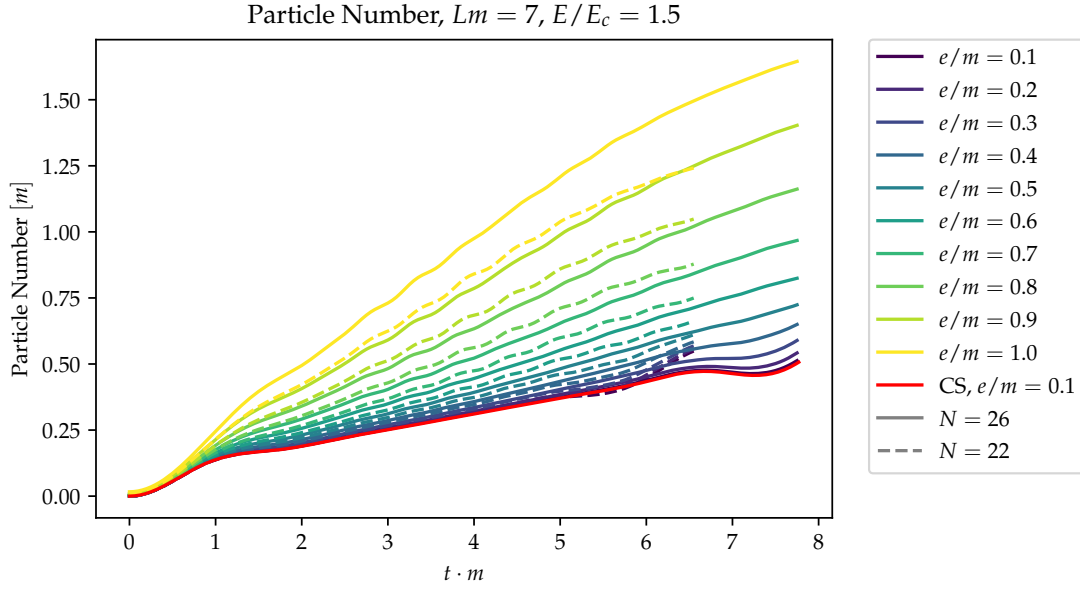


Figure 6.3: Particle number for strongly coupled QED and ‘odd’ system sizes $N = 26$, marked with solid lines, and $N = 22$, marked with dashed lines. For comparison in red the result at same N but $e/m = 0.1$ with classical-statistical (CS) simulation. (a) For small and medium couplings $e/m \leq 1$ the particle production rate grows, and it is less converged in the UV as e/m grows as can be seen in Figure 6.5. (b) The step from $e/m = 1 \rightarrow 1.5$ marks a clear cut as the particle number is already at $tm = 0$ non-vanishing. Beyond $e/m = 1.5$ the Schwinger mechanism effectively cannot produce particles as the zero mode of those vacuum states are fully occupied (cf. Figure 6.2). The UV convergence with larger couplings appears to worsen.

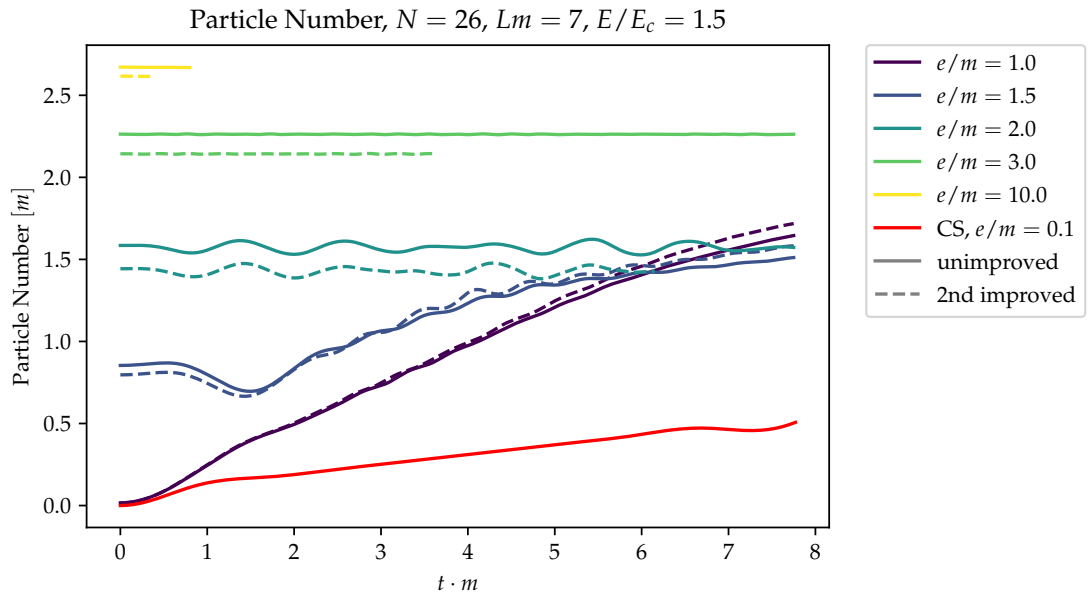
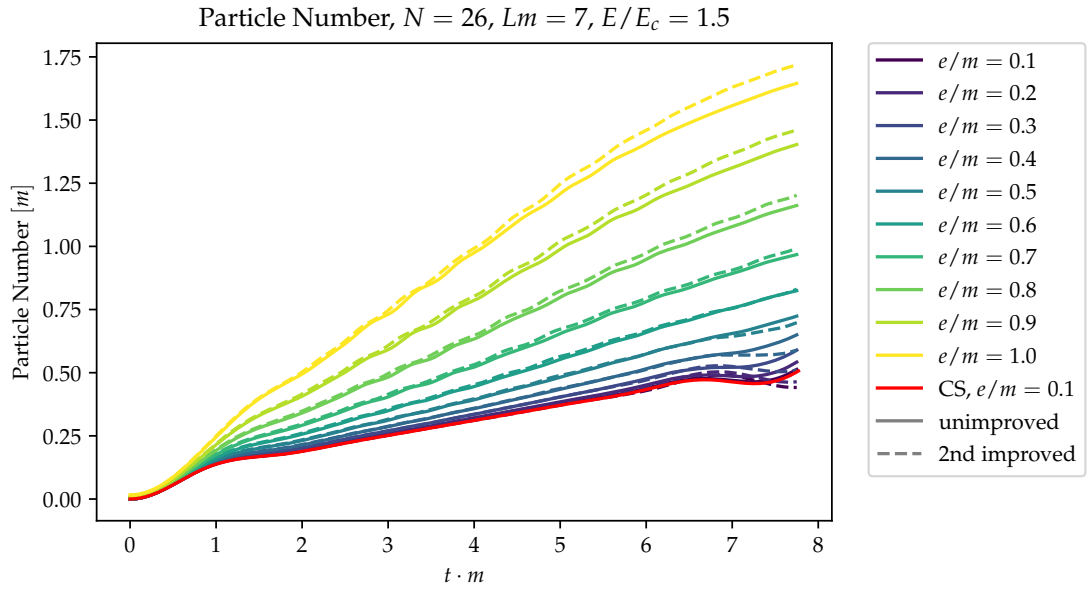


Figure 6.4: Particle number for strongly coupled QED $N = 26$, unimproved in solid lines, and 2nd order improvement marked with dashed lines. For comparison in red the result at same N but $e/m = 0.1$ with classical-statistical (CS) simulation. (a) For small and medium couplings $e/m \leq 1$ the particle production rate grows, and the 2nd order improved curve yields quantitatively very similar results. ?? Only beyond $e/m = 1.5$ the improved curve and the unimproved yield quantitative different results. As we derived the improvement coefficients for the free theory, we can not expect the improved and unimproved curve to yield similar results at strong couplings.

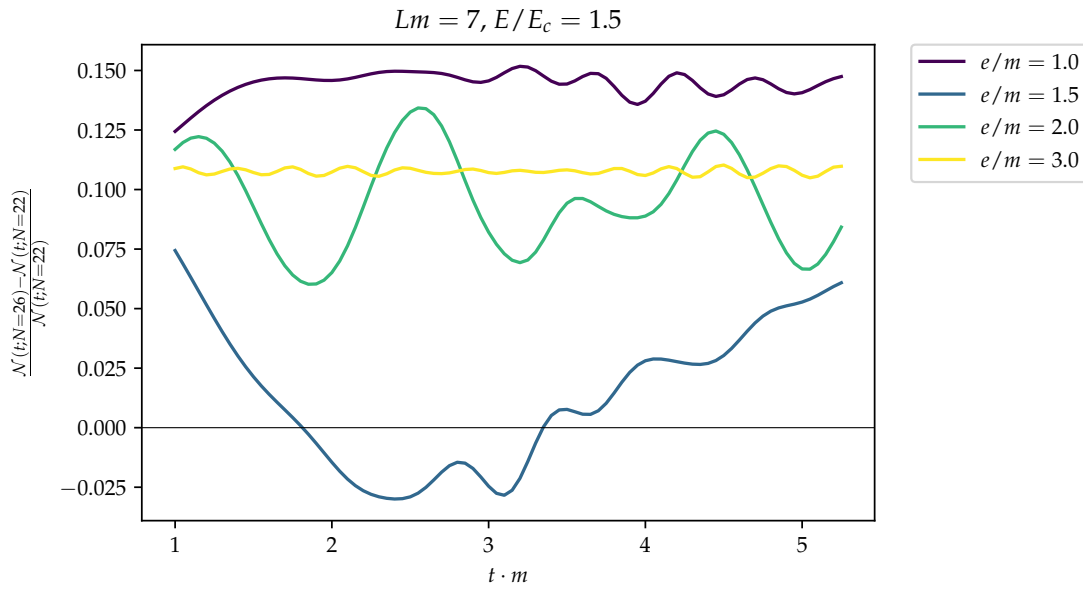
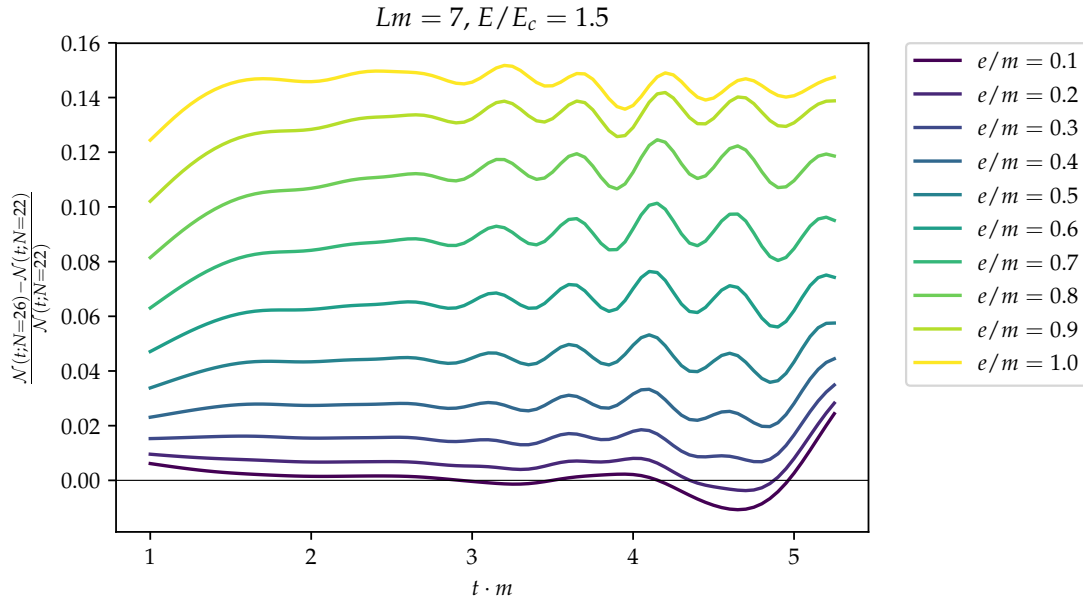


Figure 6.5: UV-convergence of particle number of systems with decreasing the lattice spacing from $am \simeq 0.32$ to $am \simeq 0.27$. (a) A clear tendency from low to strong coupling the UV convergence worsens. This is expected as at strong couplings the continuum limit is given by $ae \rightarrow 0$.

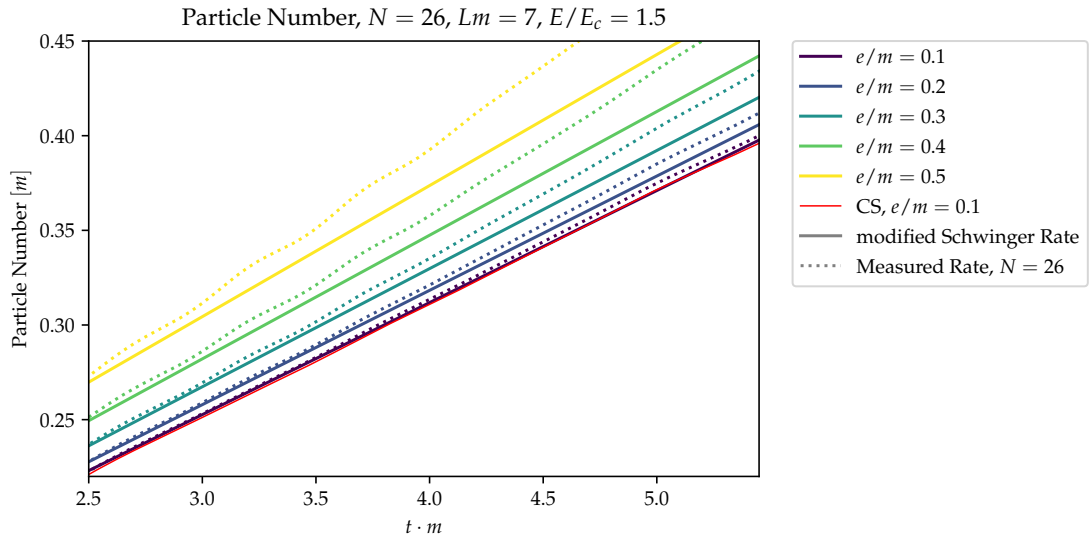
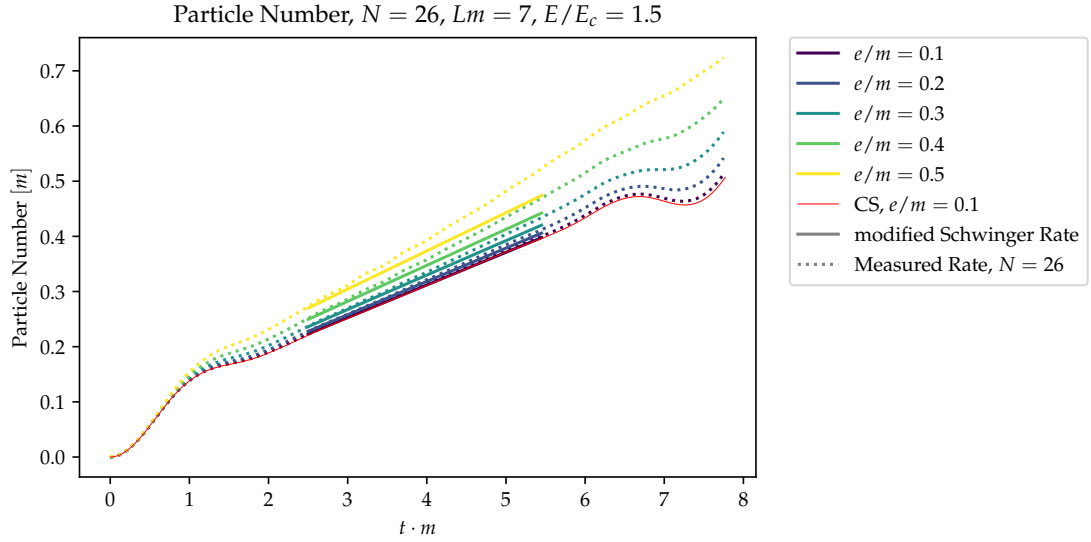


Figure 6.6: Plotted in solid lines is the modified particle production rate according to (6.7). In dotted lines is the production rate measured on ‘odd’ lattice sizes. (a) Albeit yielding the qualitative same tendency, the modified production rate is numerically not realised in our simulations as can be also inspected in the close-up in (b). The numerical difference is smaller for smaller couplings. This naive first order correction marks only a qualitative reference as renormalisation on the lattice depends also on lattice spacing a as well as physical volume Lm , and we are with $am = 0.27$ and $Lm = 7$ neither in infinite volume nor continuum limit.

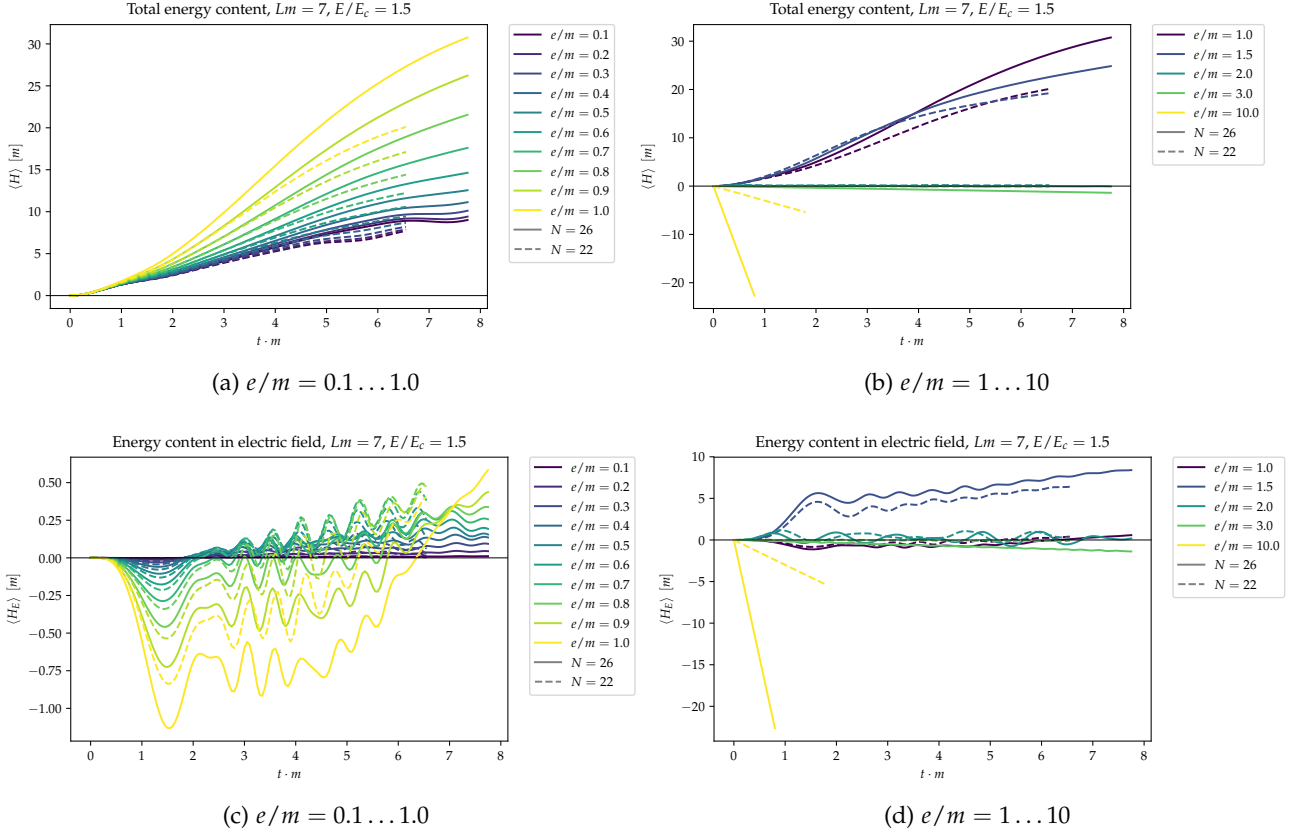


Figure 6.7: Total energy $\langle H \rangle$ of ‘odd’ system sizes: (a) for small to medium couplings the total energy grows reflecting on particle pair production, while (b) for strong couplings the picture changes dramatically from $e/m = 1.5$ to $e/m = 3.0$ where the growth in energy transitions positive gain over steady-state to energy loss. Upon further increasing the coupling for the simulation times accessible the system only loses energy. UV-convergence is at large couplings far from reached. We take it, we cannot trust the simulation of the dynamics at such large couplings. Electric field energy $\langle H_E \rangle$ of ‘odd’ system sizes: (c) for small to medium couplings the initial drop in $\langle H_E \rangle$ may be considered as a result of the quench, since the time window corresponds also to the settling of the particle production rate to the linear growth of late times (cf. Figure 6.3a). Overall the electric field energy is still growing. (d) Here, too, behaviour from $e/m = 1.5$ to $e/m = 2.0$ changes dramatically in $\langle H_E \rangle$. We can observe with (b) at such large couplings the energy is almost completely contained in $\langle H_E \rangle$. UV-convergence is at large couplings far from reached.

CONCLUSION & OUTLOOK

7.1 CONCLUSION

In [Section 2.4](#), after having introduced Symanzik’s improvement programme, we opted only for irrelevant kinetic operators to improve our theory. In [Section 2.4.6](#) we diagonalised the improved free theory and found the 1st order improved dispersion relation to have a more accurate coverage throughout the Brillouin zone which we quantified to be about 1.5 times larger compared to the unimproved curve given reasonable error margins of a few per cent. We then showed in [Section 2.5.3](#), the average current is upon improving more accurate both in powers of a and powers of t . This was confirmed by an illustrating classical-statistical simulation (cf. [Figure 2.3b](#)). Even at such large system sizes and small lattice spacings chosen in this illustrating simulation, the current displays clear benefits upon improving—quantitatively reminiscent of the gain in [Section 2.4.6](#), while the particle production rate has already converged to its continuum value. Subsequently, we investigated the UV-convergence of the particle production rate on small system sizes with exact diagonalisation methods and observed no obvious benefits upon improving our theory. Consequently, we expanded the search for better UV-convergence upon improving by using classical-statistical simulations to reach larger system sizes and smaller lattice spacings. By employing statistics over view simple fit procedures to extract faithfully a linear growth rate, we observe clear benefits of view, i.e. one digit, per cent points upon improving in certain parameter regimes. Considering the parameters we realised, improvements are particularly beneficial for the particle production rate when the electric field strength is between 1 or 2 critical field strengths. Higher critical field strengths render the benefits insignificant. Parameters, we realised, displaying most benefits from improvements include $Lm = 7$ and $E/E_c = 1$ ([Figure 5.3c](#)), $Lm = 7$ and $E/E_c = 1.5$ ([Figure 5.4b](#)), as well as $Lm = 5.5$ and $E/E_c = 2$ ([Figure 5.5c](#)). However, none of those improved runs, to first and second order, can reproduce our previous finding of a gain of 1.5 as seen in the dispersion relation and the average current, although we covered a wide range of parameters for E/E_c and Lm in which we always sampled from low cutoff and small system size, such that the linear growth in particle production was hardly observable, to clearly converged system size and large cutoff, such that $2t_{max}$ was long enough to retrieve a faithful averaged fit.

We therefore conclude that neither the improved dispersion relation, which is disposed of lattice artefacts up to $\mathcal{O}(a^{2(n+1)})$ given improvement order n , nor the average current, which we showed is also disposed of lattice artefacts up to $\mathcal{O}(a^{2(n+1)})$ given improvement order n , reduce the lattice artefacts in the particle number significantly, nor is the particle production rate positively affected by the same amount above mentioned observables are. Since the dispersion relation is most significantly improved in the upper half of the Brillouin zone (cf. [Figure 2.1](#)), while the current is most significantly improved at late times (cf. [Figure 2.3b](#) when the particles in the system reached

high momenta (cf. [Figure A.1c](#)), we must conclude that improving our theory with only irrelevant higher derivatives mostly leads to an improvement in observables which are sensitive to the high momentum range within the Brillouin zone. The particle number is apparently no such observable as we infer it tests merely the low end of the momentum spectrum.

In hindsight, the substantial benefits improvements yield in Refs. [64–66] may be due to a combination of two things. Firstly, the (in)accuracy of the *ibid.* employed unimproved Wilson fermions to $\mathcal{O}(a)$. As unimproved staggered fermions are already precise to $\mathcal{O}(a^2)$ they have an innate advantage over Wilson fermions regarding the low momentum description of our system. We suggest this innate advantage suffices to let staggered fermions adequately describe the momentum range which the particle number is sensitive to. And more important secondly, above mentioned Refs. incorporated back reactions from the fermion current onto the electric field. This allows for a negative feedback loop in which, naively viewed, particles are created homogeneously and accelerated in the strong electric field. This builds up a current which in turn reduces the electric field whenever energy is conserved. Clearly then, one can benefit from the longer and more accurate description of the currents and improvements find their way into the particle number via the current. However, within the approximation of a constant electric field, we are neither conserving energy nor allowing for a feedback from the currents onto the field. Thus, the particle number appears to be sensitive only to the low momentum range.

In [Chapter 6](#), we investigated the Schwinger mechanism for particle pair production in a constant background field for a system which we restricted to the physical subspace where we implemented Gauss law. Together with unbiased exact diagonalisation methods this enabled us to perform simulations in the strong coupling regime of QED in $1 + 1d$. We found strong disagreement between systems of sizes divisible by 4, which we called ‘even’, and system sizes only divisible by 2, which we called ‘odd’, as they have only an odd amount of modes realised in the Brillouin zone, and vice versa. We discarded the simulations with ‘even’ lattice size by virtue of knowing the vacuum expectation value of the chiral order parameter $\langle \bar{\psi}\psi \rangle_0$ to take a non-vanishing value which is given for our parameter set given by (2.48). The systems of ‘even’ sites however realised a numerically vanishing expectation value, while the systems of ‘odd’ size yielded a result corroboratively close to the continuum value. Furthermore, we found the vacuum state to display further disagreement in the particle number distribution, as ‘odd’ systems realise beyond $e/m = 1.5$ a zero mode in the Brillouin zone completely filled with 2 fermions, while ‘even’ lattice sites behave diametrically opposite; they realise throughout the tested range of e/m an empty zero mode.

Subsequently, having settled for ‘odd’ system sizes we investigated the dynamics of its vacuum state upon quenching the electric field from off to $1.5E_c$. We observed for small to medium couplings ($e/m \leq 1$) a rise in particle pair production. Our choice of ‘odd’ system size was substantiated after discussing a naive first-order correction to Schwinger’s formula of the particle pair production rate (6.7). This first-order correction captures the (finite) renormalisation of the bare mass to the physical mass and comes about when one demands to measure the electric field strengths in ‘unrenormalised’ critical fields while Schwinger’s formula is modified by replacing the bare mass with the physical mass. Our lattice simulations could not quantitatively agree with this

modified formula. This should however not be of great concern as renormalisation on the lattice manifestly incorporates the cutoff $\sim \frac{1}{a}$ and the physical volume Lm . Since we simulated on a coarse lattice with $am \simeq 0.26$ and Lm we do not expect the continuum renormalisation formula to hold. We take this modified formula as a qualitative reference whose demand we meet. As the particle number of the vacuum state changes from $e/m = 1$ to $e/m = 1.5$ dramatically from numerically zero to a significant non-vanishing quantity, it reflects on the phase transition from the unbroken phase to the spontaneously broken phase (cf. [Figure 6.1](#)). Furthermore, the growth of the very same reveals the inadequacy of the concept we attach to its observable. The particle picture fails in such ‘intermediate’ regimes of the Schwinger model—only in the ultra strong coupling limit we shall retrieve a free model.

We then emphasised at couplings beyond $e/m \sim 1.5$ the dynamics of the Schwinger model is most probably not accurately captured as the total energy as well as the electric field energy in the system display ever less UV-convergence with ever larger couplings.

The unbiased method of exact diagonalisation combined with the restriction of the Hilbert space on the physical subspace via implementing Gauß’s law allowed us to take an unprecedented approach to strong coupling dynamics in the Schwinger model, namely from the *massive* theory starting gradually approaching $e/m \rightarrow \infty$. Consequently, we were able to quantitatively estimate the correction to Schwinger’s formula of particle pair production for small to medium couplings $e/m \leq 1$. We found a linear growth with significant higher production rate already for relatively small couplings. Our findings can offer a benchmark to other numerical methods being valid only to low order in coupling as to how large the coupling may be to faithfully reproduce the Schwinger rate in the weak coupling limit.

7.2 OUTLOOK

Concerning the outlook with regards to improvements, we suggest that further investigation must comprise interaction terms, as we concluded improving only with irrelevant higher derivative terms will mostly be reflected in a better description of the kinematics of the constituents of our system. This may be even performed in a non-perturbative fashion since this would entail an improvement in the strong coupling regime of the Schwinger model, to which our approach via exact diagonalisation offers an accessible route.

Regarding the methodology, one might like to depart from the approximation of a constant background field, as it allows the observation of plasma oscillation. Moreover, the particle number can then derive benefit from improving our theory only with higher derivatives. This would particularly mean one has to account for the two boundary degrees of freedom in a suitable way, such that their dynamics is depicted accurately in some sense while their Hilbert space must be truncated, in order to still be suitable for the exact diagonalisation approach. Naturally, one might think of a quantum link model to implement this. Furthermore, the methodology can be expanded and larger system sizes realised using more symmetries of our system to restrict the Hilbert space in size, as this by fare the most significant constraint in the numerical simulation.

Lastly, we managed to retrieve the spontaneously broken phase of the Schwinger model in the strong coupling limit yet we have at present no satisfying *ab initio* answer at hand why this requires an ‘odd’ system sizes. One can only speculate over the behaviour at larger N —not at least an other reason to use further symmetries to restrict the Hilbert space. The peculiarities of ‘even’ and ‘odd’ system sizes ought to be investigated further. Particularly, since such behaviour can also be observed in similar systems [67], but also since we are unaware of any other reference confirming our finding of reaching the spontaneously broken phase from the massive theory only via ‘odd’ system sizes.

ILLUSTRATION OF THE SCHWINGER EFFECT IN THE BRILLOUIN ZONE



Here we append the plots of the particle number distribution as well as the energy density and the dispersion relation in the Brillouin zone for the setup discussed in [Section 2.5.5](#).

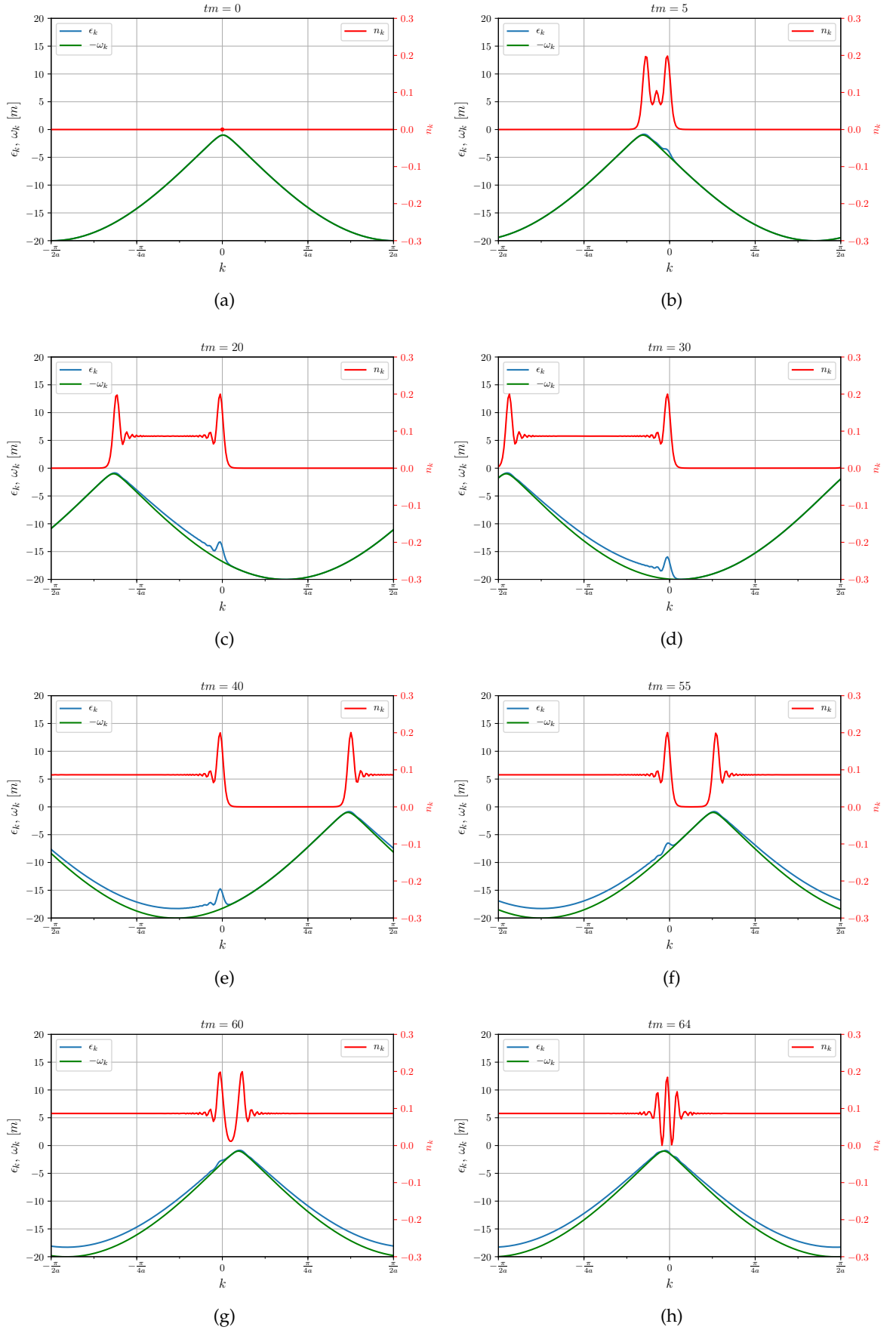


Figure A.1: A series of plots with the Brillouin zone on the horizontal axis. On the right vertical axis is displayed the value of ω_k and ϵ_k while on the left vertical axis one finds the value of n_k . Series goes through different time steps, starting at $tm = 0$ and ending at $tm = 64 \simeq 2t_{max}m$. Demonstrating periodic boundary conditions, the particle number distribution crosses at $t_{max}m$ the BZ edge and comes back at opposite momenta undisturbed. Only at $2t_{max}m$ it interferes with itself.

FERMIONIC OPERATORS IN SPIN DOF

B.1 JORDAN-WIGNER TRANSFORM

Here, we explain how to map fermionic degrees of freedom onto spin degrees of freedom. This is necessary as a direct matrix representation for any spin operator with arbitrary but finite spin length exists.

While spin operators $S_n^+ = S_n^x + iS_n^y$ and $S_n^- = S_n^x - iS_n^y$ fulfil the canonical anti-commutation relation on-site ($\{S_n^-, S_n^+\} = 1$), they *commute* offsite ($[S_n^-, S_m^+] = 0, n \neq m$). If one would be able to 'dress' them in such a way they *anti-commute* off-site ($\{\tilde{S}_n^-, \tilde{S}_m^+\} = \delta_{nm}$), the map of fermionic DoF to spin DoF would be complete. This 'dressing' in one dimension was first discovered by Jordan and Wigner 1928 [68].

In one dimension, the map of a single (spinless) fermionic degree of freedom onto a spin (qubit) degree of freedom reads as

$$\psi_n = \prod_{l=0}^{n-1} [i\sigma_l^z] \sigma_n^- = \exp\left\{i\frac{\pi}{2} \sum_{l=0}^{n-1} \sigma_l^z\right\} \sigma_n^-, \quad (\text{B.1})$$

$$\psi_n^\dagger = \prod_{l=0}^{n-1} [-i\sigma_l^z] \sigma_n^+ = \exp\left\{-i\frac{\pi}{2} \sum_{l=0}^{n-1} \sigma_l^z\right\} \sigma_n^+, \quad (\text{B.2})$$

$$\psi_n^\dagger \psi_n = \frac{1}{2} (\sigma_n^z + 1). \quad (\text{B.3})$$

Thus, we charge operator reads in qubit DoF as

$$Q_n = \frac{1}{2} (\sigma_n^z + (-1)^n). \quad (\text{B.4})$$

Since we require the total number of lattice sites to be even, we can deduce in the case of total vanishing charge,

$$0 = \sum_{n=0}^{2N-1} Q_n = \frac{1}{2} \sum_{n=0}^{2N-1} \sigma_n^z, \quad (\text{B.5})$$

translates to total vanishing 'magnetisation' in qubit degrees of freedom.

B.2 HAMILTONIAN

Applying the Jordan–Wigner transform to the Hamiltonian (3.28) we obtain

$$\begin{aligned}
H &= -\frac{i}{2a}c_1 \sum_{n=0}^{2N-2} (\bar{U}\sigma_n^+ i\sigma_n^z \sigma_{n+1}^- - \text{h.c.}) - \frac{i}{2a}c_3 \sum_{n=2N-2}^{2N-4} (\bar{U}^3 \sigma_n^+ i\sigma_n^z i\sigma_{n+1}^z i\sigma_{n+2}^z \sigma_{n+3}^- - \text{h.c.}) \\
&\quad - \frac{i}{2a}c_1 \bar{U}\sigma_{N-1}^+ \exp\left\{-i\frac{\pi}{2} \sum_{l=0}^{2N-1} \sigma_l^z\right\} i\sigma_{2N-1}^z \sigma_0^- \\
&\quad - \frac{i}{2a}c_3 \bar{U}^3 \sigma_{N-3}^+ \exp\left\{-i\frac{\pi}{2} \sum_{l=0}^{2N-1} \sigma_l^z\right\} i\sigma_{N-3} i\sigma_{N-2} i\sigma_{N-1} \sigma_0^- - \text{h.c.} \\
&\quad + m \sum_{n=0}^{2N-1} (-1)^n \sigma_n^+ \sigma_n^- \\
&\quad + H_E
\end{aligned} \tag{B.6}$$

$$\begin{aligned}
&= -\frac{1}{2a}c_1 \sum_{n=0}^{2N-1} (\bar{U}\sigma_n^+ \sigma_{n+1}^- + \text{h.c.}) + \frac{1}{2a}c_3 \sum_{n=0}^{2N-1} (\bar{U}^3 \sigma_n^+ \sigma_{n+1}^z \sigma_{n+2}^z \sigma_{n+3}^- + \text{h.c.}) \\
&\quad + m \sum_{n=0}^{2N-1} (-1)^n \sigma_n^+ \sigma_n^- \\
&\quad + H_E,
\end{aligned} \tag{B.7}$$

where

$$\begin{aligned}
H_E &= -e^2 \frac{2N-3}{2(2N-2)} \sum_{n=0}^{2N-1} \left[\sum_{d=0}^N \left(d + \frac{d^2-3d+2}{2N-3} \right) Q_n (Q_{n+d} + Q_{n-d}) \right. \\
&\quad \left. + Q_n (Q_{n+1} + Q_{n-1}) + \frac{4N^2-8}{4(2N-3)} Q_n Q_{n+N} \right],
\end{aligned} \tag{B.8}$$

and according to (B.4)

$$\begin{aligned}
Q_n (Q_{n+d} + Q_{n-d}) &\simeq \frac{1}{4} \left[\sigma_n^z (\sigma_{n+d}^z + \sigma_{n-d}^z) + (-1)^n (\sigma_{n+d}^z + \sigma_{n-d}^z) \right. \\
&\quad \left. + \sigma_n^z \left((-1)^{n+d} + (-1)^{n-d} \right) \right],
\end{aligned} \tag{B.9}$$

$$Q_n Q_{n+N} \simeq \frac{1}{4} \left[\sigma_n^z \sigma_{n+N}^z + (-1)^n \sigma_{n+N}^z + (-1)^{n+N} \sigma_n^z \right], \tag{B.10}$$

where ‘ \simeq ’ implies equality up to constant terms.

B.3 TRANSLATION OF STATISTICAL PROPAGATOR

Here, we formulate the statistical propagator

$$F_{nm} = F(n, m; t) := \frac{1}{2} \langle \Psi(t) | [\psi_n, \psi_m^\dagger] | \Psi(t) \rangle, \tag{B.11}$$

in terms of qubit degrees of freedom.

First, it shall be noted that F_{nm} is self-adjoint w.r.t. the coordinates n and m . Hence, we can assume w.l.o.g. $n > m$ and taking the hermitian conjugate in the other case.

We find

$$\frac{1}{2} \langle [\psi_n, \psi_m^\dagger] \rangle = \frac{1}{2} \left\langle \left[\sigma_n^- \prod_{l < n} [i\sigma_l^z], \prod_{k < m} [-i\sigma_k^z] \sigma_m^+ \right] \right\rangle \quad (\text{B.12})$$

$$= \frac{1}{2} i^{n-m} \langle [\sigma_n^- \sigma_{n-1}^z \cdots \sigma_m^z, \sigma_m^+] \rangle \quad (\text{B.13})$$

$$= \frac{1}{2} i^{n-m} \langle \sigma_n^- \sigma_{n-1}^z \cdots \sigma_{m+1}^z [\sigma_m^z, \sigma_m^+] \rangle \quad (\text{B.14})$$

$$= i^{n-m} \langle \sigma_n^- \sigma_{n-1}^z \cdots \sigma_{m+1}^z \sigma_m^+ \rangle, \quad (\text{B.15})$$

and in the case $n = m$, we have

$$\frac{1}{2} \langle [\psi_n, \psi_n^\dagger] \rangle = -\frac{1}{2} \langle \sigma_n^z \rangle \quad (\text{B.16})$$

B.4 CURRENT OPERATOR

Here, we want to express the fermion current operator (2.190) in terms of spin operators. Recalling $\sigma^+ \sigma^z = -\sigma^+$, we may write the current as

$$j_n = \frac{-i}{2a} \left[c_1 (\bar{\mathcal{U}} \sigma_n^+ \sigma_{n+1}^- - \text{h.c.}) - c_3 (\bar{\mathcal{U}}^3 \sigma_n^+ \sigma_{n+1}^z \sigma_{n+2}^z \sigma_{n+3}^- - \text{h.c.}) \right]. \quad (\text{B.17})$$

SUPPLEMENTARY PLOTS: UV CONVERGENCE SERIES



C.1 EXACT DIAGONALISATION

The supplementary plots to [Section 5.1](#) for the convergence series of exact diagonalisation simulations without implementing Gauß's law can be found in [Figure C.1](#) and [Figure C.2](#)

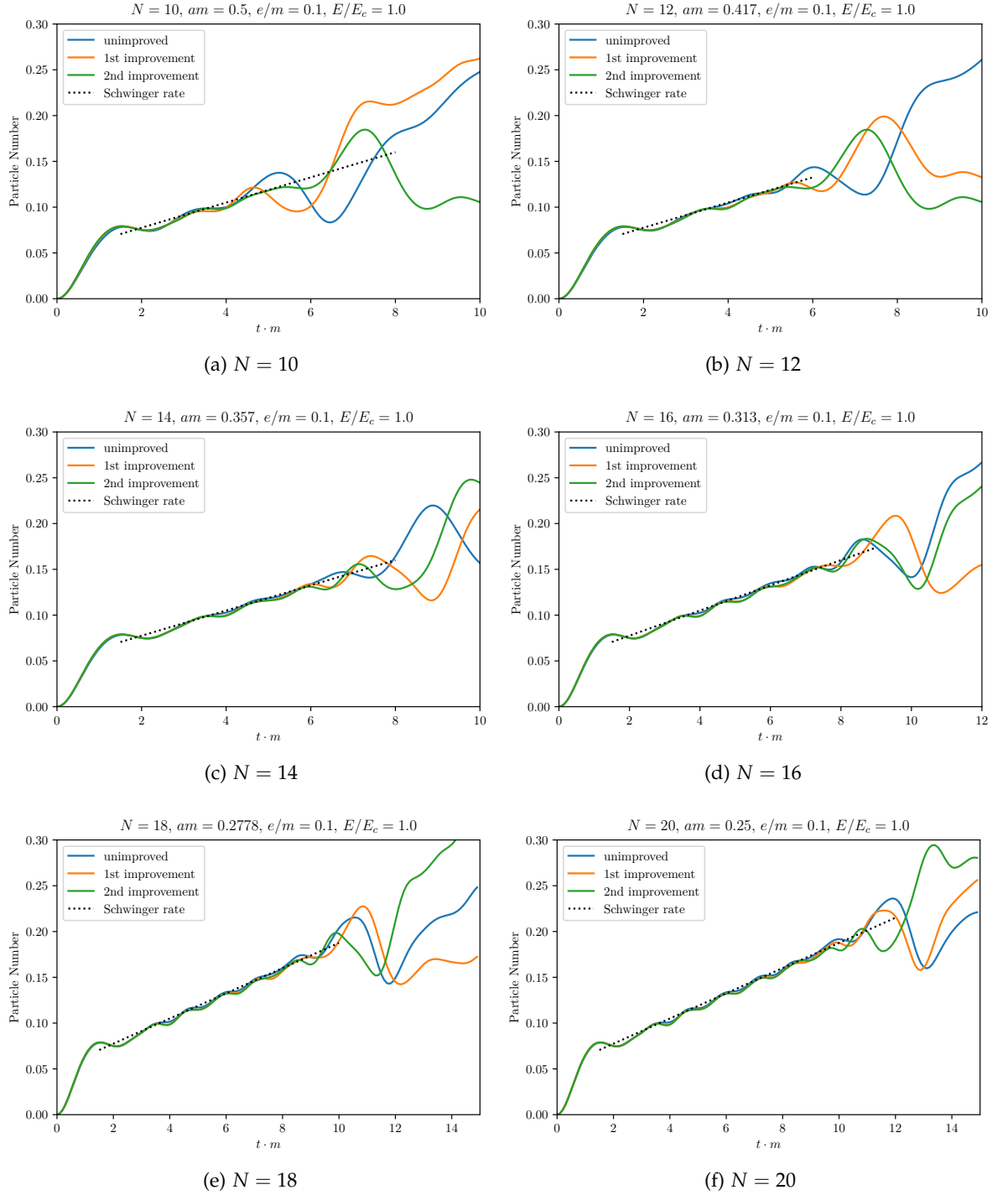


Figure C.1: UV convergence series with $Lm = 5$, $E/E_c = 1$, $e/m = 0.1$. For reference we indicated the analytic prediction for late times with a black dotted line together with the label ‘Schwinger rate’.

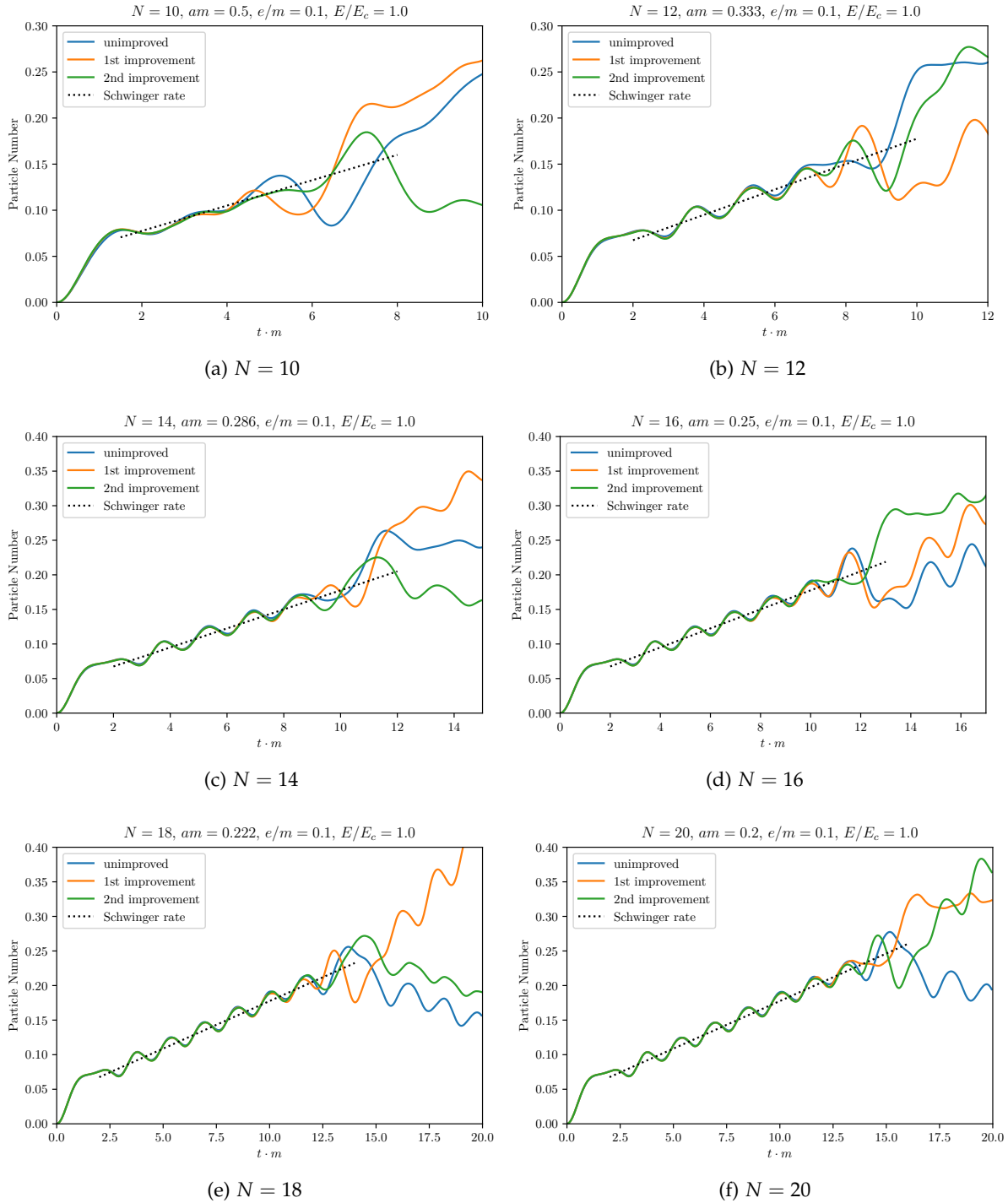
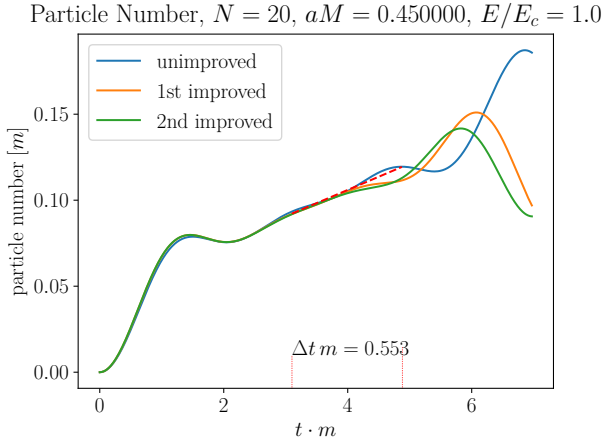


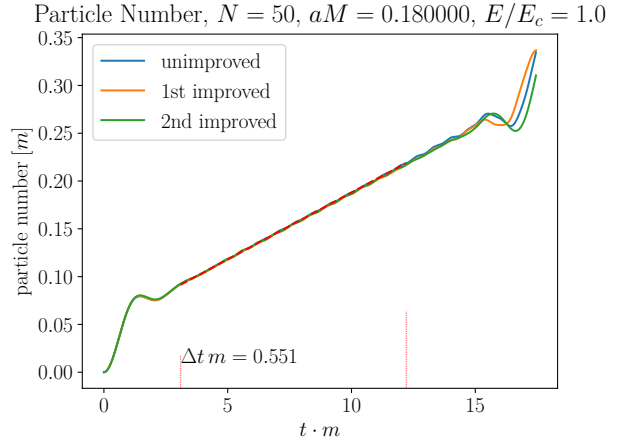
Figure C.2: UV convergence series with $Lm = 4$, $E/E_c = 1$, $e/m = 0.1$. For reference we indicated the analytic prediction for late times with a black dotted line together with the label 'Schwinger rate'.

C.2 CLASSICAL STATISTICAL SIMULATION

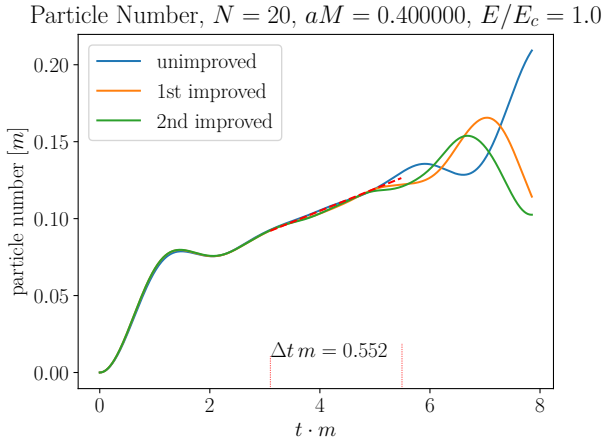
The supplementary plots to [Section 5.2](#) for the convergence series of classical-statistical simulations can be found in [Figure C.2](#) for $E/E_c = 1$, for $E/E_c = 1.5$ in [Figure C.2](#), for $E/E_c = 2$ in [Figure C.3](#), for $E/E_c = 5$ in [Figure C.4](#), and for $E/E_c = 7$ in [Figure C.5](#)



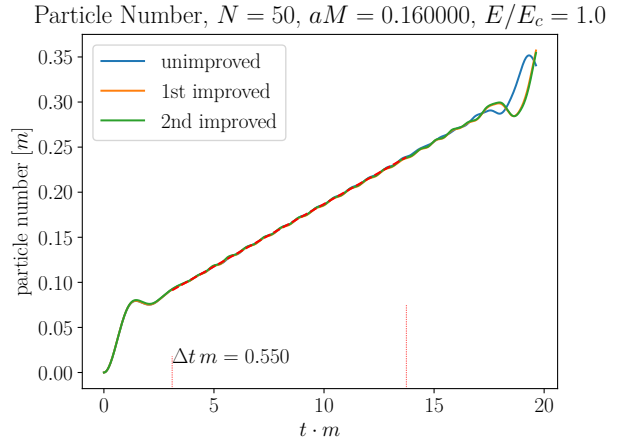
(a) $Lm = 9$, $N = 20$



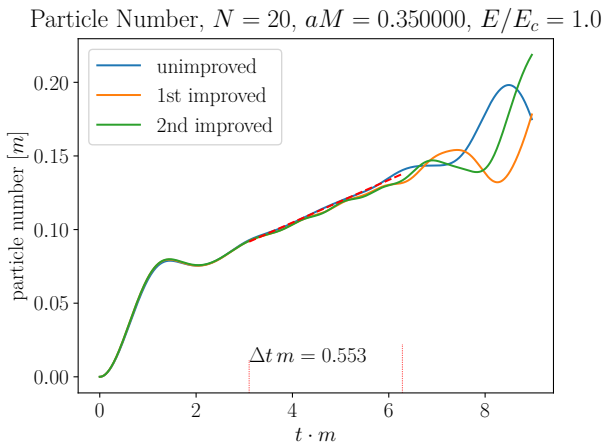
(b) $Lm = 9$, $N = 50$



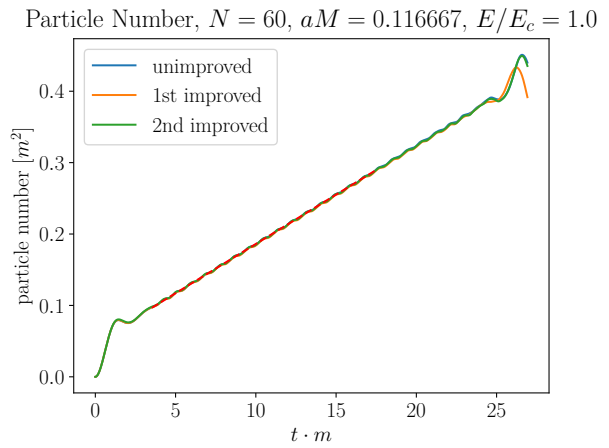
(c) $Lm = 8$, $N = 20$



(d) $Lm = 8$, $N = 50$



(e) $Lm = 7$, $N = 20$



(f) $Lm = 7$, $N = 60$

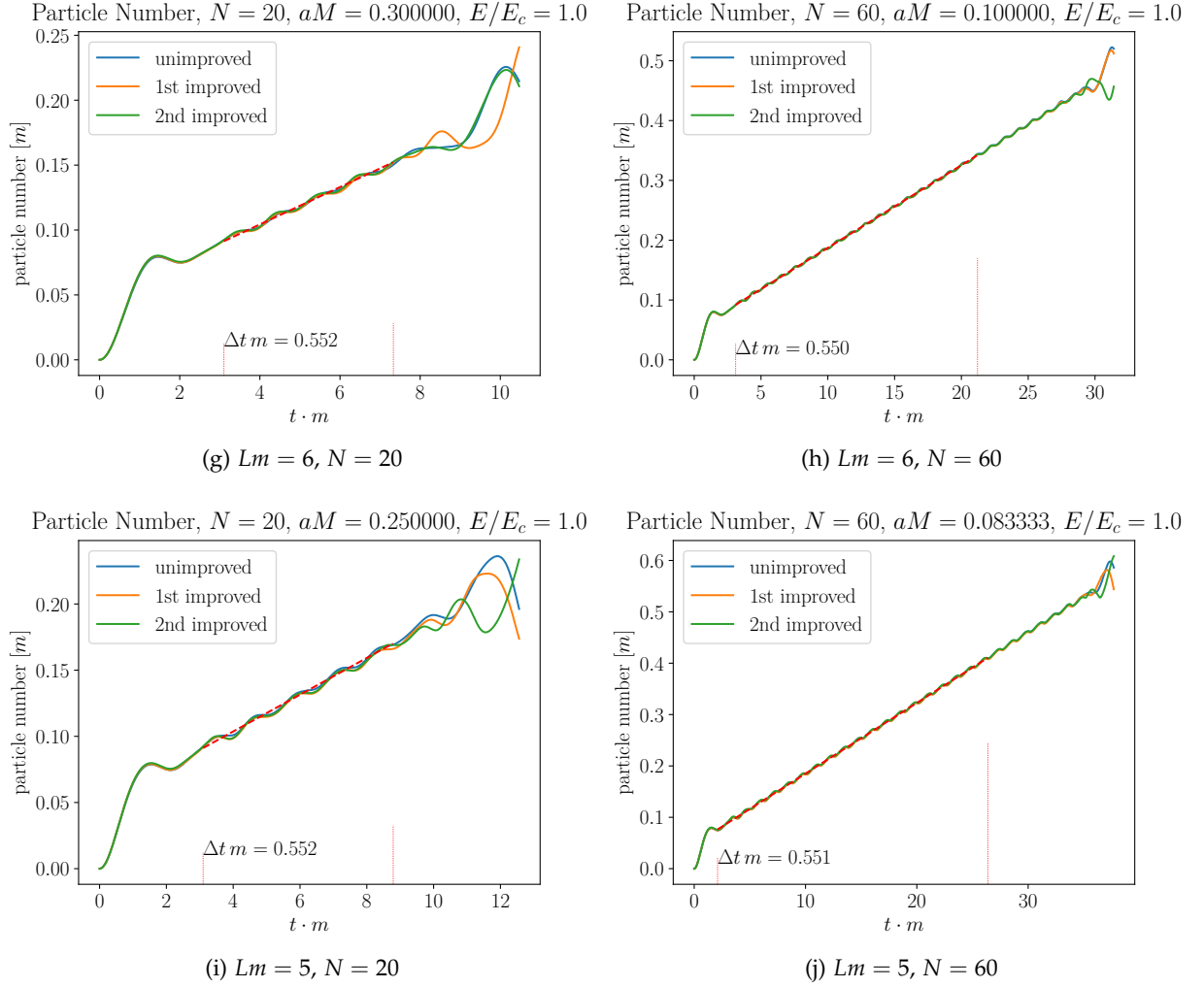
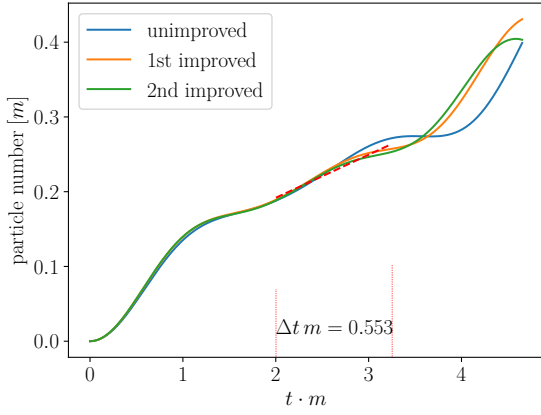


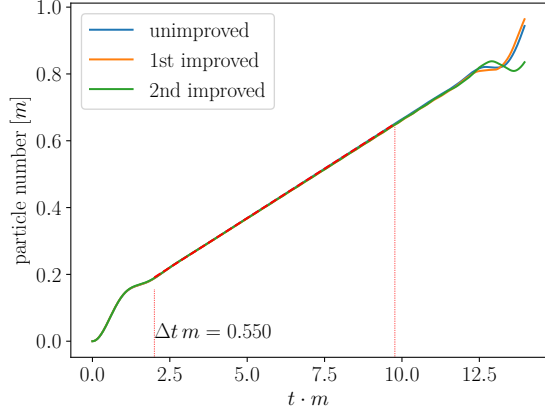
Figure C.2: UV convergence series with $E/E_c = 1$, $e/m = 0.1$. We show the first and the last run of the series, respectively. Linear function was fitted (red line) to suitable time window where quench dynamics already faded up until $1.5t_{max}$. Time window was varied with $\Delta t m \approx 0.5$.

Particle Number, $N = 20$, $aM = 0.450000$, $E/E_c = 1.5$



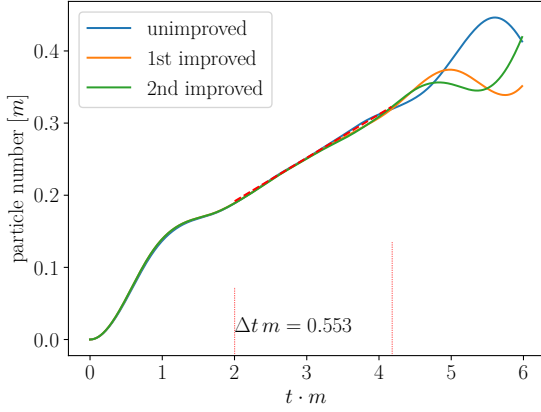
(a) $Lm = 9$, $N = 20$

Particle Number, $N = 60$, $aM = 0.150000$, $E/E_c = 1.5$



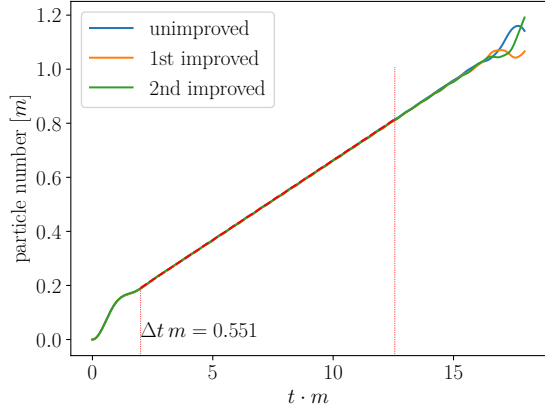
(b) $Lm = 9$, $N = 60$

Particle Number, $N = 20$, $aM = 0.350000$, $E/E_c = 1.5$



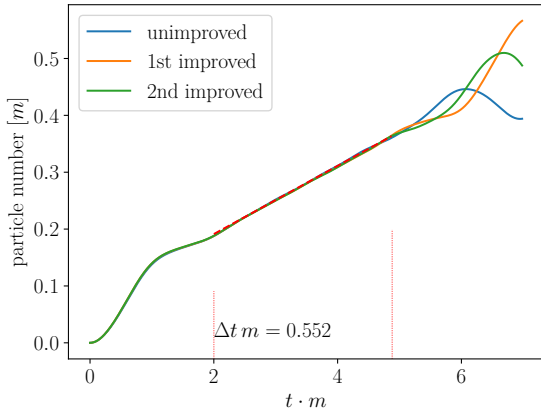
(c) $Lm = 7$, $N = 20$

Particle Number, $N = 60$, $aM = 0.116667$, $E/E_c = 1.5$



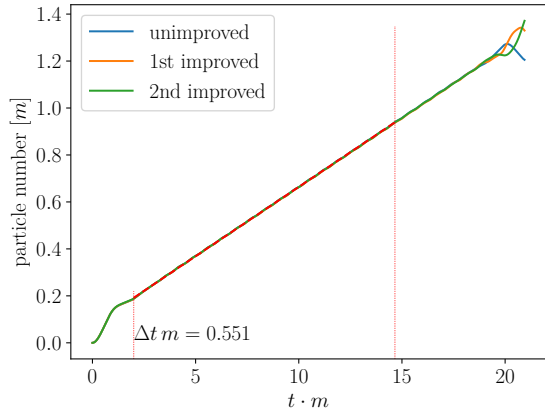
(d) $Lm = 7$, $N = 60$

Particle Number, $N = 20$, $aM = 0.300000$, $E/E_c = 1.5$



(e) $Lm = 6$, $N = 20$

Particle Number, $N = 60$, $aM = 0.100000$, $E/E_c = 1.5$



(f) $Lm = 6$, $N = 60$

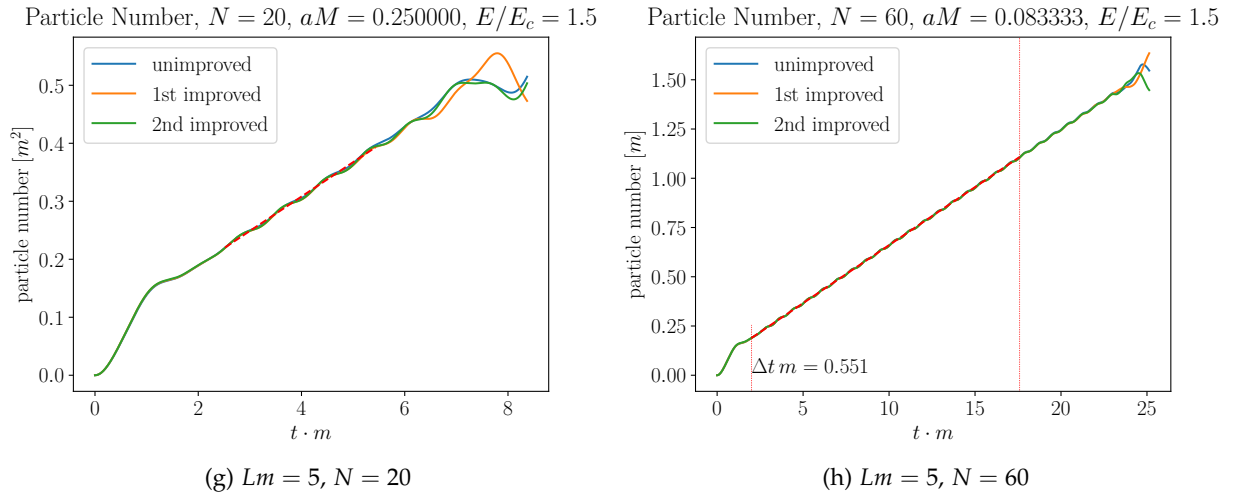


Figure C.2: UV convergence series with $E/E_c = 1.5$, $e/m = 0.1$. We show the first and the last run of the series, respectively. Linear function was fitted (red line) to suitable time window where quench dynamics already faded up until $1.5t_{max}$. Time window was varied with $\Delta tm \approx 0.5$.

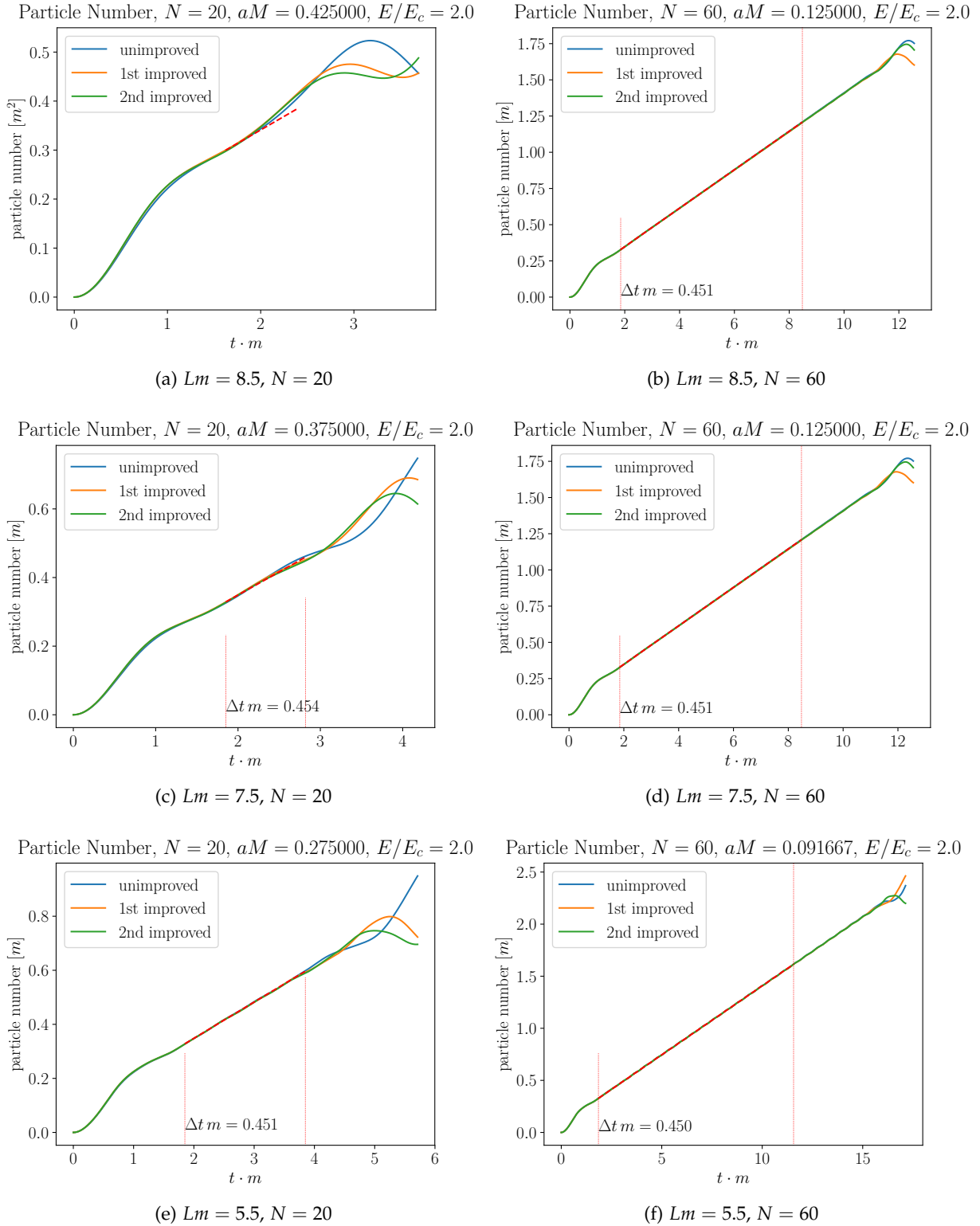


Figure C.3: UV convergence series with $E/E_c = 2$, $e/m = 0.1$. We show the first and the last run of the series, respectively. Linear function was fitted (red line) to suitable time window where quench dynamics already faded up until $1.5t_{max}$. Time window was varied with $\Delta t m \approx 0.5$.

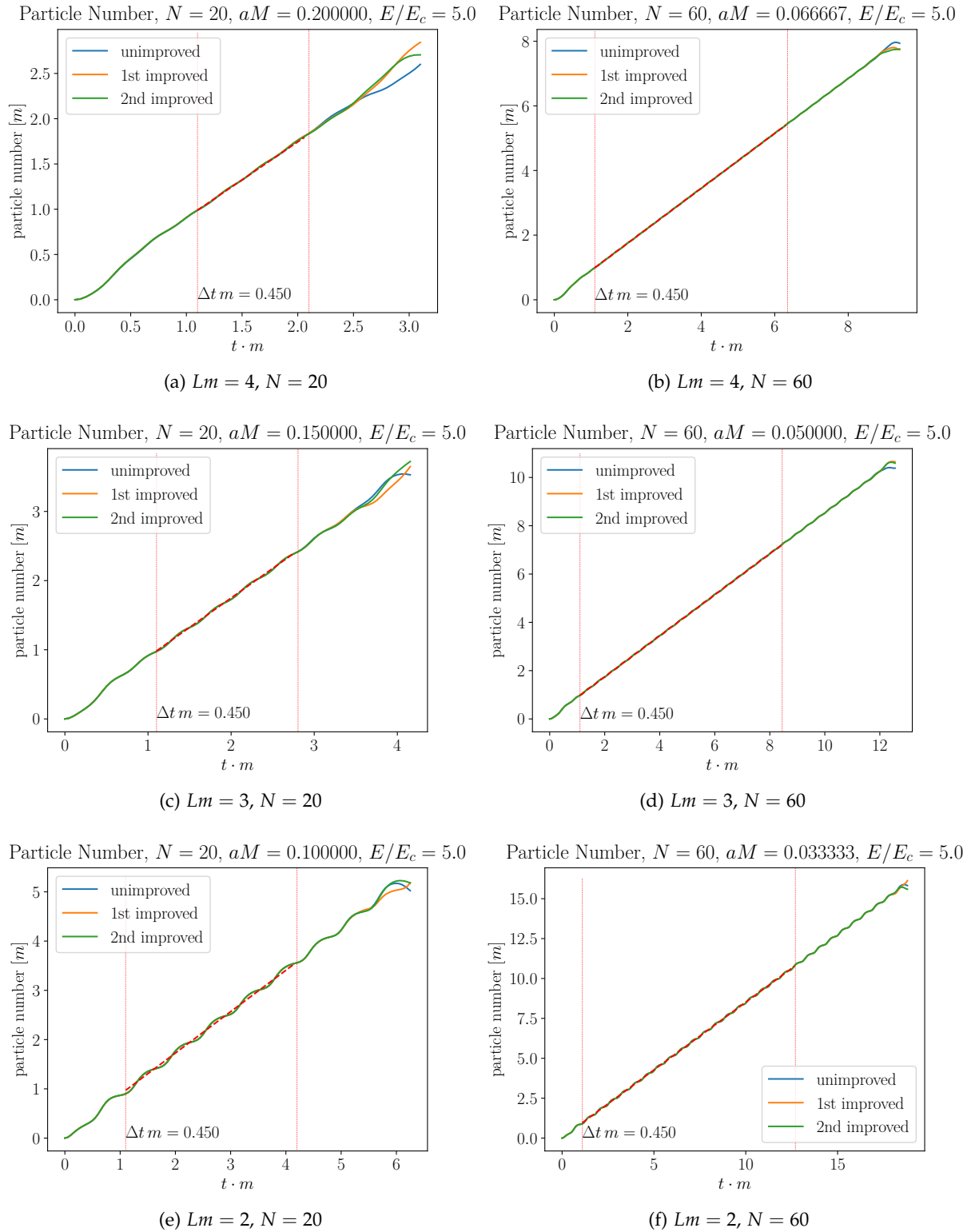


Figure C.4: UV convergence series with $E/E_c = 5$, $e/m = 0.1$. We show the first and the last run of the series, respectively. Linear function was fitted (red line) to suitable time window where quench dynamics already faded up until $1.5t_{max}$. Time window was varied with $\Delta t m \approx 0.5$.

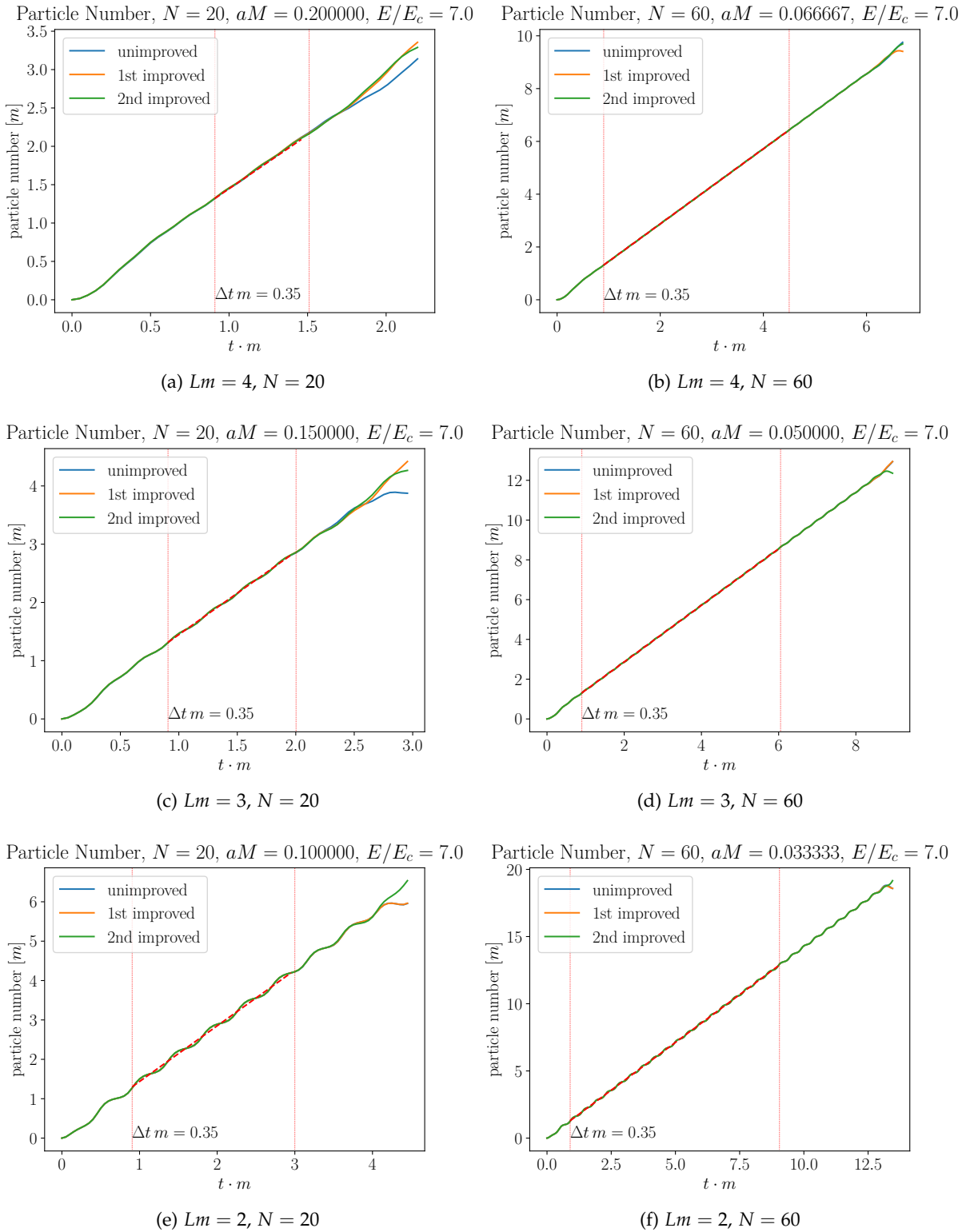


Figure C.5: UV convergence series with $E/E_c = 7$, $e/m = 0.1$. We show the first and the last run of the series, respectively. Linear function was fitted (red line) to suitable time window where quench dynamics already faded up until $1.5t_{max}$. Time window was varied with $\Delta t m \approx 0.35$.

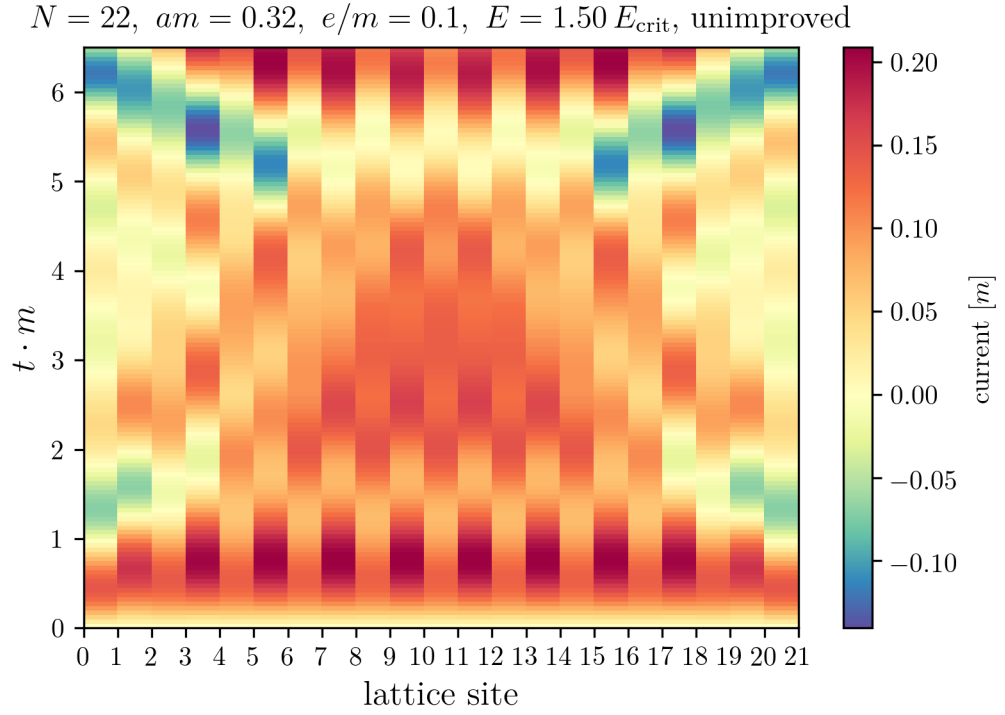
ON THE EFFECTS OF OPEN BOUNDARY CONDITIONS

In this appendix we wish to show the effects of open boundary conditions.

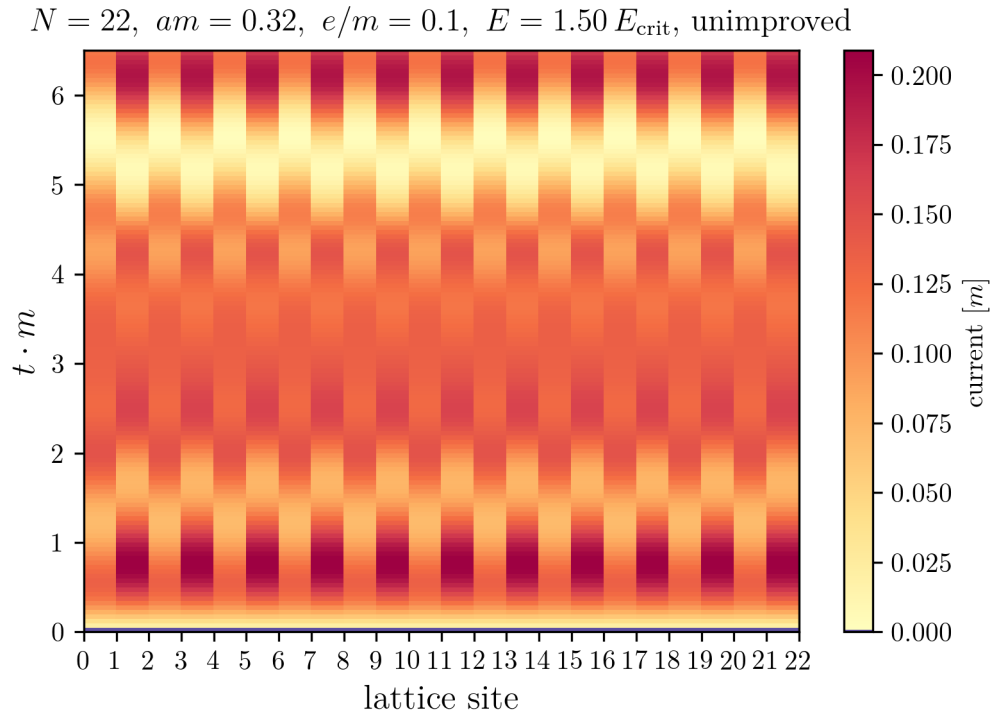
Tho this end, we inspect the current density plotted against time and location. For a system size of $2N$ sites one has for open boundary conditions $2N - 1$ different DoF for the current density opposed to $2N$ for the current with periodic boundary conditions.

We briefly looked at the boundary effects on a small systems with $N = 22$, $am = 0.32$, $e/m = 0.1$, and $E/E_c = 1.5$. [Figure D.1](#) shows the current heat map of the respective system. One observes that boundary effects find their way into the centre of the system within the runtime of $1t_{max}m$. Displayed in [Figure D.2](#) is the current averaged over two neighbouring sites which is in the case of PBC and a homogeneous field identical to space averaging over the entire system. Although the disturbance due to boundary effects at the centre of the system is admittedly mild, we still opted for periodic boundary conditions.

If one was to choose OBC one can eliminate the extra boundary degrees of freedom in [\(3.17\)](#). However, one would have to alter the analysis of diagonalising the Hamiltonian (and everything which is built on it) as plain waves would no longer constitute the diagonalising set of basis, i.e. the Fourier transform will not yield a diagonal matrix.



(a) Open Boundary Conditions



(b) Periodic Boundary Conditions

Figure D.1: Comparison of open boundary conditions and periodic boundary conditions. Both runs are performed with the same set of parameters: $N = 22$, $am = 0.32$, $e/m = 0.1$, $E/E_c = 1.5$ without improvement. Within $1t_{\text{max}}m \approx 6.5$ the boundary effects in (a) find their way into the centre of the system.

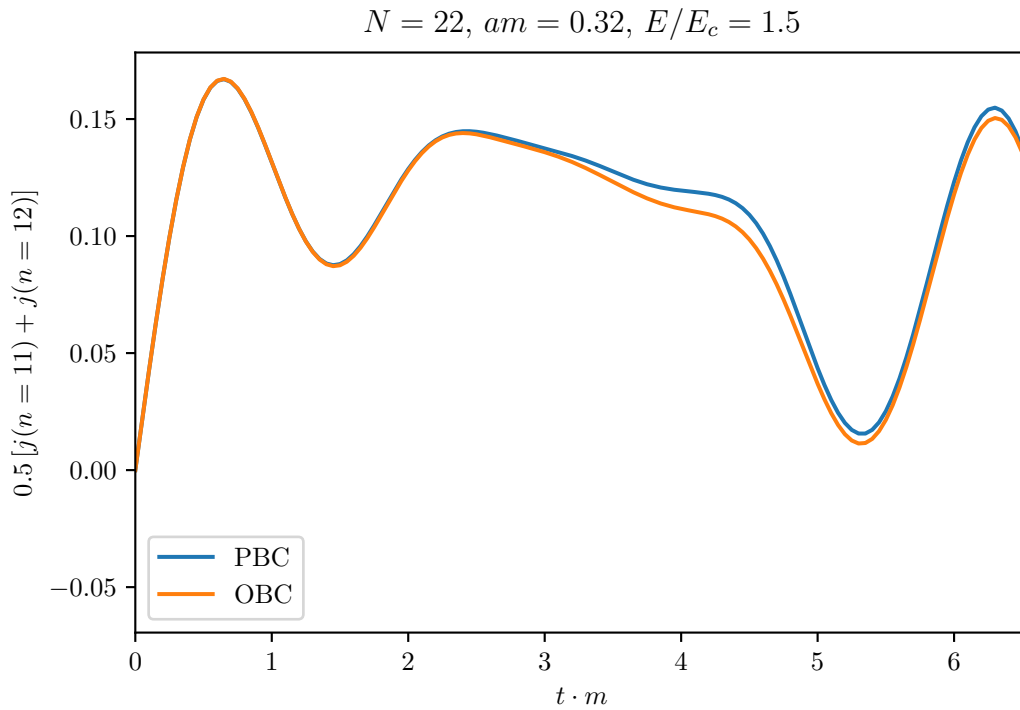
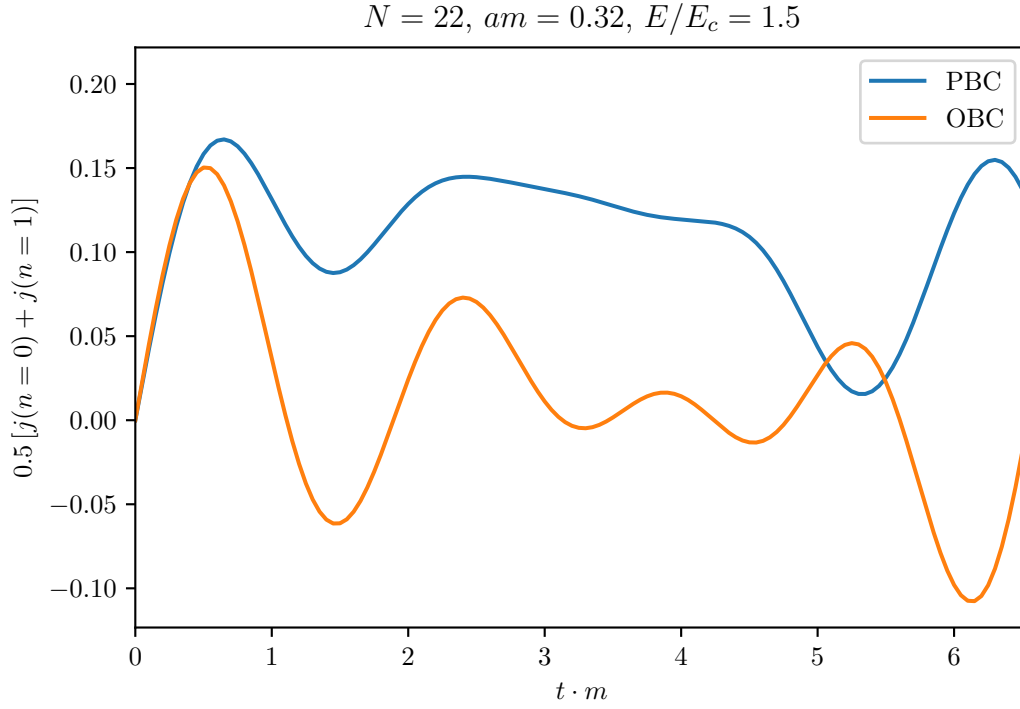
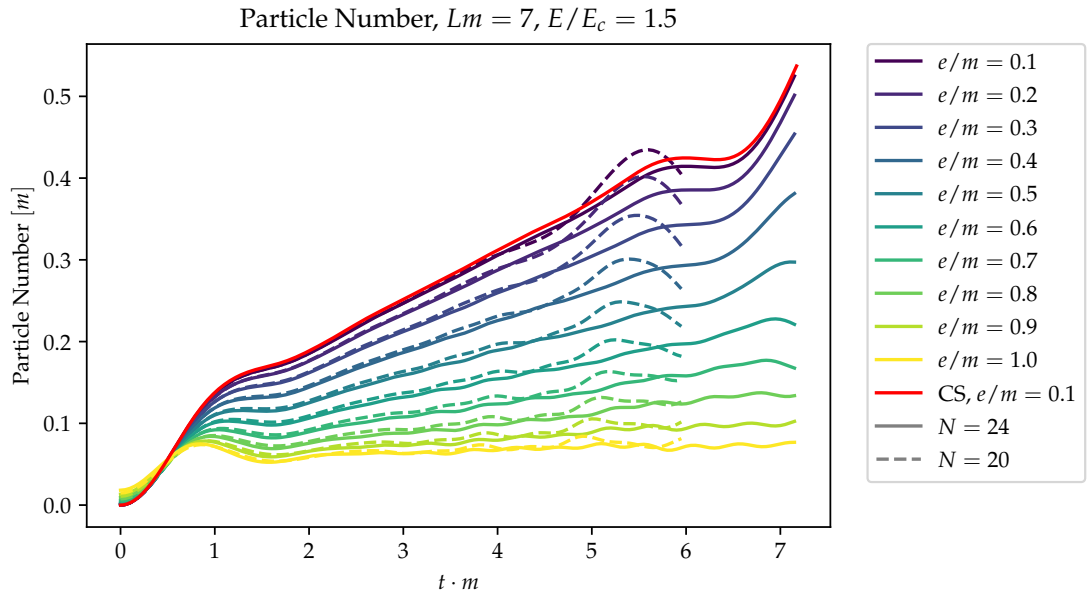


Figure D.2: Comparison of open boundary conditions and periodic boundary conditions. Both runs are performed with the same set of parameters: $N = 22, am = 0.32, e/m = 0.1, E/E_c = 1.5$ without improvement. In the case of PBC the average current discussed in Section 2.5.3 is plotted as it is in a homogeneous field identical to the average over two neighbouring sites. To no surprise, the OBC system displays strong boundary effects at the boundary. Even within $1t_{max}m$ mild boundary effects find their way into the centre of the system (cf. (b)).

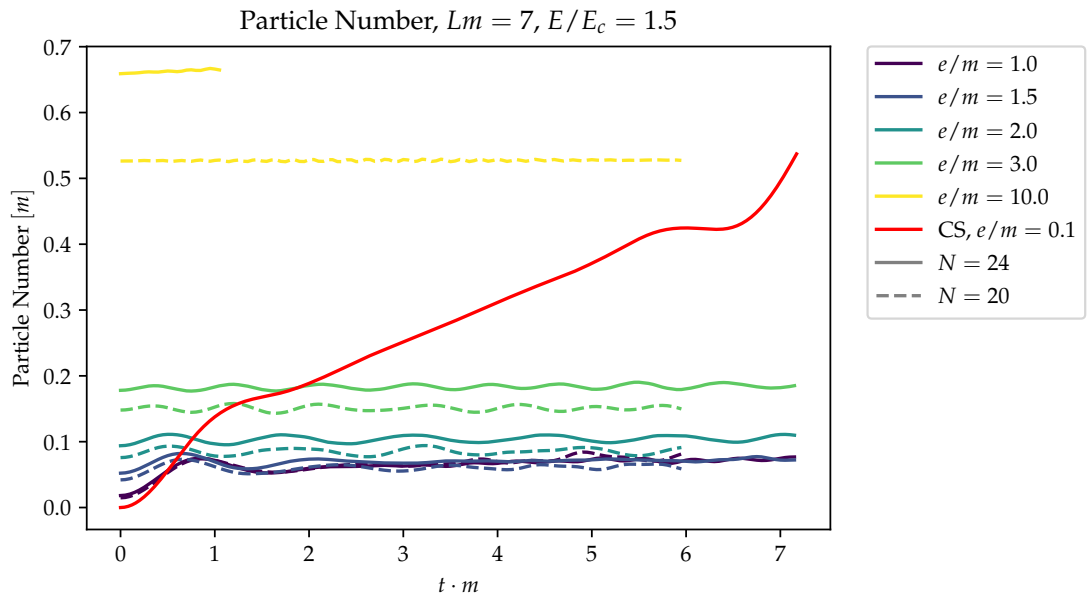
SUPPLEMENTARY PLOTS: STRONGLY COUPLED QED AT $Lm = 7$, $E/E_c = 1.5$ AND 'EVEN' SYSTEM SIZE

E

For the sake of transparency we shall enclose the plots for 'even' system size in this appendix.



(a) $N/2 = \text{even}$, $e/m = 0.1 \dots 1.0$



(b) $N/2 = \text{even}$, $e/m = 1 \dots 10$

Figure E.1: Particle number for strongly coupled QED at 'even' system sizes.

BIBLIOGRAPHY

- [1] M.E. Peskin and D.V. Schroeder. *An Introduction To Quantum Field Theory*. Frontiers in Physics. Avalon Publishing, 1995. ISBN: 9780813345437.
- [2] Heinz J. Rothe. *Lattice gauge theories. an introduction*. eng. 3. ed. World Scientific lecture notes in physics. New Jersey, NJ [u.a.]: World Scientific, 2005, XVII, 588 S. ISBN: 981-256-062-9 and 981-256-168-4 and 978-981-256-168-8 and 978-981-256-062-9.
- [3] R. P. Feynman. ‘The Theory of Positrons’. In: *Phys. Rev.* 76 (6 Sept. 1949), pp. 749–759. DOI: [10.1103/PhysRev.76.749](https://doi.org/10.1103/PhysRev.76.749). URL: <https://link.aps.org/doi/10.1103/PhysRev.76.749>.
- [4] Kenneth G. Wilson. ‘Confinement of quarks’. In: *Phys. Rev. D* 10 (8 Oct. 1974), pp. 2445–2459. DOI: [10.1103/PhysRevD.10.2445](https://doi.org/10.1103/PhysRevD.10.2445). URL: <https://link.aps.org/doi/10.1103/PhysRevD.10.2445>.
- [5] Matthias Troyer and Uwe-Jens Wiese. ‘Computational Complexity and Fundamental Limitations to Fermionic Quantum Monte Carlo Simulations’. In: *Phys. Rev. Lett.* 94 (17 May 2005), p. 170201. DOI: [10.1103/PhysRevLett.94.170201](https://doi.org/10.1103/PhysRevLett.94.170201). URL: <https://link.aps.org/doi/10.1103/PhysRevLett.94.170201>.
- [6] Valentin Kasper, Florian Hebenstreit and Jürgen Berges. ‘Fermion production from real-time lattice gauge theory in the classical-statistical regime’. In: *Phys. Rev. D* 90.2 (2014), p. 025016. DOI: [10.1103/PhysRevD.90.025016](https://doi.org/10.1103/PhysRevD.90.025016). arXiv: [1403.4849](https://arxiv.org/abs/1403.4849) [hep-ph].
- [7] Mark Mace, Niklas Mueller, Sören Schlichting and Sayantan Sharma. ‘Nonequilibrium study of the chiral magnetic effect from real-time simulations with dynamical fermions’. In: *Phys. Rev. D* 95 (3 Feb. 2017), p. 036023. DOI: [10.1103/PhysRevD.95.036023](https://doi.org/10.1103/PhysRevD.95.036023). URL: <https://link.aps.org/doi/10.1103/PhysRevD.95.036023>.
- [8] F. Hebenstreit, J. Berges and D. Gelfand. ‘Real-Time Dynamics of String Breaking’. In: *Phys. Rev. Lett.* 111 (20 Nov. 2013), p. 201601. DOI: [10.1103/PhysRevLett.111.201601](https://doi.org/10.1103/PhysRevLett.111.201601). URL: <https://link.aps.org/doi/10.1103/PhysRevLett.111.201601>.
- [9] Boye Buyens, Jutho Haegeman, Karel Van Acoleyen, Henri Verschelde and Frank Verstraete. ‘Matrix product states for gauge field theories’. In: *Phys. Rev. Lett.* 113 (2014), p. 091601. DOI: [10.1103/PhysRevLett.113.091601](https://doi.org/10.1103/PhysRevLett.113.091601). arXiv: [1312.6654](https://arxiv.org/abs/1312.6654) [hep-lat].
- [10] T. Pichler, M. Dalmonte, E. Rico, P. Zoller and S. Montangero. ‘Real-Time Dynamics in U(1) Lattice Gauge Theories with Tensor Networks’. In: *Phys. Rev. X* 6 (1 Mar. 2016), p. 011023. DOI: [10.1103/PhysRevX.6.011023](https://doi.org/10.1103/PhysRevX.6.011023). URL: <https://link.aps.org/doi/10.1103/PhysRevX.6.011023>.
- [11] Ulrich Schollwöck. ‘The density-matrix renormalization group in the age of matrix product states’. In: *Annals of Physics* 326.1 (2011). January 2011 Special Issue, pp. 96–192. ISSN: 0003-4916. DOI: <https://doi.org/10.1016/j.aop.2010.09.012>. URL: <http://www.sciencedirect.com/science/article/pii/S0003491610001752>.

- [12] Richard P. Feynman. ‘Simulating physics with computers’. In: *International Journal of Theoretical Physics* 21.6 (June 1982), pp. 467–488. ISSN: 1572-9575. DOI: [10.1007/BF02650179](https://doi.org/10.1007/BF02650179). URL: <https://doi.org/10.1007/BF02650179>.
- [13] Seth Lloyd. ‘Universal Quantum Simulators’. In: *Science* 273.5278 (1996), pp. 1073–1078. ISSN: 0036-8075. DOI: [10.1126/science.273.5278.1073](https://doi.org/10.1126/science.273.5278.1073). eprint: <http://science.sciencemag.org/content/273/5278/1073.full.pdf>. URL: <http://science.sciencemag.org/content/273/5278/1073>.
- [14] Erez Zohar, J. Ignacio Cirac and Benni Reznik. ‘Quantum Simulations of Lattice Gauge Theories using Ultracold Atoms in Optical Lattices’. In: *Rept. Prog. Phys.* 79.1 (2016), p. 014401. DOI: [10.1088/0034-4885/79/1/014401](https://doi.org/10.1088/0034-4885/79/1/014401). arXiv: [1503.02312](https://arxiv.org/abs/1503.02312) [quant-ph].
- [15] ‘Quantum theory, the Church–Turing principle and the universal quantum computer’. In: *Proceedings of the Royal Society of London A: Mathematical, Physical and Engineering Sciences* 400.1818 (1985), pp. 97–117. ISSN: 0080-4630. DOI: [10.1098/rspa.1985.0070](https://doi.org/10.1098/rspa.1985.0070). eprint: <http://rspa.royalsocietypublishing.org/content/400/1818/97.full.pdf>. URL: <http://rspa.royalsocietypublishing.org/content/400/1818/97>.
- [16] Peter W. Shor. ‘Scheme for reducing decoherence in quantum computer memory’. In: *Phys. Rev. A* 52 (4 Oct. 1995), R2493–R2496. DOI: [10.1103/PhysRevA.52.R2493](https://doi.org/10.1103/PhysRevA.52.R2493). URL: <https://link.aps.org/doi/10.1103/PhysRevA.52.R2493>.
- [17] A. M. Steane. ‘Error Correcting Codes in Quantum Theory’. In: *Phys. Rev. Lett.* 77 (5 July 1996), pp. 793–797. DOI: [10.1103/PhysRevLett.77.793](https://doi.org/10.1103/PhysRevLett.77.793). URL: <https://link.aps.org/doi/10.1103/PhysRevLett.77.793>.
- [18] H. Häffner, C.F. Roos and R. Blatt. ‘Quantum computing with trapped ions’. In: *Physics Reports* 469.4 (2008), pp. 155–203. ISSN: 0370-1573. DOI: <https://doi.org/10.1016/j.physrep.2008.09.003>. URL: <http://www.sciencedirect.com/science/article/pii/S0370157308003463>.
- [19] I. M. Georgescu, S. Ashhab and Franco Nori. ‘Quantum simulation’. In: *Rev. Mod. Phys.* 86 (1 Mar. 2014), pp. 153–185. DOI: [10.1103/RevModPhys.86.153](https://doi.org/10.1103/RevModPhys.86.153). URL: <https://link.aps.org/doi/10.1103/RevModPhys.86.153>.
- [20] V Kasper, F Hebenstreit, F Jendrzejewski, M K Oberthaler and J Berges. ‘Implementing quantum electrodynamics with ultracold atomic systems’. In: *New Journal of Physics* 19.2 (2017), p. 023030. URL: <http://stacks.iop.org/1367-2630/19/i=2/a=023030>.
- [21] Thomas Schweigler, Valentin Kasper, Sebastian Erne, Bernhard Rauer, Tim Langen, Thomas Gasenzer, Jürgen Berges and Jörg Schmiedmayer. ‘On solving the quantum many-body problem’. In: (2015). arXiv: [1505.03126](https://arxiv.org/abs/1505.03126) [cond-mat.quant-gas].
- [22] J. Smith, A. Lee, P. Richerme, B. Neyenhuis, P. W. Hess, P. Hauke, M. Heyl, D. A. Huse and C. Monroe. ‘Many-body localization in a quantum simulator with programmable random disorder’. In: *Nature Physics* 12 (June 2016), 907 EP -. URL: <http://dx.doi.org/10.1038/nphys3783>.
- [23] Esteban A. Martinez et al. ‘Real-time dynamics of lattice gauge theories with a few-qubit quantum computer’. In: *Nature* 534 (June 2016), 516 EP -. URL: <http://dx.doi.org/10.1038/nature18318>.

- [24] J. Q. You and Franco Nori. ‘Atomic physics and quantum optics using superconducting circuits’. In: *Nature* 474 (June 2011). Review Article, 589 EP -. URL: <http://dx.doi.org/10.1038/nature10122>.
- [25] K. Symanzik. ‘Cutoff Dependence in Lattice ϕ_4^4 Theory’. In: *Recent Developments in Gauge Theories*. Ed. by G. ’t Hooft, C. Itzykson, A. Jaffe, H. Lehmann, P. K. Mitter, I. M. Singer and R. Stora. Boston, MA: Springer US, 1980, pp. 313–330. ISBN: 978-1-4684-7571-5. DOI: [10.1007/978-1-4684-7571-5_18](https://doi.org/10.1007/978-1-4684-7571-5_18). URL: https://doi.org/10.1007/978-1-4684-7571-5_18.
- [26] Julian Schwinger. ‘On Gauge Invariance and Vacuum Polarization’. In: *Phys. Rev.* 82 (5 June 1951), pp. 664–679. DOI: [10.1103/PhysRev.82.664](https://link.aps.org/doi/10.1103/PhysRev.82.664). URL: <https://link.aps.org/doi/10.1103/PhysRev.82.664>.
- [27] Kirill Melnikov and Marvin Weinstein. ‘Lattice Schwinger model: Confinement, anomalies, chiral fermions, and all that’. In: *Phys. Rev. D* 62 (9 Oct. 2000), p. 094504. DOI: [10.1103/PhysRevD.62.094504](https://link.aps.org/doi/10.1103/PhysRevD.62.094504). URL: <https://link.aps.org/doi/10.1103/PhysRevD.62.094504>.
- [28] Elcio Abdalla, Maria Cristina B. Abdalla and Klaus D. Rothe. *Non-perturbative methods in 2 dimensional quantum field theory*. eng. 2. ed. Includes bibliographical references and index. Singapore [u.a.]: World Scientific, 2001, 832 S. ISBN: 981-02-4596-3 and 978-981-02-4596-2.
- [29] C.J. Hamer, J. Kogut, D.P. Crewther and M.M. Mazzolini. ‘The massive Schwinger model on a lattice: Background field, chiral symmetry and the string tension’. In: *Nuclear Physics B* 208.3 (1982), pp. 413–438. ISSN: 0550-3213. DOI: [https://doi.org/10.1016/0550-3213\(82\)90229-2](https://doi.org/10.1016/0550-3213(82)90229-2). URL: <http://www.sciencedirect.com/science/article/pii/0550321382902292>.
- [30] J.H Lowenstein and J.A Swieca. ‘Quantum electrodynamics in two dimensions’. In: *Annals of Physics* 68.1 (1971), pp. 172–195. ISSN: 0003-4916. DOI: [https://doi.org/10.1016/0003-4916\(71\)90246-6](https://doi.org/10.1016/0003-4916(71)90246-6). URL: <http://www.sciencedirect.com/science/article/pii/0003491671902466>.
- [31] H.B. Nielsen and M. Ninomiya. ‘A no-go theorem for regularizing chiral fermions’. In: *Physics Letters B* 105.2 (1981), pp. 219–223. ISSN: 0370-2693. DOI: [https://doi.org/10.1016/0370-2693\(81\)91026-1](https://doi.org/10.1016/0370-2693(81)91026-1). URL: <http://www.sciencedirect.com/science/article/pii/0370269381910261>.
- [32] John Kogut and Leonard Susskind. ‘Hamiltonian formulation of Wilson’s lattice gauge theories’. In: *Phys. Rev. D* 11 (2 Jan. 1975), pp. 395–408. DOI: [10.1103/PhysRevD.11.395](https://link.aps.org/doi/10.1103/PhysRevD.11.395). URL: <https://link.aps.org/doi/10.1103/PhysRevD.11.395>.
- [33] Christof Gattringer and Christian B. Lang. *Quantum Chromodynamics on the Lattice. An Introductory Presentation*. eng. Lecture notes in physics ARRAY(0x41e71e0). Berlin, Heidelberg: Springer Berlin Heidelberg, 2010, Online-Ressource (XV, 343p. 34 illus, digital). ISBN: 978-3-642-01850-3. DOI: [10.1007/978-3-642-01850-3](https://doi.org/10.1007/978-3-642-01850-3). URL: <http://dx.doi.org/10.1007/978-3-642-01850-3>.
- [34] Kenneth G. Wilson and J. Kogut. ‘The renormalization group and the ϵ expansion’. In: *Physics Reports* 12.2 (1974), pp. 75–199. ISSN: 0370-1573. DOI: [https://doi.org/10.1016/0370-1573\(74\)90023-4](https://doi.org/10.1016/0370-1573(74)90023-4). URL: <http://www.sciencedirect.com/science/article/pii/0370157374900234>.

- [35] P. Weisz. ‘Continuum limit improved lattice action for pure Yang-Mills theory (I)’. In: *Nuclear Physics B* 212.1 (1983), pp. 1–17. ISSN: 0550-3213. DOI: [https://doi.org/10.1016/0550-3213\(83\)90595-3](https://doi.org/10.1016/0550-3213(83)90595-3). URL: <http://www.sciencedirect.com/science/article/pii/0550321383905953>.
- [36] Stefan Sint. ‘An introduction to Symanzik’s $O(a)$ improvement programme’. STRONGnet Summer School 2011, Bielefeld. 2011. URL: https://www2.physik.uni-bielefeld.de/fileadmin/user_upload/workshops/strongnet/sint_bielefeld_11.pdf.
- [37] G. Peter Lepage. ‘Redesigning lattice QCD’. In: *Lect. Notes Phys.* 479 (1997), pp. 1–48. DOI: [10.1007/BFb0104288](https://doi.org/10.1007/BFb0104288). arXiv: [hep-lat/9607076](https://arxiv.org/abs/hep-lat/9607076) [hep-lat].
- [38] P. Hasenfratz. ‘Prospects for perfect actions’. In: *Nuclear Physics B - Proceedings Supplements* 63.1 (1998). Proceedings of the XVth International Symposium on Lattice Field Theory, pp. 53–58. ISSN: 0920-5632. DOI: [https://doi.org/10.1016/S0920-5632\(97\)00696-8](https://doi.org/10.1016/S0920-5632(97)00696-8). URL: <http://www.sciencedirect.com/science/article/pii/S0920563297006968>.
- [39] W. Bietenholz and U.-J. Wiese. ‘Perfect lattice actions for quarks and gluons’. In: *Nuclear Physics B* 464.1 (1996), pp. 319–350. ISSN: 0550-3213. DOI: [https://doi.org/10.1016/0550-3213\(95\)00678-8](https://doi.org/10.1016/0550-3213(95)00678-8). URL: <http://www.sciencedirect.com/science/article/pii/0550321395006788>.
- [40] Xiang-Qian Luo, Shuo-Hong Guo, Helmut Kröger and Dieter Schütte. ‘Improved lattice gauge field Hamiltonian’. In: *Phys. Rev. D* 59 (3 Jan. 1999), p. 034503. DOI: [10.1103/PhysRevD.59.034503](https://doi.org/10.1103/PhysRevD.59.034503). URL: <https://link.aps.org/doi/10.1103/PhysRevD.59.034503>.
- [41] Satchidananda Naik. ‘On-shell improved action for QCD with suskind fermions and the asymptotic freedom scale’. In: *Nuclear Physics B* 316.1 (1989), pp. 238–268. ISSN: 0550-3213. DOI: [http://dx.doi.org/10.1016/0550-3213\(89\)90394-5](https://doi.org/10.1016/0550-3213(89)90394-5). URL: <http://www.sciencedirect.com/science/article/pii/0550321389903945>.
- [42] V Kasper, F Hebenstreit, F Jendrzejewski, M K Oberthaler and J Berges. ‘Implementing quantum electrodynamics with ultracold atomic systems’. In: *New Journal of Physics* 19.2 (2017), p. 023030. URL: <http://stacks.iop.org/1367-2630/19/i=2/a=023030>.
- [43] Naoto Tanji. ‘Dynamical view of pair creation in uniform electric and magnetic fields’. In: *Annals Phys.* 324 (2009), pp. 1691–1736. DOI: [10.1016/j.aop.2009.03.012](https://doi.org/10.1016/j.aop.2009.03.012). arXiv: [0810.4429](https://arxiv.org/abs/0810.4429) [hep-ph].
- [44] F. Hebenstreit, J. Berges and D. Gelfand. ‘Simulating fermion production in 1+1 dimensional QED’. In: *Phys. Rev. D* 87 (10 May 2013), p. 105006. DOI: [10.1103/PhysRevD.87.105006](https://doi.org/10.1103/PhysRevD.87.105006). URL: <https://link.aps.org/doi/10.1103/PhysRevD.87.105006>.
- [45] Michel Caffarel and Werner Krauth. ‘Exact diagonalization approach to correlated fermions in infinite dimensions: Mott transition and superconductivity’. In: *Phys. Rev. Lett.* 72 (10 Mar. 1994), pp. 1545–1548. DOI: [10.1103/PhysRevLett.72.1545](https://doi.org/10.1103/PhysRevLett.72.1545). URL: <https://link.aps.org/doi/10.1103/PhysRevLett.72.1545>.

- [46] Steven R. White. ‘Density matrix formulation for quantum renormalization groups’. In: *Phys. Rev. Lett.* 69 (19 Nov. 1992), pp. 2863–2866. DOI: [10.1103/PhysRevLett.69.2863](https://doi.org/10.1103/PhysRevLett.69.2863). URL: <https://link.aps.org/doi/10.1103/PhysRevLett.69.2863>.
- [47] D. Banerjee, M. Bögli, M. Dalmonte, E. Rico, P. Stebler, U.-J. Wiese and P. Zoller. ‘Atomic Quantum Simulation of $U(N)$ and $SU(N)$ Non-Abelian Lattice Gauge Theories’. In: *Phys. Rev. Lett.* 110 (12 Mar. 2013), p. 125303. DOI: [10.1103/PhysRevLett.110.125303](https://doi.org/10.1103/PhysRevLett.110.125303). URL: <https://link.aps.org/doi/10.1103/PhysRevLett.110.125303>.
- [48] L. Tagliacozzo, A. Celi, A. Zamora and M. Lewenstein. ‘Optical Abelian lattice gauge theories’. In: *Annals of Physics* 330 (2013), pp. 160–191. ISSN: 0003-4916. DOI: <https://doi.org/10.1016/j.aop.2012.11.009>. URL: <http://www.sciencedirect.com/science/article/pii/S0003491612001819>.
- [49] V. Kasper, F. Hebenstreit and J. Berges. ‘Fermion production from real-time lattice gauge theory in the classical-statistical regime’. In: *Phys. Rev. D* 90 (2 July 2014), p. 025016. DOI: [10.1103/PhysRevD.90.025016](https://doi.org/10.1103/PhysRevD.90.025016). URL: <https://link.aps.org/doi/10.1103/PhysRevD.90.025016>.
- [50] V. Kasper, F. Hebenstreit, M.K. Oberthaler and J. Berges. ‘Schwinger pair production with ultracold atoms’. In: *Physics Letters B* 760 (2016), pp. 742–746. ISSN: 0370-2693. DOI: <https://doi.org/10.1016/j.physletb.2016.07.036>. URL: <http://www.sciencedirect.com/science/article/pii/S037026931630377X>.
- [51] T V Zache, F Hebenstreit, F Jendrzejewski, M K Oberthaler, J Berges and P Hauke. ‘Quantum simulation of lattice gauge theories using Wilson fermions’. In: *Quantum Science and Technology* 3.3 (2018), p. 034010. URL: <http://stacks.iop.org/2058-9565/3/i=3/a=034010>.
- [52] C. J. Hamer, Zheng Weihong and J. Oitmaa. ‘Series expansions for the massive Schwinger model in Hamiltonian lattice theory’. In: *Phys. Rev. D* 56 (1 July 1997), pp. 55–67. DOI: [10.1103/PhysRevD.56.55](https://doi.org/10.1103/PhysRevD.56.55). URL: <https://link.aps.org/doi/10.1103/PhysRevD.56.55>.
- [53] Torsten Victor Zache. ‘Massive Schwinger Model on the lattice: solution to Gauß’ Law with periodic boundary conditions’. unpublished thesis. 2018.
- [54] Phillip Weinberg and Marin Bukov. ‘QuSpin: a Python Package for Dynamics and Exact Diagonalisation of Quantum Many Body Systems part I: spin chains’. In: *SciPost Phys.* 2 (1 2017), p. 003. DOI: [10.21468/SciPostPhys.2.1.003](https://doi.org/10.21468/SciPostPhys.2.1.003). URL: <https://scipost.org/10.21468/SciPostPhys.2.1.003>.
- [55] Richard B Lehoucq, Danny C Sorensen and Chao Yang. *ARPACK users’ guide: solution of large-scale eigenvalue problems with implicitly restarted Arnoldi methods*. Vol. 6. Siam, 1998.
- [56] Anders Soerensen and Klaus Moelmer. ‘Quantum computation with ions in thermal motion’. In: *Phys. Rev. Lett.* 82 (1999), pp. 1971–1974. DOI: [10.1103/PhysRevLett.82.1971](https://doi.org/10.1103/PhysRevLett.82.1971). arXiv: [quant-ph/9810039](https://arxiv.org/abs/quant-ph/9810039) [quant-ph].
- [57] M Müller, K Hammerer, Y L Zhou, C F Roos and P Zoller. ‘Simulating open quantum systems: from many-body interactions to stabilizer pumping’. In: *New Journal of Physics* 13.8 (2011), p. 085007. URL: <http://stacks.iop.org/1367-2630/13/i=8/a=085007>.

- [58] J. I. Cirac and P. Zoller. ‘Quantum Computations with Cold Trapped Ions’. In: *Phys. Rev. Lett.* 74 (20 May 1995), pp. 4091–4094. DOI: [10.1103/PhysRevLett.74.4091](https://doi.org/10.1103/PhysRevLett.74.4091). URL: <https://link.aps.org/doi/10.1103/PhysRevLett.74.4091>.
- [59] T. Banks, Leonard Susskind and John Kogut. ‘Strong-coupling calculations of lattice gauge theories: (1 + 1)-dimensional exercises’. In: *Phys. Rev. D* 13 (4 Feb. 1976), pp. 1043–1053. DOI: [10.1103/PhysRevD.13.1043](https://doi.org/10.1103/PhysRevD.13.1043). URL: <https://link.aps.org/doi/10.1103/PhysRevD.13.1043>.
- [60] F. Berruto, G. Grignani and P. Sodano. ‘Chiral symmetry breaking in strongly coupled (1+1)-dimensional lattice gauge theories’. In: *Lattice fermions and structure of the vacuum. Proceedings, NATO Advanced Research Workshop, Dubna, Russia, October 5-9, 1999*. 1999, pp. 91–98. arXiv: [hep-lat/0001012](https://arxiv.org/abs/hep-lat/0001012) [hep-lat].
- [61] Ashok K. Das, J. Frenkel and C. Schubert. ‘Infrared divergences, mass shell singularities and gauge dependence of the dynamical fermion mass’. In: *Phys. Lett. B* 720 (2013), pp. 414–418. DOI: [10.1016/j.physletb.2013.02.036](https://doi.org/10.1016/j.physletb.2013.02.036). arXiv: [1212.2057](https://arxiv.org/abs/1212.2057) [hep-th].
- [62] F. Berruto, G. Grignani, G. W. Semenoff and P. Sodano. ‘Chiral symmetry breaking on the lattice: A study of the strongly coupled lattice Schwinger model’. In: *Phys. Rev. D* 57 (8 Apr. 1998), pp. 5070–5083. DOI: [10.1103/PhysRevD.57.5070](https://doi.org/10.1103/PhysRevD.57.5070). URL: <https://link.aps.org/doi/10.1103/PhysRevD.57.5070>.
- [63] T. Banks, Leonard Susskind and John Kogut. ‘Strong-coupling calculations of lattice gauge theories: (1 + 1)-dimensional exercises’. In: *Phys. Rev. D* 13 (4 Feb. 1976), pp. 1043–1053. DOI: [10.1103/PhysRevD.13.1043](https://doi.org/10.1103/PhysRevD.13.1043). URL: <https://link.aps.org/doi/10.1103/PhysRevD.13.1043>.
- [64] Daniel Spitz and Jürgen Berges. ‘Fermion production and color string dynamics in real-time lattice QCD₂’. in preparation. 2018.
- [65] Mark Mace, Niklas Müller, Sören Schlichting and Sayantan Sharma. ‘Nonequilibrium study of the chiral magnetic effect from real-time simulations with dynamical fermions’. In: *Phys. Rev. D* 95 (3 Feb. 2017), p. 036023. DOI: [10.1103/PhysRevD.95.036023](https://doi.org/10.1103/PhysRevD.95.036023). URL: <https://link.aps.org/doi/10.1103/PhysRevD.95.036023>.
- [66] Mark Mace, Niklas Mueller, Sören Schlichting and Sayantan Sharma. ‘Simulating chiral magnetic effect and anomalous transport phenomena in the pre-equilibrium stages of heavy-ion collisions’. In: *Nuclear Physics A* 967 (2017). The 26th International Conference on Ultra-relativistic Nucleus-Nucleus Collisions: Quark Matter 2017, pp. 752–755. ISSN: 0375-9474. DOI: <https://doi.org/10.1016/j.nuclphysa.2017.05.040>. URL: <http://www.sciencedirect.com/science/article/pii/S0375947417301574>.
- [67] Torsten V. Zache. private communication. 2018.
- [68] P. Jordan and E. Wigner. ‘Über das Paulische Äquivalenzverbot’. In: *Zeitschrift für Physik* 47.9 (Sept. 1928), pp. 631–651. ISSN: 0044-3328. DOI: [10.1007/BF01331938](https://doi.org/10.1007/BF01331938). URL: <https://doi.org/10.1007/BF01331938>.

DECLARATION

Erklärung:

Ich versichere, dass ich diese Arbeit selbstständig verfasst habe und keine anderen als die angegebenen Quellen und Hilfsmittel benutzt habe.

Heidelberg, August 2018

.....